Acta Universitatis Agriculturae Sueciae

Doctoral Thesis No. 2025:13
Faculty of Forest Sciences

Methane emissions from high latitude peatlands:

Controls of their spatio-temporal dynamics across a mire complex

Koffi Dodji Noumonvi

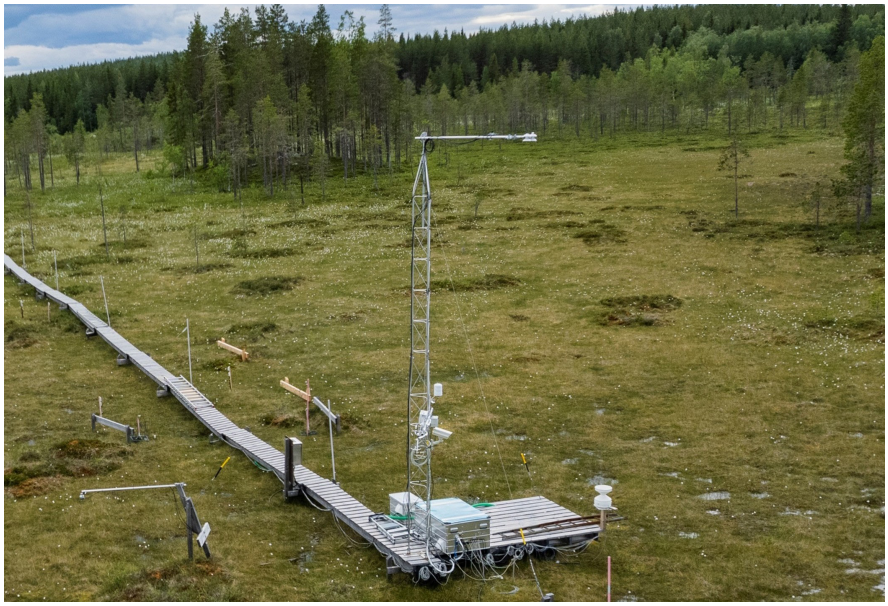

Methane emissions from high latitude peatlands:

Controls of their spatio-temporal dynamics across a mire complex

Koffi Dodji Noumonvi
Faculty of Forest Sciences
Department of Forest Ecology and Management
Umeå

SWEDISH UNIVERSITY
OF AGRICULTURAL
SCIENCES

DOCTORAL THESIS
Umeå 2025

Acta Universitatis Agriculturae Sueciae
2025:13

Cover: Aerial view of Hålmyran, photo by Andreas Palmén

ISSN 1652-6880
ISBN (print version) 978-91-8046-448-2
ISBN (electronic version) 978-91-8046-498-7
https://doi.org/10.54612/a.7rle58mqf6

Swedish University of Agricultural Sciences, Department of Forest Ecology and Management, Umeå, Sweden

Print: SLU Grafisk service, Uppsala 2025

Methane emissions from high latitude peatlands: Controls of their spatio-temporal dynamics across a mire complex

Abstract

Northern peatlands are significant natural sources of atmospheric methane (CH_4), yet high uncertainties remain in estimates of global CH_4 budgets. A key source of this uncertainty is a limited understanding of spatial variations at the mesoscale of peatland complexes. Current estimates typically rely on single-site measurements at the local scale. This thesis utilized the Kulbäcksliden Research Infrastructure (KRI) in northern Sweden, comprising four eddy covariance tower stations across a peatland complex, with the overall aim to investigate and predict mesoscale variations in CH_4 fluxes (FCH_4). The research first documented the infrastructure's unique configuration with replicated ecosystem-scale measurements and detailed mapping of vegetation (**Paper I**), then developed the Hummock-Hollow-Lawn (HuHoLa) model for peatland microtopography classification (**Paper II**). Using data from the KRI, spatial patterns in FCH_4 across the mire complex and their environmental controls were investigated (**Paper III**), followed by the development of data-driven approaches for upscaling single-site measurements (**Paper IV**). Key findings demonstrated that replicated ecosystem-scale measurements are essential for understanding spatial heterogeneity in peatland processes and developing upscaling approaches. The HuHoLa model advanced peatland surface characterization beyond traditional binary classifications by identifying three distinct microform classes and providing proxies for mapping water table depth and soil temperature (Ts). Spatial variability in FCH_4 within the mire complex matched that typically observed among geographically distant mire systems, with C:N ratio setting the baseline for spatial variations while Ts and plant productivity controlled temporal dynamics. The developed upscaling approaches reduced uncertainty in mire complex FCH_4 estimates by up to 50% compared to simple single-site extrapolation. These advances provide new understanding and tools for reducing uncertainties in global CH_4 budget estimates, crucial for predicting peatland-climate feedbacks under changing environmental conditions.

Keywords: methane flux, eddy covariance, peatland, microtopography, upscaling, machine learning, C:N ratio, footprint analysis, research infrastructure.

Metanemissioner från nordliga myrar: Reglering av spatio-temporala dynamik över ett myrkomplex

Sammanfattning

Nordliga myrar är viktiga naturliga källor till atmosfärisk metan (CH_4), men det finns betydande osäkerheter kring hur stor denna källa är, vilket påverkar globala CH_4-budgetskattningar. En viktig källa till denna osäkerhet är begränsad förståelse för rumsliga variationer inom myrkomplex på mesoskalan. Nuvarande skattningar förlitar sig ofta på empiriska mätningar från enstaka platser, som sedan antas vara representativa för ett större område. Denna avhandling använde Kulbäckslidens Forskningsinfrastruktur (KRI) i norra Sverige, som omfattar fyra eddy covariance-stationer spridda över ett myrkomplex, för att undersöka variationer i CH_4-flöden (FCH_4) på mesoskala. Först dokumenterades infrastrukturens unika konfiguration med replikerade ekosystemmätningar och kartering av vegetationen (**Artikel I**). Sedan utvecklades HuHoLa modellen för klassificering av torvmarksmikrotopografi (**Artikel II**). Vidare undersöktes rumsliga mönster i FCH_4 över myrkomplexet och faktorer som reglerar CH_4-utbytet (**Artikel III**). Slutligen utvecklades datadrivna metoder för uppskalning av mätningar från enstaka platser till ett större geografiskt område (**Artikel IV**). Resultaten visade att replikerade ekosystem-skaliga mätningar är nödvändiga för att förstå rumslig variation och utveckla uppskalningsmetoder. HuHoLa förbättrade karakteriseringen av myrelement, bortom traditionella binära klassificeringar, genom att identifiera tre mikroformklasser och tillhandahålla indikatorer för kartläggning av grundvattennivå och marktemperatur (Ts). Rumslig variation i FCH_4 inom myrkomplexet motsvarade den som vanligtvis observeras bland geografiskt avlägsna myrlokaler, där C:N-förhållandet sätter utgångspunkten för rumsliga variationer medan Ts och växtproduktivitet reglerade tidsvariationer. De utvecklade uppskalningsmetoderna minskade osäkerheten i uppskattningar av FCH_4 från myrkomplex med upp till 50% jämfört med enklare extrapolering från enstaka lokaler. Resultaten bidrar till ny förståelse och verktyg för att minska osäkerheter i skattningen av den globala CH_4-budgeten, vilket är avgörande för att förutsäga myrar-klimat återkopplingar under miljöförändringar.

Nyckelord: metanflöde, eddy covariance, torvmark, mikrotopografi, uppskalning, maskininlärning, C:N förhållande, footprint-analys, forskningsinfrastruktur.

Photo: Andreas Palmén

Photo: Andreas Palmén

Dedication

In the memory of my father Koffi Kodédjro Noumonvi (1959–2020)

Photo: Andreas Palmén

Contents

List of publications

This thesis is based on the work contained in the following papers, referred to by Roman numerals in the text:

I. Noumonvi, K. D., Ågren, A. M., Ratcliffe, J. L., Öquist, M. G., Ericson, L., Tong, C. H. M., Järveoja, J., Zhu, W., Osterwalder, S., Peng, H., Erefur, C., Bishop, K., Laudon, H., Nilsson, M. B., & Peichl, M. (2023). The Kulbäcksliden Research Infrastructure: A unique setting for northern peatland studies. Frontiers in Earth Science, 11, 1194749. https://doi.org/10.3389/feart.2023.1194749

II. Noumonvi, K. D., Havertz, N. H., Bohlin, J., van der Linden, S., Nilsson, M. B., & Peichl, M. (2025). HuHoLa: A novel Hummock-Hollow-Lawn mire microtopography modelling approach. (submitted)

III. Noumonvi, K. D., Nilsson, M. B., Ratcliffe, J. L., Öquist, M. G., Kljun, N., Fransson, J. E. S., Järveoja, J., Lindroth, A., Simpson, G., Smeds, J., & Peichl, M. (2025). Variations in ecosystem-scale methane fluxes across a boreal mire complex assessed by a network of flux towers. (submitted)

IV. Noumonvi, K. D., Kljun, N., Ratcliffe, J. L., Öquist, M. G., Fransson, J. E. S., Nilsson, M. B., & Peichl, M. (2025). Data-driven modelling of methane fluxes across a peatland complex based on eddy-covariance measurements and spatially resolved driver information. (Manuscript)

Paper I (open access) was reproduced with the permission of the publisher.

The contribution of Koffi Dodji Noumonvi to the papers included in this thesis was as follows:

I. Led the synthesis of site information and instrumentation, coordinated co-author contributions, and led the writing of the manuscript.

II. Developed the model concept, improved the model with co-authors, implemented the model, performed validation analysis with co-authors, and led the writing of the manuscript.

III. Designed the study with co-authors, performed data analysis, and led the writing of the manuscript.

IV. Designed the study with co-authors, performed data analysis and modelling, and led the writing of the manuscript.

List of tables

Photo: Andreas Palmén

List of figures

Abbreviations

CH_4	Methane
C:N ratio	Carbon-to-nitrogen ratio
CO_2	Carbon dioxide
DEM	Digital elevation model
EC	Eddy covariance
FCH_4	Methane fluxes
FFP	Flux footprint prediction
GPP	Gross primary production
HuHoLa	Hummock-Hollow-Lawn
HHDH	Hollow-hummock-depth-height
KRI	Kulbäcksliden Research Infrastructure
MSE	Mean squared error
NDVI	Normalized difference vegetation index
NEE	Net ecosystem CO_2 exchange
PAR	Photosynthetically active radiation
PARin	Incoming photosynthetically active radiation
PARout	Outgoing photosynthetically active radiation
RH	Relative humidity
RMSE	Root mean square error
Ts	Soil temperature
UAV	Unmanned aerial vehicle
VPD	Vapor pressure deficit
WTD	Water table depth

Photo: Andreas Palmén

1. Introduction

1.1 The role of northern peatlands in the global carbon cycle

Carbon storage and methane emissions

Northern peatlands are key ecosystems in the global carbon cycle, storing approximately one-third of the world's soil carbon despite covering less than 3% of the global land area (Frolking et al., 2011; Limpens et al., 2008). These ecosystems have accumulated carbon over millennia through the imbalance between primary production and decomposition under cold, waterlogged conditions (Frolking et al., 2011; Gorham, 1957). This high carbon density makes them the most efficient carbon storing ecosystem type on Earth on a per area basis (Joosten and Couwenberg, 2008). At the same time, the anaerobic conditions that preserve carbon also promote methane (CH_4) production, making northern peatlands significant natural sources of atmospheric CH_4, contributing between 9 and 53 Tg CH_4-C annually to global emissions (Peltola et al., 2019; Saunois et al., 2020; Yuan et al., 2024; Zhuang et al., 2006). This emission from northern peatlands represents approximately 5 to 25% of recent multi-model estimates of global wetland CH_4 emissions (Zhang et al., 2025). The production, oxidation and emission of CH_4 in peatlands is controlled by complex interactions between hydrology, vegetation, and microbial communities (Lai, 2009; Yuan et al., 2022), which are increasingly sensitive to the impacts of climate change.

Feedbacks between peatland CH_4 exchanges and the global climate

The importance of northern peatlands in global CH_4 dynamics is amplified as high-latitude regions are experiencing warming at more than twice the global average rate (Rantanen et al., 2022; Walsh, 2014). This amplified warming affects peatland carbon cycling through multiple pathways, including direct temperature effects on microbial activity and enhanced vegetation productivity, which increases CH_4 emissions by providing substrates for methanogens and pathways for gas transport (Heffernan et al., 2022; Hopple et al., 2020). Given that CH_4 is a potent greenhouse gas with approximately 28 times the warming potential of carbon dioxide (CO_2) over a 100-year period (IPCC, 2023), these warming-induced changes represent a positive feedback loop that will further accelerate

climate warming (Dean et al., 2018; Yuan et al., 2024). Beyond temperature effects, changes in precipitation patterns and increasing evaporative demand are altering peatland water balances (Helbig et al., 2020), which can significantly impact both their carbon storage capacity (Kettridge et al., 2016) and CH_4 emissions. However, quantifying these complex interactions and their impacts on CH_4 emissions remains challenging.

Current uncertainties in global CH_4 budgets

Despite the critical role of northern peatlands in the global CH_4 cycling, significant uncertainties remain in quantifying their contribution to global CH_4 budgets. The wide range in estimated annual CH_4 emissions (9–53 Tg CH_4-C) reflects challenges in accurately measuring and upscaling CH_4 fluxes (FCH_4) across heterogeneous peatland landscapes (Ingle et al., 2023; McNicol et al., 2023). Such uncertainties stem from multiple sources, including limitations in mapping wetland extent, structural and parametric uncertainties in biogeochemical processes, and limited observational constraints that make it difficult to capture CH_4 flux (FCH_4) variations across different spatial scales (Knox et al., 2019; Zhu et al., 2025). While plot-scale (1–10 m^2) measurements are relatively common, there is a notable scarcity of replicated ecosystem-scale measurements at the mesoscale (0.5–20 km^2; Rydin and Jeglum, 2013) and landscape level (> 20 km^2), creating a critical gap in our understanding of CH_4 dynamics at these intermediate scales (Zhu et al., 2025). Improving our understanding of these multi-scale dynamics is crucial for better predicting the role of peatlands in future climate feedbacks and for incorporating these processes into land surface models.

1.2 Spatio-temporal dynamics of peatland methane fluxes

Plot-scale variability (microtopography)

Peatland FCH_4 exhibit substantial spatial variability at the microform level (1–10 m^2), driven by variations in microtopography. These fine-scale differences create distinct microenvironments with varying water table depth (WTD), soil temperature (Ts), and vegetation composition (Bubier et al., 1993; Granberg et al., 1997; Juottonen et al., 2015; Perryman et al., 2022). Higher CH_4 emissions typically occur in wetter microforms such as hollows and lawns, while elevated hummocks generally show lower emissions

(Bubier et al., 1993; Waddington and Roulet, 1996; Welpelo et al., 2024). These differences stem from varying oxygen availability at the different microforms and the related methanogenic (i.e., CH_4 production) and methanotrophic (i.e., CH_4 oxidation) activity, but is also influenced by the presence of vascular plants which provide substrate for methanogenesis, and direct transport channels for CH_4 to the atmosphere (Bellisario et al., 1999; Öquist and Svensson, 2002; Welpelo et al., 2024).

Ecosystem-scale patterns

At the ecosystem scale (~0.1–0.5 km²), FCH_4 flux patterns emerge from the integration of multiple microforms and their associated biogeochemical processes (Juottonen et al., 2015). Ecosystem-scale FCH_4 are determined by both the relative abundance of different microforms and their related characteristics across the site (Määttä and Malhotra, 2023; Webster et al., 2018). Site-level gradients in vegetation, hydrology, and nutrient availability create distinct zones of high and low emissions that contribute to the overall ecosystem pattern (Rydin and Jeglum, 2013; Zhang et al., 2020). These site-level patterns of FCH_4 then integrate into higher-order dynamics across large peatland complexes.

Mesoscale variation within peatland complexes

At the mesoscale (0.5–20 km²), additional patterns emerge as large peatlands, or peatland complexes, can contain peatland types with distinct characteristics. Fen and bog sections within the same peatland complex can exhibit markedly different FCH_4 patterns (Euskirchen et al., 2024; Zhang et al., 2021). Even peatland complexes containing only a single peatland type can exhibit varying properties and FCH_4 at different locations. These variations arise from the position in the landscape, catchment properties, and nutrient inputs from surrounding areas, which create distinct zones with varying biogeochemical functioning (Arsenault et al., 2023; Ehnvall et al., 2023; Zhang et al., 2020). The interaction between local topography, hydrology, and vegetation creates complex spatial patterns that can result in substantial variations in FCH_4 across a peatland complex. For example, areas receiving greater mineral-rich groundwater inputs often show enhanced FCH_4 compared to more isolated sections, with different gradients along the transitions between these hydrological zones (Bubier et al., 1995).

Temporal dynamics and spatial interactions

The spatial patterns of FCH_4 in peatlands are not static but interact dynamically with temporal variations in environmental conditions (Armstrong et al., 2015). Seasonal changes in Ts and WTD can amplify or diminish spatial differences in FCH_4 (Feng et al., 2020), with FCH_4 often exhibiting hysteresis relationships with both WTD and Ts fluctuations (Chang et al., 2021; Goodrich et al., 2015), which complicate the understanding and quantification of FCH_4 patterns in relation to these drivers. During wet periods, microtopographic differences become more pronounced as biomass and nutrients might concentrate on higher microforms, enhancing the contrasts in FCH_4 among microforms (Diamond et al., 2020). Warming conditions modify spatial patterns by accelerating methanogenesis in water-saturated areas while enhancing methanotrophy in oxic layers, often resulting in lower FCH_4 in drier years (Rinne et al., 2020). Additionally, interannual variations in climate can alter the relative importance of different spatial controls on FCH_4, making it essential to consider both spatial and temporal dynamics when understanding peatland FCH_4.

1.3 Methods for quantifying peatland methane fluxes

Plot-scale measurements

Chamber measurements have long been used to study plot-scale variations in methane fluxes (Bubier et al., 1993; Perryman et al., 2022; Turetsky et al., 2014) and continue to provide valuable insights into the controls on emissions at the microform scale. These measurements offer high spatial resolution and the ability to isolate specific processes and controls at fine plot scales (1–10 m^2) or for comparing FCH_4 between different microforms across a peatland. However, scaling these measurements to larger areas remains challenging due to the high spatial heterogeneity of peatland landscapes and the labor-intensive nature of chamber-based sampling.

Ecosystem-scale measurements

The eddy covariance (EC) technique has emerged as the state-of-the-art method for measuring ecosystem-scale greenhouse gas fluxes, providing continuous measurements at high temporal resolution (Baldocchi, 2014;

Burba and Anderson, 2010; Knox et al., 2019). EC measurements integrate fluxes over footprint areas of several hectares (Kljun et al., 2002; Vesala et al., 2008), thereby capturing the combined effect of different microforms and vegetation types (Kowalska et al., 2013). However, in large peatland complexes, the representativeness of FCH_4 measurements from a single location remains uncertain due to potential variations in vegetation, hydrology, and biogeochemical conditions across the peatland complex.

Challenges in estimating mire complex-scale CH_4 budgets

Quantifying FCH_4 across peatland complexes presents significant methodological challenges. Due to the high cost and maintenance requirements of EC systems, most studies are limited to measurements at a single location within a peatland complex (Lees et al., 2018). This constraint creates uncertainty in regional and global estimates of peatland methane emissions, as single-site measurements may not capture the full range of spatial variations across large mire systems (McNicol et al., 2023). This limitation of single-site measurements emphasizes the need for approaches that can account for this variability when only single-site measurements are available. Bottom-up modelling approaches for estimating wetland CH_4 emissions have evolved to address these challenges through three predominant methodologies (Zhu et al., 2025): (1) empirical biogeochemical modelling that combines relationships between wetland CH_4 emissions and environmental variables; (2) process-based biogeochemical modelling that explicitly represents CH_4 production, consumption, and transport processes; and (3) data-driven machine learning approaches trained against field observations. These different bottom-up approaches can differ by up to 80 Tg CH_4 yr^{-1} in their global estimates (Zhu et al., 2025), reflecting differences in model assumptions and parameterizations. To improve and validate these models at regional scales, there is a critical need for spatially well-replicated observations across larger scales.

1.4 Research infrastructure for studies of peatland biogeochemistry

Historical context

Understanding how peatlands respond to global change requires research infrastructures that can capture both long-term dynamics and spatial

variations across heterogeneous peatland complexes. Historically, peatland research has concentrated around accessible sites that could support long-term monitoring, resulting in research hubs (e.g., Degerö Stormyr or SE-Deg (Nilsson et al., 2008), Siikaneva or SE-Sii (Rinne et al., 2007) and Mer Bleue or CA-Mer (Roulet et al., 2007)) where intensive studies have built up detailed understanding of local processes over decades. While these long-term research sites have been crucial in establishing our fundamental understanding of peatland functioning, they have traditionally focused on single locations within larger peatland complexes. There is therefore a critical need to upscale our understanding from these intensively studied areas to capture the cross-scale feedbacks that govern peatland development and carbon accumulation across entire peatland systems (Belyea and Baird, 2006). The complex nature of peatlands demands research infrastructures equipped for studying biogeochemical processes at both temporal and spatial scales. Despite this need, such infrastructures remain scarce, limiting our ability to understand how local variations in ecosystem characteristics influence ecosystem responses to environmental change across different scales.

Value of replicated ecosystem measurements

Research infrastructures with replicated ecosystem-scale measurements are crucial for understanding spatial variations in processes across peatland complexes. Such facilities enable investigation of how biogeochemical processes and their drivers vary across peatland landscapes, providing insights that cannot be obtained from single-site studies. While there remains a significant gap in our understanding of how well single-site measurements represent the spatial variations of biogeochemical processes across entire peatland complexes (Desai et al., 2022; Tuovinen et al., 2019), replicated measurement infrastructures can provide unique opportunities to develop and validate upscaling approaches. This is particularly important given the increasing need for accurate estimation of peatland FCH_4 at regional and global scales for climate change prediction and mitigation strategies.

Development of the Kulbäcksliden Research Infrastructure (KRI)

The Kulbäcksliden Research Infrastructure (KRI) in northern Sweden was established to address fundamental questions about peatland biogeochemistry and their responses to environmental change. Building upon research at SE-Deg that dates back to the early 1900s, this site has

provided valuable insights into carbon cycling (Granberg et al., 1997; Järveoja et al., 2020; Nilsson et al., 2008; Peichl et al., 2014), vegetation dynamics (Järveoja et al., 2018; Koebsch et al., 2020; Peichl et al., 2018), and hydrological processes (Campeau et al., 2017; Nijp et al., 2017). The KRI currently includes four research sites within a 7.6 km² peatland complex: SE-Deg, Hälsingfors Stormyran (SE-HfM), Hålmyran (SE-Hmr), and Stortjärn (SE-Srj). The unique configuration of the KRI, with its replicated ecosystem-scale measurements, creates unprecedented opportunities for developing and testing new approaches to understand and upscale ecosystem processes such as FCH_4 dynamics to the peatland complex scale (Noumonvi et al., 2023).

Photo: Andreas Palmén

2. Aim and Objectives

The main aim of this thesis was to advance our understanding of FCH_4 dynamics and their spatio-temporal variability across a boreal peatland complex. By leveraging a unique research infrastructure with replicated ecosystem-scale measurements, this was achieved through studies describing the research infrastructure (**Paper I**), developing a novel approach for characterizing peatland surface structure (**Paper II**), investigating ecosystem-scale FCH_4 variations and their drivers (**Paper III**), and developing a data-driven scaling approach to estimate FCH_4 across a mire complex based on single-site measurements (**Paper IV**). A conceptual overview of the four studies carried in this thesis are shown in Figure 1.

The specific objectives were:

I. To provide a first description of the Kulbäcksliden Research Infrastructure (KRI), including a review on research history, description of site characteristics and measurement instrumentation, highlighting the value of replicated ecosystem-scale measurements for studies of peatland biogeochemistry (**Paper I**).

II. To develop a hydrological model (HuHoLa, for Hummock-Hollow-Lawn) based on digital elevation models (DEMs) that can classify peatland microtopography and provide proxies for WTD and Ts (**Paper II**).

III. To explore the spatio-temporal variability of ecosystem-scale FCH_4 and the hierarchy of underlying environmental and biogeochemical controls across four sites within a boreal mire complex (**Paper III**).

IV. To develop and assess a data-driven approach that incorporates detailed site characteristics and dynamic EC footprint modelling to upscale single-site measurements to the mire complex (**Paper IV**).

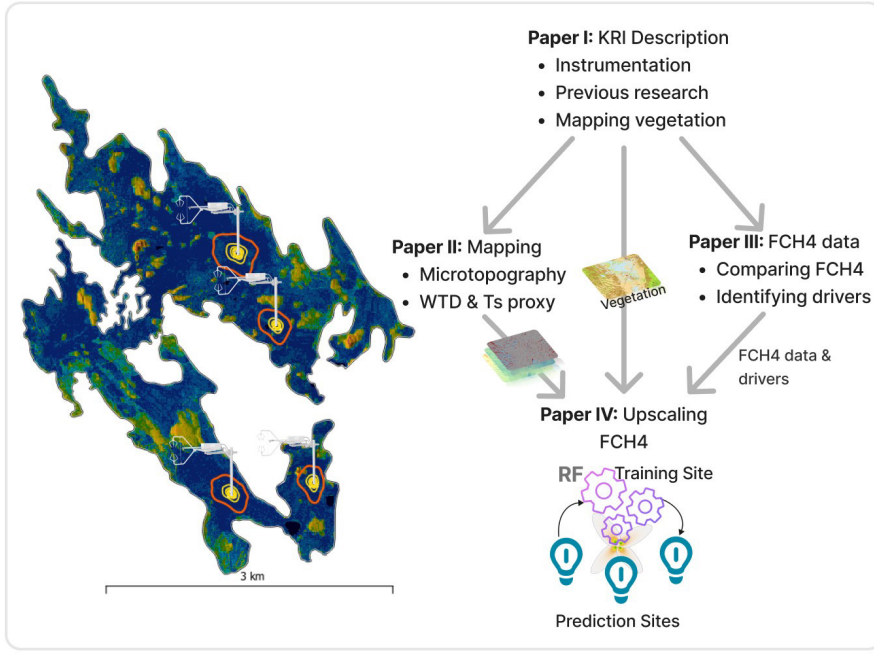

Figure 1. Overview of studies carried out in this thesis (Papers I-IV) at the peatland complex of the Kulbäcksliden Research Infrastructure (KRI, shape on the left). The background image in the peatland complex is the soil moisture map (Ågren et al., 2021). "RF" means random forests.

3. Methods

3.1 Study sites

The four studies were conducted at the Kulbäcksliden Research Infrastructure (KRI) in northern Sweden, which encompasses a peatland complex with four peatland research sites located less than 3 km apart: Degerö Stormyr (SE-Deg), Hälsingfors Stormyran (SE-HfM), Hålmyran (SE-Hmr), and Stortjärn (SE-Srj) (Figure 2). The sites are situated on an elevated land between two major rivers (Umeälven and Vindelälven), spanning latitudes 64°9'22.3"N to 64°11'22.7"N and longitudes 19°31'30"E to 19°34'24.4"E, approximately 10 km from Vindeln municipality.

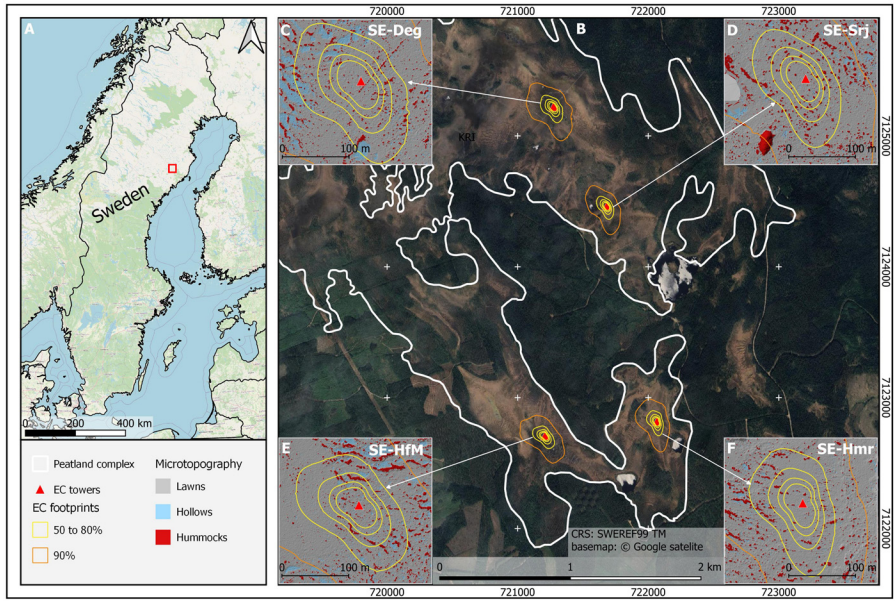

Figure 2. Location of the study sites in northern Sweden (A), and within the Kulbäcksliden Research Infrastructure (KRI) (B). The four side panels (C to F) provide close-ups into the 50 to 80% footprint climatologies and microtopography classes in the background for each site, i.e. SE-Deg (C), SE-Srj (D), SE-HfM (E), SE-Hmr (F). The footprint climatologies were calculated from all half-hour eddy covariance (EC) data available in June to August 2022 with the flux footprint prediction model (Kljun et al., 2015), while the microtopography was classified using the HuHoLa model (Noumonvi et al., 2025 - in review).

The mire complex represents a minerogenic and oligotrophic fen system underlain by paragneiss bedrock dating to the Svecokarelian orogeny (1.92–1.87 billion years ago). This geology contributes to the nutrient-poor characteristics of the system. Quaternary deposits consist primarily of till-based ridges of moraine, with peat accumulation in depressions. The catchment areas range from 30 ha at SE-Srj to 273 ha at SE-Deg, with varying proportions of mire coverage (46–76% of catchment area, Table 1).

Table 1. Coordinates of eddy covariance towers and basic catchment characteristics at each site.

Variable	SE-Deg	SE-HfM	SE-Hmr	SE-Srj
Longitude (°E)	19.55654	19.55150	19.56924	19.56381
Latitude (°N)	64.18203	64.15956	64.16000	64.17498
Altitude (m a.s.l.)	266	292	290	269
Catchment area (ha)	273	65	33	30
Mire/Catchment (%)	72	65	76	46

The climate is classified as subarctic (Dfc) according to the Köppen-Geiger classification. The annual mean air temperature (Ta) was +3.0°C for the long-term period 1991–2020 (2020–2023: +3.6°C), with total precipitation of 645 mm (2020–2023: 700 mm). The average January temperature and precipitation were -7.2°C (2020–2023: -5.8°C) and 44 mm (2020–2023: 58 mm), while the respective averages for July were +15.4°C (2020–2023: +15.3°C) and 89 mm (2020–2023: 94 mm).

3.2 Data collection

3.2.1 Eddy covariance measurements of CO_2 and CH_4

Each of the four study sites was equipped with an eddy covariance (EC) system for measuring ecosystem-scale CO_2, water vapour (H_2O) and CH_4 fluxes. The EC setup at SE-Deg, which has been operational since 2001, is currently equipped with a LI-7200 gas analyzer for CO_2 and H_2O measurements and a LGR FGGA 911-0010 analyzer for CH_4 measurements. The other three sites, established in 2019-2020, are currently operating Picarro G2311-f analyzers for CO_2, CH_4, and H_2O measurements. For measuring wind speed components and wind direction, all sites featured 3D

sonic anemometers (Gill HS-50 at SE-Deg, Metek uSonic-3 Class A at other sites) mounted at heights of 3.07 m (SE-Deg) or 2.75 m (other sites). Air inlet tubes were positioned near the anemometers with minimal separation (<5 cm vertical, <18 cm northward). For the LGR analyzer, the tube was 20 m long with a 5.3 mm diameter and maintained a flow rate of 12 l min^{-1}, while the Picarro analyzers used 6.9 m long tubes with 4.3 mm diameter and 5 l min^{-1} flow rate.

Raw EC data was processed using the EddyPro flux calculation software version 7.0.9 (LI-COR Biosciences, 2022) and followed best practices following Nemitz et al. (2018) and Sabbatini et al. (2018). Processing included compensation for time lags between wind velocity and gas concentration measurements through automatic time lag optimization with narrow search windows (typically <10 s) based on preliminary assessment. A double rotation was applied to the anemometer axes for tilt correction (Wilczak et al., 2001), and turbulent fluctuations were extracted from high-frequency time series using 30-minute block averaging. CH_4 concentrations from the LGR analyser were first converted to mixing ratios (readily available for CH_4 measurements from the Picarro analyzer) before flux calculations, eliminating the need for Webb-Pearman-Leuning (WPL) corrections. WPL corrections were only performed for the short period of measurement with an open path analyser (Li-7700) at SE-HfM from June to December 2020. Spectral attenuation was corrected following Fratini et al. (2012).

Quality control and filtering of the processed fluxes was performed in R v. 4.3.1, and was organized into the "PostEddyPro" package (v.0.1.0, available at https://github.com/bravemaster3/PostEddyPro). The quality control protocol included removing measurements taken during low instrument signal strength and filtering out data collected during non-steady state or low turbulent conditions (Mauder and Foken, 2004). Additionally, fluxes measured under low friction velocity conditions (threshold of 0.1 m s^{-1}, determined using the method described by Reichstein et al., 2005) were excluded. After all quality control steps, approximately 55–62% of the original flux data remained for analysis, with seasonal variations in data coverage between 20–75% depending on site and year.

Gap-filling of missing flux data was performed using machine learning approaches. For FCH_4, random forests were employed following Irvin et al. (2021), while NEE was gap-filled using XGBoost following Kämäräinen et

al. (2022). The models were trained using environmental variables including air temperature (Ta), Ts, WTD, incoming photosynthetically active radiation (PARin), air pressure, relative humidity, vapor pressure deficit (VPD), and precipitation, along with temporal indicators (yearly sine, cosine, and time delta). Model performance was evaluated through 10-fold cross-validation, yielding R^2 values of 0.88–0.95 for CH_4 and 0.90–0.93 for NEE, depending on the site. Gap-filled NEE was further partitioned into gross primary production (GPP) and ecosystem respiration (Reco) using the nighttime partitioning approach implemented in the REddyProc R package v. 1.3.2 (Wutzler et al., 2018). Flux uncertainties were estimated using Monte Carlo simulations following Richardson and Hollinger (Richardson and Hollinger, 2007).

3.2.2 Environmental variables

At each EC flux tower, a standard suite of instrumentation was installed to monitor meteorological and soil environmental variables. Ta and relative humidity (RH) were measured at 2 m height using Rotronic MP102H-331000 sensors at SE-Deg and HC2S3 sensors at the other sites. Incoming and outgoing shortwave/longwave radiation were measured using a CNR4 net radiometer at SE-Deg and a NR01 net radiometer at the other sites. Additionally, photosynthetically active radiation (PAR) was monitored using LI-190 quantum sensors at all sites.

Ts was measured at multiple depths (2, 10, 15, 30, and 50 cm, with an additional 5 cm measurement at SE-Deg), using Fischer Pt100 sensors at SE-Deg and TR03 TOJO Skogsteknik sensors at the other sites. WTD was monitored using CS450 pressure transducers at SE-Deg and CS451 sensors at the other sites. Ts and WTD were replicated at six locations at SE-Deg, and two locations at the other sites. Precipitation was measured using Lambrecht Rain[e]H3 gauges at SE-Deg and ARG100 tipping bucket rain gauges at the other sites. VPD was calculated from RH and Ta measurements following standard methods (Antezana-Vera and Marenco, 2022; Buck, 1981). Gaps in all environmental data were filled using linear regressions between sites when data were missing at a site and available at other locations within the mire complex.

NDVI data used in our studies were obtained from two sources. The first data source was Sentinel-2 multispectral instrument (MSI) satellite imagery processed through Google Earth Engine (GEE, 2024), providing NDVI at 10

m spatial resolution for the period 2020–2022 (**Paper III**). For the dynamic footprint modelling (**Paper IV**), this was complemented with a second data source: monthly unmanned aerial vehicle (UAV) surveys (May to September 2022–2023) using a DJI Phantom 4 equipped with a five-band multispectral camera, producing orthomosaics at 3 cm resolution. These two data sources were combined through arithmetic averaging to create fused NDVI maps that leveraged both the relatively higher temporal resolution of satellite data and the fine resolution of UAV imagery.

3.2.3 Data for mapping vegetation and microtopography (**Paper I** and **Paper II**)

*Mapping of vegetation (**Paper I**)*

Ground-based vegetation data were collected through detailed field surveys conducted in November 2021, with over 50 inventory points at each of the four mire sites. At each point, vegetation composition was recorded following an adapted version of the Finnish mire classification system (Paper I supplementary materials 4; Eurola et al., 2015, 1995, 1984). The classification accounts for vegetation types across different microforms, ranging from lawns and carpets to hummocks and forested areas.

For spatial classification of vegetation, high-resolution (6.5 cm) RGB imagery derived from a Riegl VQ-1560i-DW LiDAR scan of September 2019 was used. This dual wavelength (532 nm green, 1064 nm NIR) scanner provided both spectral and elevation data with an average point density of 20 points/m². The RGB imagery was combined with a microtopography classification layer (an early version of the HuHoLa microtopography classification presented in **Paper II**) as an additional band. The observation points from the field survey were used to delineate regions of interest (ROI) representing different vegetation groups for training the random forest classification model.

*Mapping of Microtopography (**Paper II**)*

Using elevation data from the September 2019 Riegl VQ-1560i-DW light detection and ranging (LiDAR) scan, DEMs were produced at 30 × 30 cm and 50 × 50 cm spatial resolutions. Additionally, higher resolution DEMs (3 × 3 cm) were produced using Structure-from-Motion based on the September 2023 unmanned aerial vehicle (UAV) imagery. The UAV-based DEM was also resampled to coarser resolutions (6, 10, 20, 30, 40, 50, 60, 70, 80, 90

and 100 cm) and used to evaluate the sensitivity of the microtopography classification to the DEM resolution.

For validation of the HuHoLa microtopography classification, 260 reference points were collected at the SE-Deg site using a high-precision ground positioning system (RTK-GNSS). These points were positioned 2 meters away from the boardwalk.

For calibrating the HuHoLa model's secondary outputs, time series of Ts measured with HOBO MX2303 loggers and manual WTD measurements were collected from four distinct microtopographic locations at each site. These measurements were used to evaluate the relationships between model-derived proxies and actual field measurements of Ts and WTD.

3.2.4 Peat physical and chemical properties

Core sampling and analysis

Three peat cores, 50 cm deep, were collected from lawn areas at each site in autumn 2020, and preserved by freezing until laboratory analysis. Following thawing, the samples were dried and analyzed for their physical and chemical properties. Carbon and nitrogen content were determined using a Thermo Fischer Scientific Flash EA 2000 elemental analyzer. From these measurements, C:N ratios were calculated. Bulk density was calculated as the ratio of dry mass to volume. For each site, bulk density and C:N ratio values were averaged from the three cores.

Peat CH_4 concentration profiles

During the summer of 2022, vertical profiles of peat pore space CH_4 concentrations were sampled. At each site, samples were collected from two hollows and two hummocks at five depths (5, 15, 25, 35, and 45 cm) and repeated four times (May, June, July, and August) in 2022. For sampling the air-filled pore system above the water table, 5 ml of pore gas was injected into 22 ml glass vials. For sampling peat pore water in the saturated zone, 5 ml pore water was injected into 22 ml glass vials (with N_2 at ambient pressure) containing 5 ml phosphoric acid (H_3PO_4, 85%), and preserved with a drop of ZnCl. CH_4 concentrations were analyzed by gas chromatography using a PerkinElmer Clarus 580 GC-FID equipped with a methanizer. Separation was carried out on an Elite-PLOT Q column (30 m, 0.53 mm ID, 20 μm df, PerkinElmer) at 30°C with N_2 as carrier gas (10 psi).

3.3 Data analysis

3.3.1 HuHoLa model development (**Paper II**)

The HuHoLa model is based on depression-filling in a DEM (Lindsay, 2016), and involves a four-step process (Figure 3): (1) filling depressions in the original DEM to identify hollows, (2) filling depressions in the inverted DEM to identify hummocks, (3) subtracting the filled DEMs to produce the hollow-hummock-depth-height (HHDH) layer used for classifying the microforms, or used as proxy for WTD and Ts, and (4) classification into three or five classes. To determine the optimal classification threshold, two analyses were performed: first, areas containing single classes were visually delineated to analyze the frequency distribution of fill depths in each microtopography class; second, different thresholds were tested and validated against ground truth data, with the optimal threshold identified at the equal error rate (where precision and recall curves intersect). Additionally, model sensitivity to DEM resolution (3 cm to 1 m) and fill threshold (0–10 cm) was systematically analysed using the UAV-derived resampled DEM.

Figure 3. Workflow of the HuHoLa model. Green rectangles represent the inputs of the model, blue rectangles represent intermediary outputs not used directly, red rectangles represent exported outputs, yellow diamonds represent operations performed in the model, and ellipses represent classification rules. Numbers represent the four sub-sections of the HuHoLa model: 1- filling the Digital Elevation Model (DEM), 2- filling the inverted DEM, 3- Subtracting the filled DEM from the filled inverted DEM to produce the hollow-hummock-depth-height (HHDH) proxy for water table depth (WTD) when “fix flats” is applied during subsection 1, 4- Classification into the different microforms. Classes 0, 1, 2, 3, and 4 in step 4 are respectively lawns, hollows, hummocks, lower level lawns, and upper level lawns.

3.3.2 Flux footprint analysis

The spatial source area of FCH_4 based on EC measurements was determined using the two-dimensional Flux Footprint Prediction (FFP) model (Kljun et al., 2015). The model inputs included roughness length (z_0), measurement height above displacement height (z-d), friction velocity (u*), Obukhov length (L), standard deviation of lateral wind speed (σ_v), and boundary layer height (h). Most parameters were derived directly from EC measurements, while boundary layer height was obtained from ERA5 reanalysis data (Hersbach et al., 2020).

For **Papers I** and **III**, footprint climatologies representing cumulative source areas (50% to 90%) were calculated using aggregated data from May 2020 to April 2021 to characterize the typical spatial extent of flux measurements. For **Paper IV**, half-hourly footprints were calculated to enable dynamic weighting of spatially-explicit environmental variables based on their contribution to each flux measurement.

3.3.3 Estimation of mire complex FCH_4 (**Paper IV**)

A random forest model was developed to scale FCH_4 across the mire complex using footprint-weighted and spatially-explicit environmental information. This approach integrated dynamic EC flux footprint analysis with comprehensive spatial mapping of key FCH_4 drivers (footprint-based model). Environmental variables were characterized through two pathways: spatially-explicit variables (microtopography, vegetation classes, Ts, WTD, and NDVI) were mapped and weighted by area contributions within each half-hourly EC flux footprint, while meteorological measurements were maintained as spatially-fixed time series (Figure 4). For comparison, a standard random forest model using only environmental measurements from fixed sensor locations (biomet model) was also developed. Both models were trained using data from individual sites to predict fluxes at the remaining sites, with predictions adjusted using site-specific C:N ratios to account for underlying biogeochemical differences between sites. The footprint-based approach allowed for dynamic integration of spatial heterogeneity in both static (e.g., microtopography) and temporally varying (e.g., Ts) drivers of FCH_4 within the EC measurement footprint.

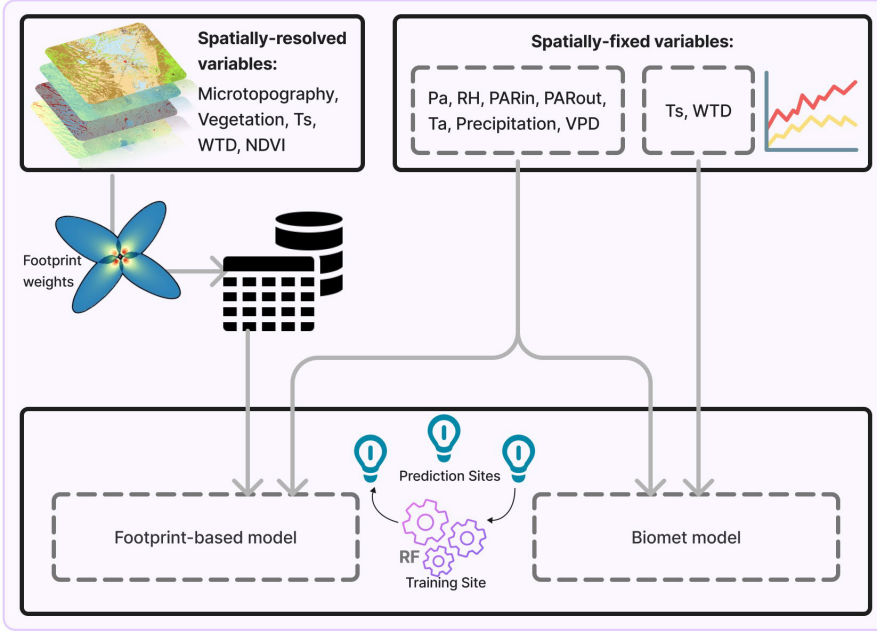

Figure 4. Summary of the methodology for combining spatially-resolved variables (through footprint analysis) and spatially-fixed time series into the modelling framework of the footprint-based, and the biomet models. "RF" means random forests.

3.3.4 Statistical approaches

Several complementary statistical methods were employed to analyze FCH_4 drivers and patterns (**Paper III**). Wavelet coherence analysis was used to examine the temporal relationships between FCH_4 and environmental variables across multiple time scales simultaneously. This method, originally developed for signal processing and time series analysis in both time and frequency domains (Weng and Lau, 1994), is particularly valuable for revealing non-stationary patterns and phase relationships that might otherwise be missed by traditional correlation analyses (Campeau et al., 2024; Cazelles et al., 2008). Commonality analysis (Newton and Spurrell, 1967) was used to partition the explained variance in FCH_4 into unique and shared components among different predictor variables. This technique helps understand how environmental variables interact in explaining flux variations. Path analysis, using multiple linear regression pathways (Streiner, 2005), helped quantify the direct and indirect effects of different drivers on FCH_4. Statistical difference in annual FCH_4 between our sites and other

peatland systems was assessed using the Kruskal-Wallis test followed by post-hoc Dunn tests with Bonferroni correction (Srinivasan et al., 2013) (**Paper III**).

The accuracy of microtopography classification was assessed using precision, recall, F1 score, overall accuracy and kappa statistics (**Paper II**), while model performance in **Paper IV** was evaluated with root mean square error (RMSE) and bias metrics.

Photo: Antonia Hartmann

4. Results and discussion

4.1 Vegetation patterns across the mire complex (**Paper I**)

The vegetation at the mire complex was categorized into six broad categories based on microtopography and plant species:

- I. Lawns dominated by short sedges, including species such as *Eriophorum vaginatum*, *Trichophorum cespitosum*, *Carex pauciflora*, *Sphagnum angustifolium*, *S. balticum*, *S. medium*, *S. rubellum*, *S. compactum*, and *S. papillosum*, *Andromeda polifolia* and *Oxycoccus palustris*.
- II. Carpets composed predominantly of similar short sedges as in the lawns, but also *Sphagnum* subg. *Cuspidata* (*S. balticum*, *S. majus*, *S. lindbergii*, *S. jensenii*), as well as *S. papillosum* or *S. compactum*.
- III. Mud and loose bottoms, and tall-sedge fens: with species like *Scheuchzeria palustris*, *Carex limosa*, *Trichophorum cespitosum*, *Drosera longifolia*, and *Menyanthes trifoliata*, *Sphagnum* subg. *Cuspidata*, *S. fallax*, and *Warnstorfia* spp.
- IV. Hummocks and sparsely treed areas: vegetation includes *Pinus sylvestris*, *Betula nana*, *Andromeda polifolia* and *Calluna vulgaris*, *Sphagnum angustifolium*, *S. fuscum*, *S. medium*, and *S. rubellum*, *Pleurozium schreberi*, *Cladonia mitis*, and *C. stygia*.

At the edges of the mire complex, a “mire forest” vegetation type with more trees occurs, while “forests on mineral soils” occur on rock outcrops, with the following vegetation species:

- V. Mire forests: with species like *Pinus sylvestris*, *Betula pubescens*, *Picea abies*, *Betula nana*, *Andromeda polifolia*, *Empetrum hermaphroditum*, *Ledum palustre*, *Oxycoccus* spp., *Vaccinium myrtillus*, *Eriophorum vaginatum*, *Carex globularis*, *Dactylorhiza maculata*, *Rubus chamaemorus*, *Sphagnum angustifolium*, *Polytrichum commune*, *Pleurozium schreberi*, *Hylocomium splendens*, *Dicranum spp*., *Cladonia* spp.
- VI. Forests on mineral soils with species like *Pinus sylvestris*, *Betula pubescens*, *Picea abies*, *Calluna vulgaris*, *Empetrum*

hermaphroditum, *Linnaea borealis*, *Vaccinium vitis-idaea*, *V. myrtillus*, *Deschampsia flexuosa*, *Dicranum* spp., *Polytrichum* spp., *Hylocomium splendens*, *Pleurozium schreberi*, *Ptilium crista-castrensis*, *Barbilophozia lycopodioides*, *Cladonia* spp.

The vegetation composition varied substantially across the mire complex (Figure 5, Table 2). At SE-Srj, lawn communities dominated by short sedges and *Sphagna* (Group I) covered nearly half (48%) of the footprint area, i.e. the highest proportion of lawn vegetation among all sites. In contrast, at SE-HfM, carpet vegetation (Group II, 35%) and mud bottoms/tall-sedge fens (Group III, 19%) were most prevalent, indicating generally wetter surface conditions. At SE-Hmr, lawn vegetation (Group I, 34%) and hummock vegetation (Group IV, 34%) covered equal portions of the 90% EC footprint area, with hummock coverage reaching its highest proportion among all sites. At SE-Deg, vegetation was more evenly distributed between lawns (33%), carpets (31%) and hummocks (20%), though wetter microform vegetation (Groups II and III combined) covered 43% of the area, i.e. a two times higher proportion than at SE-Hmr and SE-Srj. Mire forest vegetation (Group V) occupied only a small fraction (0.7–7%) of the EC footprints across all sites, while vegetation typical of mineral soil forests (Group VI) was nearly absent (0–2%). This distribution confirms that the EC towers primarily captured fluxes from the mire vegetation rather than forested areas.

The distinct vegetation patterns observed across our sites reflect the complex spatial organization typical of boreal mire complexes (Laitinen et al., 2005; Rydin and Jeglum, 2013). The notable differences in the proportions of lawn, carpet, and hummock vegetation communities have direct implications for the mire complex's FCH_4 patterns, as wetter microforms with carpet and hollow vegetation typically show higher CH_4 emissions compared to drier hummock areas (Bubier et al., 1993; Waddington and Roulet, 1996; Welpelo et al., 2024).

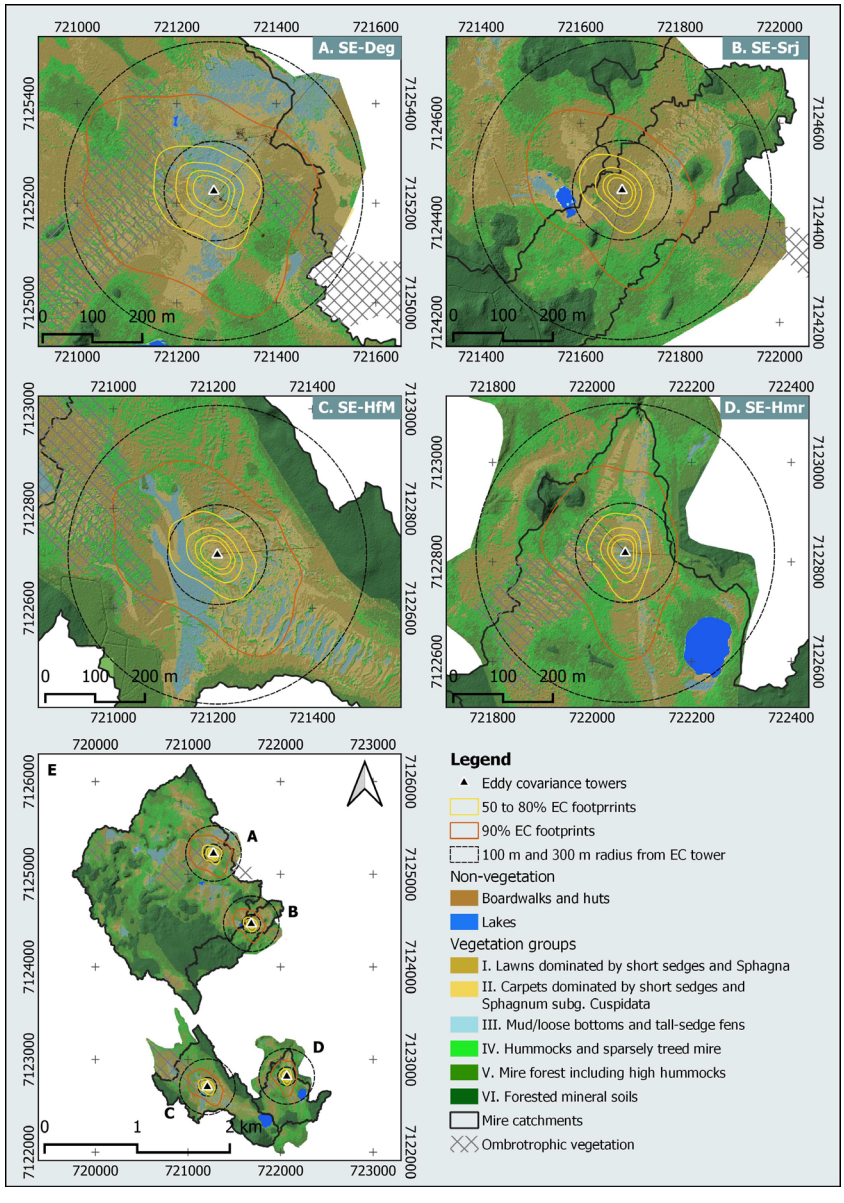

Figure 5. Vegetation classification map of the mire sites of the Kulbäcksliden Research Infrastructure with a focus on a 300 m radius from eddy covariance (EC) towers at SE-Deg (A), SE-Srj (B), SE-HfM (C), SE-Hmr (D) and an overview of all four catchments (E). The footprint climatologies were calculated from one-year data of wind speed and wind direction (May 2020 to April 2021) based on (Kljun et al., 2015). The vegetation groups layer is blended with a hillshade derived from a 0.5 m resolution digital elevation model.

Table 2. Percentage share of the different vegetation groups within the 90% tower footprint area.

Mire site	Total area (ha)	Percentage (%) of total area					
		Group I	Group II	Group III	Group IV	Group V	Group VI
SE-Deg	15	33	31	12	20	4	0
SE-HfM	10	27	35	19	20	0.7	0
SE-Hmr	7	34	18	4	34	7	2
SE-Srj	8	48	21	2	21	5	1

4.2 Microtopography patterns across the mire complex (**Paper II**)

The validation of microtopography in delineated reference areas (i.e., areas containing a single microtopography class) revealed that lawns are not completely flat, with their elevation fluctuating up to ±6 cm and ±4 cm for 30 cm and 50 cm resolution DEMs, respectively (Figure 6). This natural variation in lawn elevation had important implications for microtopography classification with the HuHoLa model, suggesting the use of a resolution-adapted threshold for accurate microtopography classification. The systematic testing of different threshold values revealed a trade-off between precision and recall, and the optimal thresholds (at equal error rate) were 5 cm for the 30 cm resolution DEM, and 4 cm for the 50 cm resolution DEM.

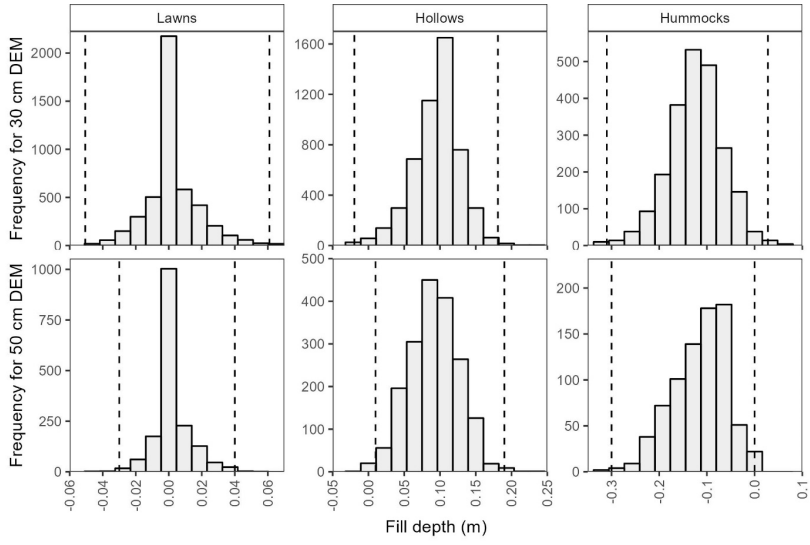

Figure 6. Histogram of fill depth per class, for small polygons considered purely as lawns (left panels), hollows (middle panels), and hummocks (right panels). Negative and positive fill depths are fill depths in the digital elevation model (DEM) and inverted DEM, respectively. Top panels represent frequency distribution with a 30 cm DEM resolution and bottom panels represent frequency distribution with a 50 cm DEM resolution. The vertical dashed lines represent the 99% percentiles of the fill depth per class. Note the different y-axis ranges for each panel.

The sensitivity of the microtopography classification to the fill threshold based on UAV-derived DEM at different resolutions revealed that higher thresholds (> 4 cm) were needed for finer resolutions (i.e., 3–30 cm) while coarser resolutions (i.e., 70–100 cm) required lower thresholds (~2 cm). This relationship reflects how finer resolution DEMs capture more surface detail, requiring larger thresholds to distinguish true microforms from subtle surface roughness within lawns. Conversely, coarser resolution DEMs inherently smooth minor surface variations, allowing for smaller thresholds to distinguish between microtopography classes.

The application of the model with a 4 cm threshold on a 50 cm resolution DEM effectively captured diverse microtopographic patterns across the mire complex (Overall accuracy = 0.94, Kappa = 0.81). The elevation profiles across different locations demonstrated the model's ability to distinguish between various microform combinations: from pronounced string-flark patterns (alternating “hummocks” and “hollows” in patterned mires) with

clear elevation differences (Figure 7-A and B), to subtle transitions between hummocks and lawns, and areas dominated by lawns with minimal elevation fluctuations (Figure 7-C and D).

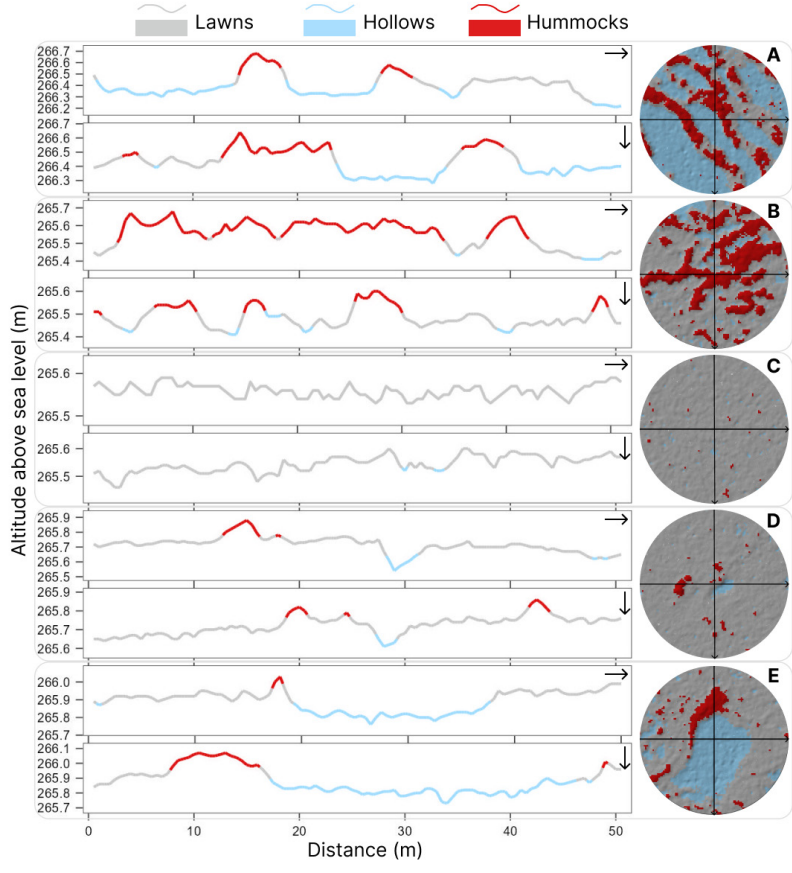

Figure 7. Elevation profiles of a few locations in the microtopography map. The fill threshold is 4 cm, for a digital elevation model (DEM) resolution of 50 cm. The locations were chosen to represent different microforms: (A) Strings and flarks; (B) hummocks and lawns; (C) Lawns; (D) and (E) hummocks, hollows and lawns. At each location, a horizontal (left to right) and a vertical (top to bottom) arrow indicates the orientation of the elevation profiles. The Y axis graduation is variable, and a spaced Y axis as in panel C indicates little amplitude in the elevation fluctuation at the lawn.

The detection of the intermediary lawn class through the threshold approach represents an advance over previous methods that typically produced binary hummock-hollow classifications (Brubaker et al., 2013; Graham et al., 2020; Kalacska et al., 2021; Lovitt et al., 2017; Moore et al.,

2019; Stovall et al., 2019). Due to the hydrological basis of the model, rooted in surface flow and relative elevation differences, rather than site-specific characteristics or training data, it is generalizable across different peatland systems. Moreover, the model provides secondary outputs that act as proxies for WTD and Ts through its HHDH secondary output (Figure 8). Despite the limited number of data points per site, the good agreement ($R^2 > 0.68$) between the proxies and observed Ts and WTD makes HuHoLa applicable for spatializing these variables in peatland landscapes.

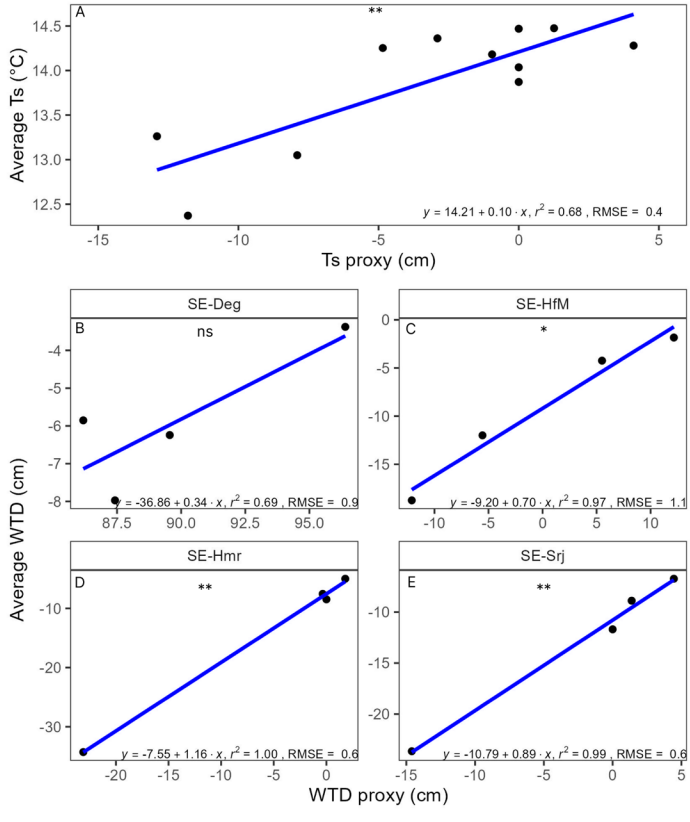

Figure 8. Correlation between (A) measured average soil temperature (Ts) at 10 cm depth and Ts proxy (i.e. the hollow-hummock-depth-height, or HHDH) using a 30 cm resolution digital elevation model (DEM), with no site distinction as HHDH is independent of site surroundings when no "fix flats" is applied, and (B-E) measured average water table depth (WTD) and 30 cm DEM-based WTD proxy (HHDH with “fix flats”) from the HuHoLa model for different sites: SE-Deg (B), SE-HfM (C), SE-Hmr (D), and SE-Srj (E), using a 30 cm resolution DEM. Statistical significance is indicated as * ($p < 0.05$), ** ($p < 0.01$), or ns (not significant).

4.3 Environmental controls on methane fluxes (**Paper III**)

4.3.1 Spatio-temporal variations of environmental variables across the mire complex

Given the close proximity of the four sites (< 3 km apart), meteorological conditions were remarkably similar across the mire complex. Air temperature and photosynthetically active radiation showed minimal spatial variation, with differences between sites remaining within instrument error (< 0.4°C and < 25 μmol m^{-2}, Figure 9-A and B). This spatial uniformity in meteorological conditions provided an ideal setting for examining how site-specific characteristics influence FCH_4 patterns.

Despite meteorological similarities, soil environmental conditions exhibited some site-specific differences, likely due to contrasting surface characteristics. Specifically, while average annual differences in Ts between sites were generally small (< 1°C), SE-Srj showed delayed warming after snowmelt (by approximately 12 days) compared to other sites during 2020 and 2022 (Figure 9-C). This delay was observed at the 10 cm depth but not at other measurement depths, suggesting local differences in soil thawing dynamics. WTD differences were consistent among sites during 2020–2023, with SE-Srj maintaining lower WTD (averaging -8.6 cm) compared to SE-Deg (-6.1 cm) (Figure 9-D).

Vegetation activity, as indicated by NDVI, showed systematic differences between sites despite their spatial proximity (Figure 9-E). Specifically, during the peak growing season 2022, SE-Srj showed consistently lower NDVI values (peaking at 0.6) compared to other sites like SE-Hmr and SE-Deg (peaking at 0.7). Such variations in vegetation indices can reflect differences in both plant productivity and vegetation water content, as water in plant tissues affects near-infrared reflectance and directly influences NDVI values in peatland ecosystems (Bubier et al., 1997; Šimanauskienė et al., 2019).

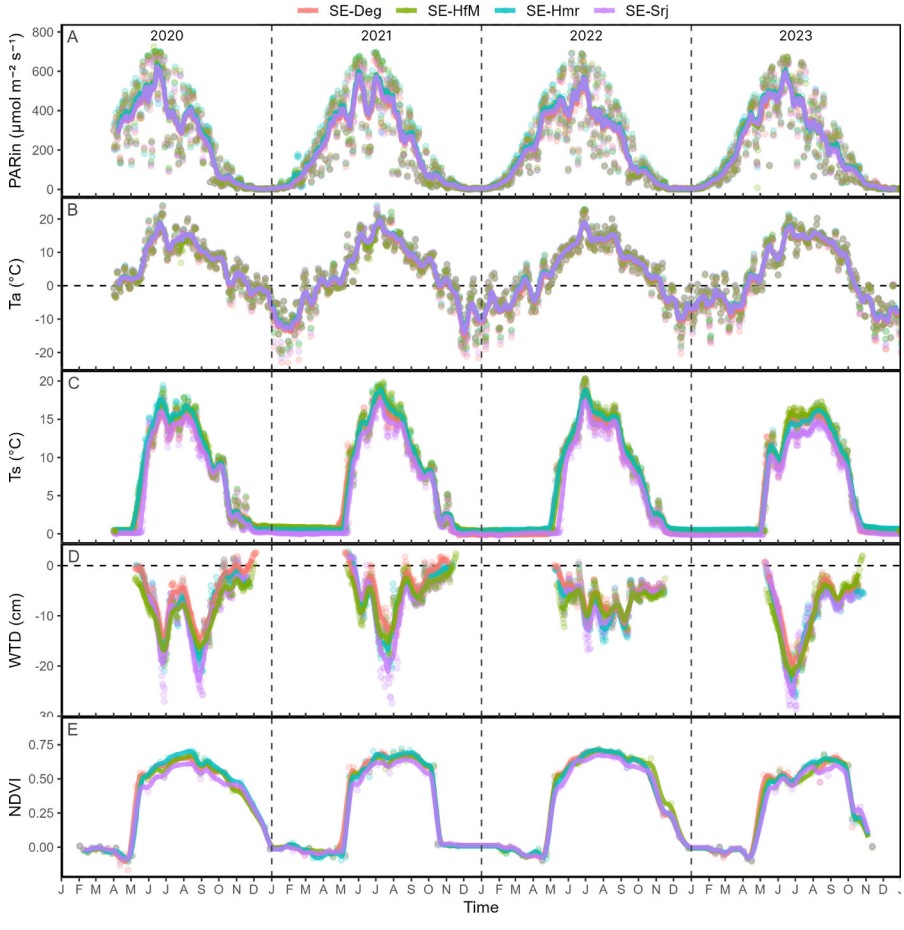

Figure 9. Daily means of environmental variables at the SE-Deg, SE-HfM, SE-Hmr, and SE-Srj sites during 2020–2023: (A) incoming photosynthetically active radiation (PARin), (B) air temperature at 2 m height (Ta), (C) soil temperature at 10 cm depth (Ts 10cm), (D) water table depth (WTD), and (E) Sentinel-2 derived normalized difference vegetation index (NDVI). Solid lines represent a 15-day running average.

4.3.2 Spatio-temporal variations of methane fluxes across the mire complex

The magnitude of FCH_4 varied substantially across the mire complex (Figure 10-A), with annual FCH_4 ranging from 7 to 11 g C m^{-2} during 2020–2023 (Figure 11). Consistent spatial patterns were observed, with SE-Srj exhibiting the lowest FCH_4 across all four years (averaging 7.6 ± 1.4 g C m^{-2}), while SE-Deg typically showed the highest emissions (averaging 11.9

± 2.1 g C m^{-2}). Annual GPP ranged from 272 to 434 g C m^{-2} during the same period (Figure 10-B), with SE-Hmr consistently showing the highest values (averaging 409 ± 28 g C m^{-2}) and SE-HfM the lowest (averaging 286 ± 13 g C m^{-2}). The coefficient of variation of ~16% across the mire complex was particularly noteworthy as it matched the variability typically observed among geographically distant mire systems (Figure 11). This suggests that mesoscale variations within mire complexes can be as significant as differences between geographically distant mire systems in the boreal region.

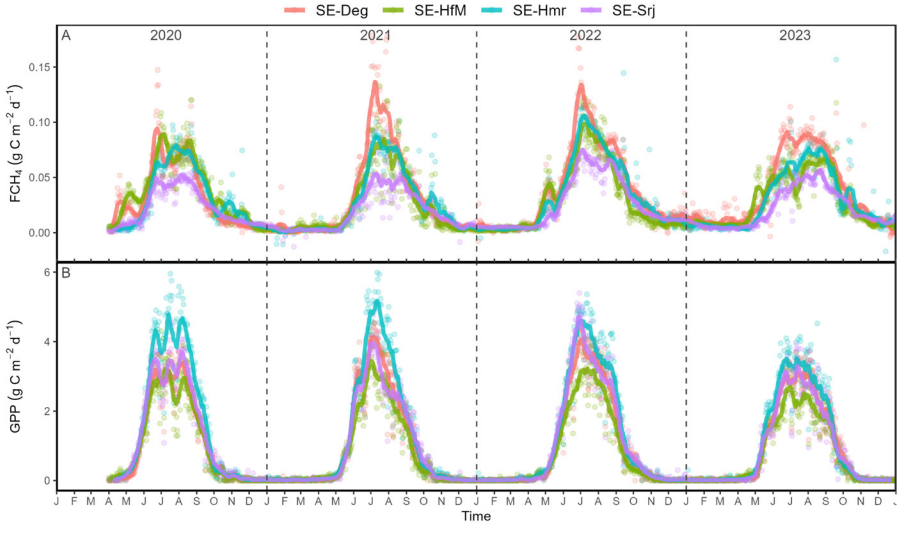

Figure 10. Daily sums of (A) methane fluxes (FCH_4) and (B) gross primary production (GPP) at the SE-Deg, SE-HfM, SE-Hmr, and SE-Srj sites during 2020-2023. Solid lines represent a 15-day running average.

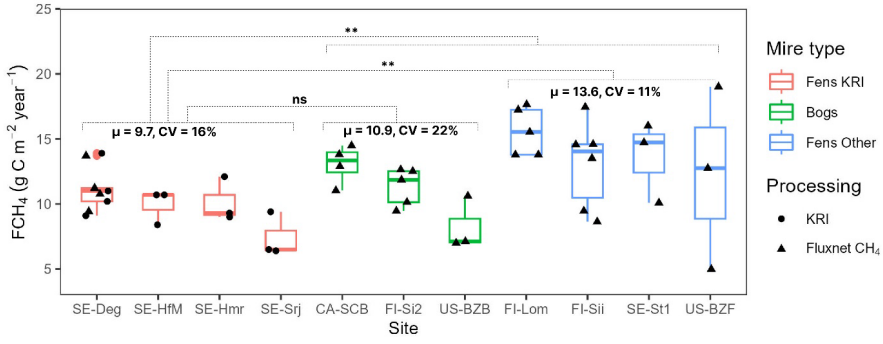

Figure 11. Annual sums of methane flux (FCH_4) at the Kulbäcksliden Research Infrastructure (KRI) compared to data from eddy covariance (EC) Fluxnet-CH_4 sites (Table 2) split by mire type (Bog vs. Fen). Point symbols (dots for data processed in this thesis, triangles for data obtained from Fluxnet-CH_4) represent individual years. The boxplots show the first quartile (Q1), the median (Q2) and the third quartile (Q3) of the available FCH_4 data per site. The whiskers stop at 1.5 × (Q3-Q1). Statistical significance from Kruskal-Wallis tests is indicated by: 'ns' (non-significant, $p > 0.05$), and '**' (highly significant, $p < 0.01$). Site names on the X axis are Degerö Stormyr (SE-Deg), Hälsingfors Stormyran (SE-HfM), Hålmyran (SE-Hmr), Stortjärn (SE-Srj), Scotty Creek Bog (CA-SCB), Siikaneva-2 Bog (FI-Si2), Bonanza Creek Thermokarst Bog (US-BZB), Lompolojänkkä (FI-Lom), Siikaneva (FI-Sii), Stordalen grassland (SE-St1), and Bonanza Creek Rich Fen (US-BZF).

The frost-free season contributed over 90% to annual FCH_4 (Table 3), as it is the case generally in northern peatlands (Knox et al., 2019). Historic data (2014–2019) from SE-Deg revealed that annual and frost-free season FCH_4 were mostly in range with more recent data (2020–2023), though extreme events like the 2018 drought could substantially impact FCH_4 (Rinne et al., 2020).

Table 3. Frost-free season (i.e. period when soil temperature at 10 cm was consistently above 1°C for at least five consecutive days) and annual sums (±standard deviation) of methane fluxes (FCH_4) and gross primary production (GPP) at the four mire sites SE-Deg, SE-HfM, SE-Hmr and SE-Srj. Standard deviations were calculated using a Monte Carlo approach.

Site	Year	Frost-free season		Annual	
		FCH_4 (g C m^{-2})	GPP (g C m^{-2})	FCH_4 (g C m^{-2})	GPP (g C m^{-2})
SE-Deg	2014	10.1 ± 0.03	292 ± 6	13.7 ± 0.03	304 ± 5
	2015	9.4 ± 0.02	277 ± 6	11.2 ± 0.03	278 ± 5
	2016	9.4 ± 0.02	206 ± 3	11.2 ± 0.03	207 ± 3
	2017	9.3 ± 0.03	221 ± 4	10.8 ± 0.03	222 ± 3
	2018	7.8 ± 0.02	116 ± 1	9.4 ± 0.02	117 ± 1
	2019	8.8 ± 0.05	272 ± 6	10.2 ± 0.06	298 ± 5
	2020	8 ± 0.04	317 ± 5	9.3 ± 0.04	320 ± 5
	2021	10.2 ± 0.06	342 ± 8	11 ± 0.06	344 ± 7
	2022	12.2 ± 0.06	362 ± 4	13.9 ± 0.06	366 ± 4
	2023	10.9 ± 0.03	327 ± 8	13.3 ± 0.05	328 ± 8
SE-HfM	2020	9.8 ± 0.07	295 ± 14	11 ± 0.07	298 ± 21
	2021	7.7 ± 0.03	275 ± 6	8.4 ± 0.03	277 ± 6
	2022	9.2 ± 0.03	290 ± 6	10.7 ± 0.03	296 ± 5
	2023	8 ± 0.03	268 ± 8	10.2 ± 0.03	272 ± 10
SE-Hmr	2020	8.3 ± 0.03	431 ± 7	9.4 ± 0.03	435 ± 7
	2021	8.3 ± 0.03	405 ± 8	9 ± 0.03	406 ± 8
	2022	10.8 ± 0.03	418 ± 7	12.1 ± 0.04	424 ± 7
	2023	8.9 ± 0.03	368 ± 8	10.5 ± 0.03	371 ± 9
SE-Srj	2020	5.6 ± 0.02	351 ± 6	6.4 ± 0.02	354 ± 6
	2021	5.7 ± 0.02	330 ± 7	6.5 ± 0.02	333 ± 7
	2022	7.9 ± 0.03	387 ± 8	9.4 ± 0.03	392 ± 9
	2023	6.1 ± 0.04	320 ± 26	7.8 ± 0.04	322 ± 29

4.3.3 Drivers of the temporal variations in methane fluxes

Wavelet coherence analysis revealed a consistent hierarchy of temporal controls on FCH_4 across the mire complex (Figure 12). At the daily timescale, a strong coherence was observed between Ts and FCH_4 throughout the frost-free season at all sites (Figure 12-A to D), particularly at SE-Deg where it persisted from June through September (Figure 12-A). The inconsistent phase relationships (lead/lag) between FCH_4 and Ts suggest

complex interactions in CH_4 production and transport processes, aligning with previous findings about temperature sensitivity of methanogenic and methanotrophic activities (Bergman et al., 1998; Chang et al., 2021).

Similar to Ts, a strong coherence was observed between GPP and FCH_4 at daily to five-day timescales, especially during summer months at SE-Deg (Figure 12-E) and SE-HfM (Figure 12-F). The phase relationships revealed some differences between sites, with FCH_4 generally in phase with GPP at SE-Deg but lagging behind GPP by 4–6 hours at SE-HfM. This close coupling between GPP and FCH_4 depending on the site is likely related to the role of vegetation in both substrate provision for methanogenesis, and transport of the produced CH_4 into the atmosphere (Salmon et al., 2022; Wang et al., 2013).

While the coherence between WTD and FCH_4 was not strong at daily timescales, stronger relationships emerged at multi-day to bi-weekly scales, particularly during mid-summer and autumn periods (Figure 12-I to L). The weak coherence likely results from seasonal dynamics, where wettest conditions occur during spring and autumn when temperatures are lower, while WTD shows irregular fluctuations throughout the growing season. These temporal patterns create potential confounding effects that make it challenging to isolate the distinct impact of WTD on FCH_4 (Koebsch et al., 2015).

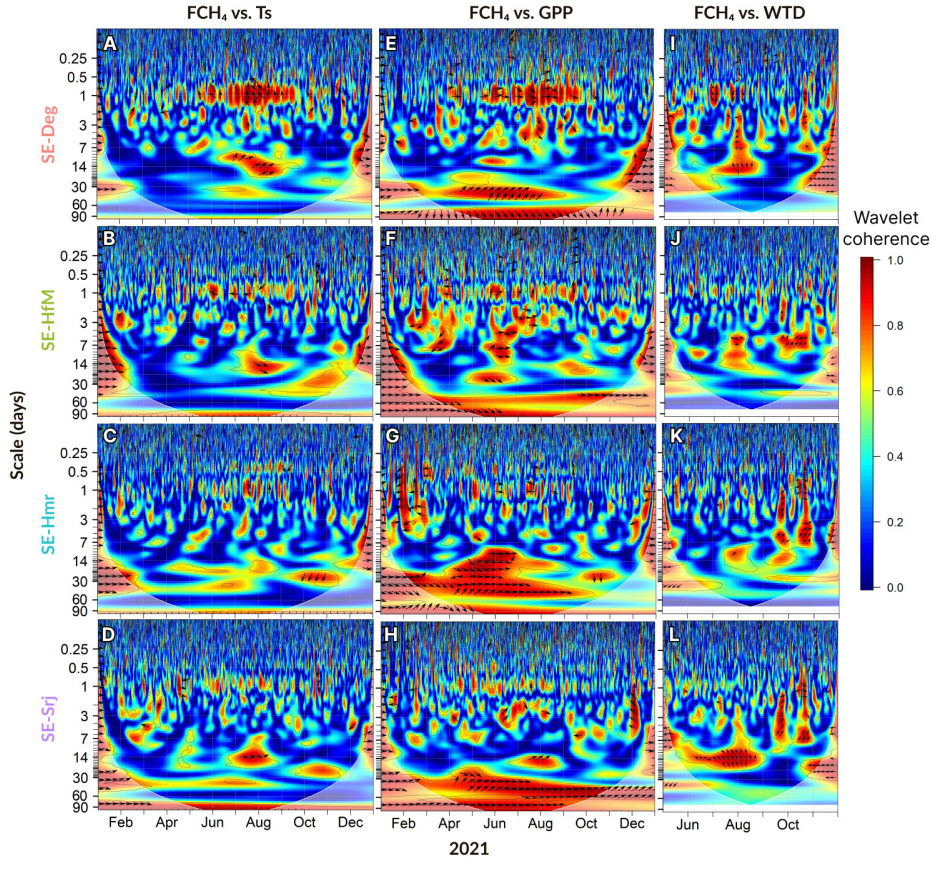

Figure 12. Wavelet coherence between half-hourly methane fluxes (FCH4) and soil temperature at 10 cm depth (Ts) (A-D), gross primary production (GPP) (E-H), and water table depth (WTD) (I-L) in 2021, with each row representing one site (SE-Deg, SE-HfM, SE-Hmr, SE-Srj). Shaded areas at the bottom-right and bottom-left of each panel indicate areas outside the cone of influence, i.e. impacted by edge effects. Arrows indicate the phase relationship between the two variables during high coherence periods (in red): in-phase (rightward), in anti-phase (leftward), variable x leading y (upward), or lagging y (downward) (Grinsted et al., 2004). Note the different x-axis for panels I-L, where WTD is limited to the frost-free season.

Path analysis further clarified these relationships by quantifying the relative importance of different drivers (Figure 13). GPP had the highest direct effect size (0.43–0.64) on FCH_4, reflecting its role in both substrate provision for methanogens and regulation of plant-mediated transport pathways (Lai, 2009; McEwing et al., 2015; Öquist and Svensson, 2002). WTD consistently showed the lowest effect size (<0.15) across all sites,

suggesting that within the observed range of water table fluctuations, other factors (e.g., vegetation and Ts) were more important in controlling the temporal variations in FCH_4. Furthermore, the high second-order GPP-mediated Ts effect (43–50% of explained variance) and significant third-order effects involving GPP, Ts and WTD (37–49%), as revealed by the commonality analysis, indicate that these drivers operate interactively rather than independently. This supports the understanding that FCH_4 are controlled by complex interactions between biotic and abiotic factors rather than single dominant controls (Lhosmot et al., 2023).

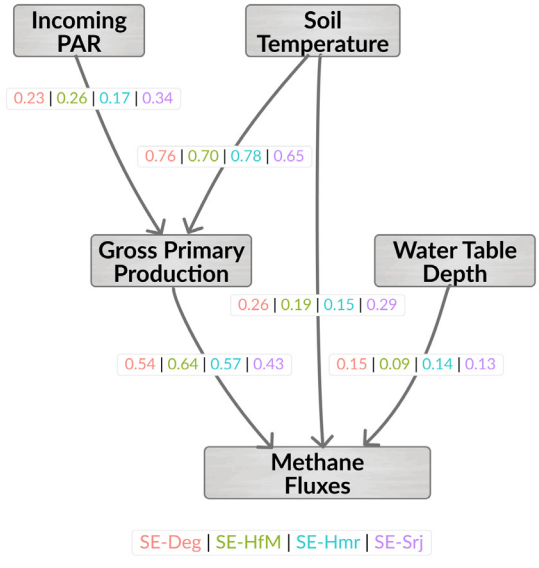

Figure 13. Path diagram showing the paths and effect sizes of soil temperature, incomings photosynthetically active radiation (incoming PAR), gross primary production and water table depth, in explaining daily methane fluxes. Colors correspond to site names (SE-Deg, SE-HfM, SE-Hmr, and SE-Srj) shown in the legend.

4.3.4 Drivers of the spatial variations in methane fluxes

Physical and chemical peat properties emerged as key factors explaining spatial variations in FCH_4 across the mire complex, with higher annual CH_4 emissions observed at sites with higher C:N ratios and lower bulk density (Figure 14). Specifically, the site SE-Deg with the highest C:N ratio (43 ± 3) and lowest bulk density (75 ± 10 kg/m³), exhibited the highest average CH_4 emissions over the period 2020–2022 (11.4 ± 1.3 g C m^{-2} $year^{-1}$), while the

site SE-Srj, which had the lowest C:N ratio (34 ± 2) and the highest bulk density (96 ± 9 kg/m³) also had the lowest average CH_4 emissions over the same period (7.4 ± 1.0 g C m^{-2} $year^{-1}$). A significant relationship was found between annual FCH_4 and C:N ratio (positive) or bulk density (negative) in both 2021 and 2022, while the relationship was not significant in 2020 and was only significant with C:N ratio when averaging FCH_4 over the three years (i.e. 2020, 2021, and 2022). These patterns suggest that peat decomposition stage influences both substrate quality for methanogenesis and physical gas transport pathways (Krüger et al., 2015; Leifeld et al., 2020), hence regulating FCH_4 across the mire complex. C:N ratios typically decrease during decomposition due to preferential loss of carbon while nitrogen is retained in these nitrogen-limited systems (Biester et al., 2014; Watmough et al., 2022), while the higher bulk density at more decomposed sites could further limit gas transport due to collapsed pore networks (Baird et al., 2004; Kleimeier et al., 2017).

While the mire-to-catchment ratio showed a positive trend with FCH_4, this relationship was not statistically significant. Interestingly, while NDVI showed significant correlation with FCH_4 in 2021 and when averaged across years, sedge biomass and GPP did not correlate significantly with FCH_4. This discrepancy between NDVI and both GPP and sedge biomass suggests that NDVI might be capturing broader ecosystem properties beyond vegetation productivity, potentially including variations in water regime and nutrient status that affect spectral properties of different *Sphagnum* moss species (Bubier et al., 1997).

Differences in peat pore CH_4 concentrations were observed across sites, mirroring those observed in FCH_4. In fact, CH_4 averaged across all depths (5 to 45 cm) was highest at SE-Deg (2389 ± 824 ppm), and lowest at SE-Srj (873 ± 239 ppm), with differences persisting through the peat profile, suggesting fundamental differences in CH_4 production and/or oxidation, rather than differences in only transport processes.

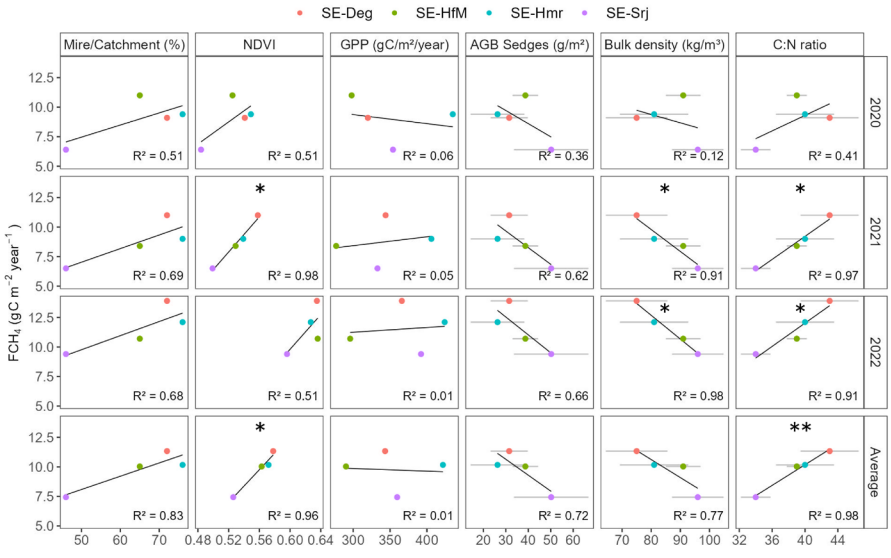

Figure 14. Correlation between annual methane fluxes (FCH_4; for each year 2020–2022, and averaged for all three years) with site characteristics, i.e. mire/catchment ratio, bulk density and C:N ratio at 0–50 cm depth, and vegetation metrics, i.e. the normalized difference vegetation index (NDVI), gross primary production (GPP) and above-ground biomass (AGB) of sedges. The grey horizontal lines represent the standard errors across the spatial replicates. The black lines represent linear regression fit lines. The '*' represents p-values <0.05 and '**' represents $p < 0.01$, i.e. the significance levels of the linear relationships. Panels without '*' means no significant linear relationship.

4.4 Upscaling FCH_4 to the mire complex (**Paper IV**)

4.4.1 Variability within footprint

The analysis of spatially-resolved information for each of the half-hourly EC flux footprints revealed substantial spatio-temporal variations in environmental conditions within individual flux footprints, as illustrated by four example 80% footprints at SE-Deg (Figure 15). These variations arose both from the spatio-temporal heterogeneity of surface properties and from changes in wind properties that define the source area of measured fluxes. The microtopography proportions showed relatively consistent patterns across the mire complex, with lawns comprising 85–95% of footprint areas while hollows and hummocks cover smaller proportions (< 10%). However, vegetation composition exhibited greater variability depending on the site

and footprint, with SE-Srj dominated by lawns with short sedges (80–90% of footprint area), while SE-HfM showed higher proportions of carpet vegetation (50–80%).

After removing temporal trends, NDVI variations remained within ±0.025 during 2022 but showed larger deviations from spatially-fixed values (+0.025 to -0.05) during 2023. Ts variations were generally small (±2°C) but reached up to +4°C above spatially-fixed values during June and July 2023. WTD showed site-specific patterns of variation, with the largest footprint-related deviations from spatially-fixed values (up to +8 cm) observed at SE-HfM, while remaining within ±2 cm at other sites. These patterns highlight the complex spatial heterogeneity captured by EC measurements, demonstrating why footprint analysis is crucial for correctly interpreting flux measurements in heterogeneous landscapes (Peltola et al., 2015; Vesala et al., 2008) and for improving EC flux upscaling approaches (Ingle et al., 2023; Tuovinen et al., 2019).

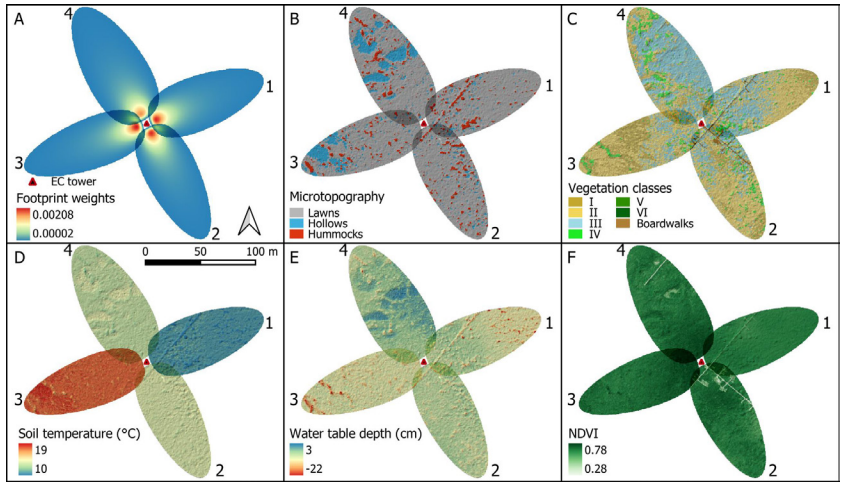

Figure 15. Example 80% footprints weights (A) at the site SE-Deg for four sample half-hours, 1: 2022-09-15 10:30 to 11:00, 2: 2022-06-11 10:30 to 11:00, 3: 2022-07-05 10:30 to 11:00, 4: 2022-06-15 10:30 to 11:00 (The similar footprint shapes are selected for visualization, but in reality, they vary with wind conditions). The extracted thematic layers for the same half-hours and footprint areas represent microtopography classes (B); vegetation classes as defined in section 4.1: I for "lawns dominated by short sedges", II for "carpets with short sedges and *Sphagnum* subg. Cuspidata", III for "mud and loose bottoms/tall-sedge fens", IV for "hummocks and sparsely treed areas", V for "mire forests", and VI for "forests on mineral soils" (C); soil temperature (D); water table depth with negative values below surface (E); and the normalized difference vegetation index (NDVI) (F).

4.4.2 Model performance and uncertainty

The two random forest approaches showed comparable overall performance but with some differences. Depending on the site used for training the random forest, the biomet model achieved RMSE values ranging from 0.39 to 0.78 mg C m^{-2} 30 min^{-1} (mean: 0.60), while the footprint-based model showed RMSE from 0.46 to 0.80 mg C m^{-2} 30 min^{-1} (mean: 0.61).

Estimating FCH_4 across the entire mire complex based on a simple extrapolation from a single measurement location (i.e. assuming representativity over the entire mire complex) would have introduced substantial uncertainty in mire complex FCH_4 estimates. In fact, direct extrapolation from any individual site would have resulted in under- or overestimation of actual mire complex average FCH_4 by up to 22% in 2022 and 32% in 2023 (Figure 16). On the other hand, both random forest modelling approaches reduced this uncertainty, with the footprint-based model achieving under- or overestimation up to 8% in 2022 and 25% in 2023, while the biomet model showed under- or overestimation up to 11% and 30%, respectively. The larger uncertainties observed in 2023 for both approaches reflect the challenges of such models during drier conditions, suggesting potential limitations as climate extremes become more frequent.

While the footprint-based model showed marginally better performance in estimating mire complex FCH_4 compared to the biomet model (8–25% vs 11–30% deviation from observed average, respectively), the biomet model offers practical advantages through simpler implementation and continuous temporal coverage. The footprint-based approach requires extensive spatial data collection and processing, including mapping the spatio-temporal dynamics of different environmental variables. It also depends on wind-related variables for footprint calculations, which inherently creates temporal gaps in estimates as these variables cannot be reliably gap-filled over long periods. In contrast, the biomet model's reliance on fixed sensor measurements allows for continuous estimates through gap-filling. These make the biomet model a more efficient choice over larger areas where the spatial data might be more difficult to acquire.

The accuracy of our random forest models (RMSE = 0.61 mg C m^{-2} 30 min^{-1} or approximately 0.03 g C m^{-2} d^{-1}) is similar to results achieved using the process-based CoupModel at SE-Deg, which showed prediction errors of about 0.02 g C m^{-2} d^{-1} (Duan et al., 2025 - in review). This comparable performance suggests that machine learning approaches may offer a viable

alternative to process-based modelling for estimating FCH_4. Nevertheless, their broader applicability needs further testing, particularly at multiple mire complexes with different characteristics or environmental conditions.

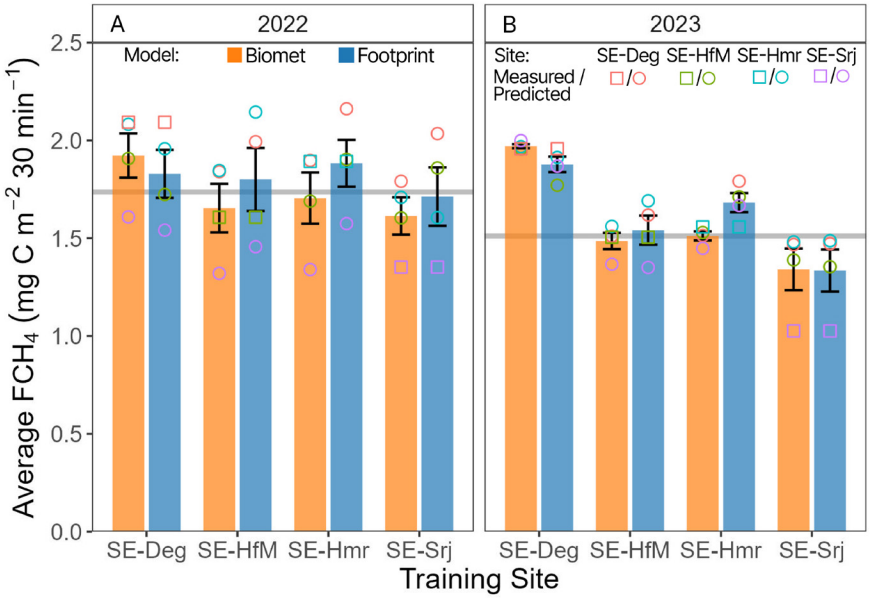

Figure 16. Comparison of mire complex methane flux (FCH_4) estimates using different measurement and modelling approaches in 2022 (A) and 2023 (B). For each site (SE-Deg, SE-HfM, SE-Hmr, SE-Srj), coloured squares show the measured flux at that training site, while coloured circles show model-predicted fluxes for the other three sites. The orange and blue bars represent the mean values across all sites (one measured, i.e. square, and three predicted, i.e. circles) when using the biomet model and footprint-based model respectively. The horizontal grey bar represents the observed mire complex average based on measurements from all four sites, with black vertical error bars showing standard errors of the means.

Variable importance analysis revealed NDVI as the strongest predictor across both models (30–55% and 45–65% increase in MSE for biomet and footprint-based models, respectively), followed by air pressure (30–45%), Ts and WTD (both 20–40% increase in MSE across sites). This relative importance supports the long-known drivers of FCH_4, i.e. substrate supply (Ström et al., 2015; Turner et al., 2020), Ts and WTD (Rinne et al., 2022; Turetsky et al., 2014), while highlighting air pressure's importance due to its role in regulating CH_4 transport, particularly ebullition processes in peatlands (Männistö et al., 2019; Tokida et al., 2007). The significant

improvement (up to 42% reduction in RMSE at some sites) in both models following C:N ratio adjustment suggests that C:N ratio sets a baseline for FCH_4 across the mire complex due to its reflection of organic matter quality and decomposition stage (Krüger et al., 2015; Leifeld et al., 2020). These findings suggest that while meteorological and hydrological variables drive temporal patterns, landscape-scale biogeochemical properties significantly constrain spatial variations in FCH_4.

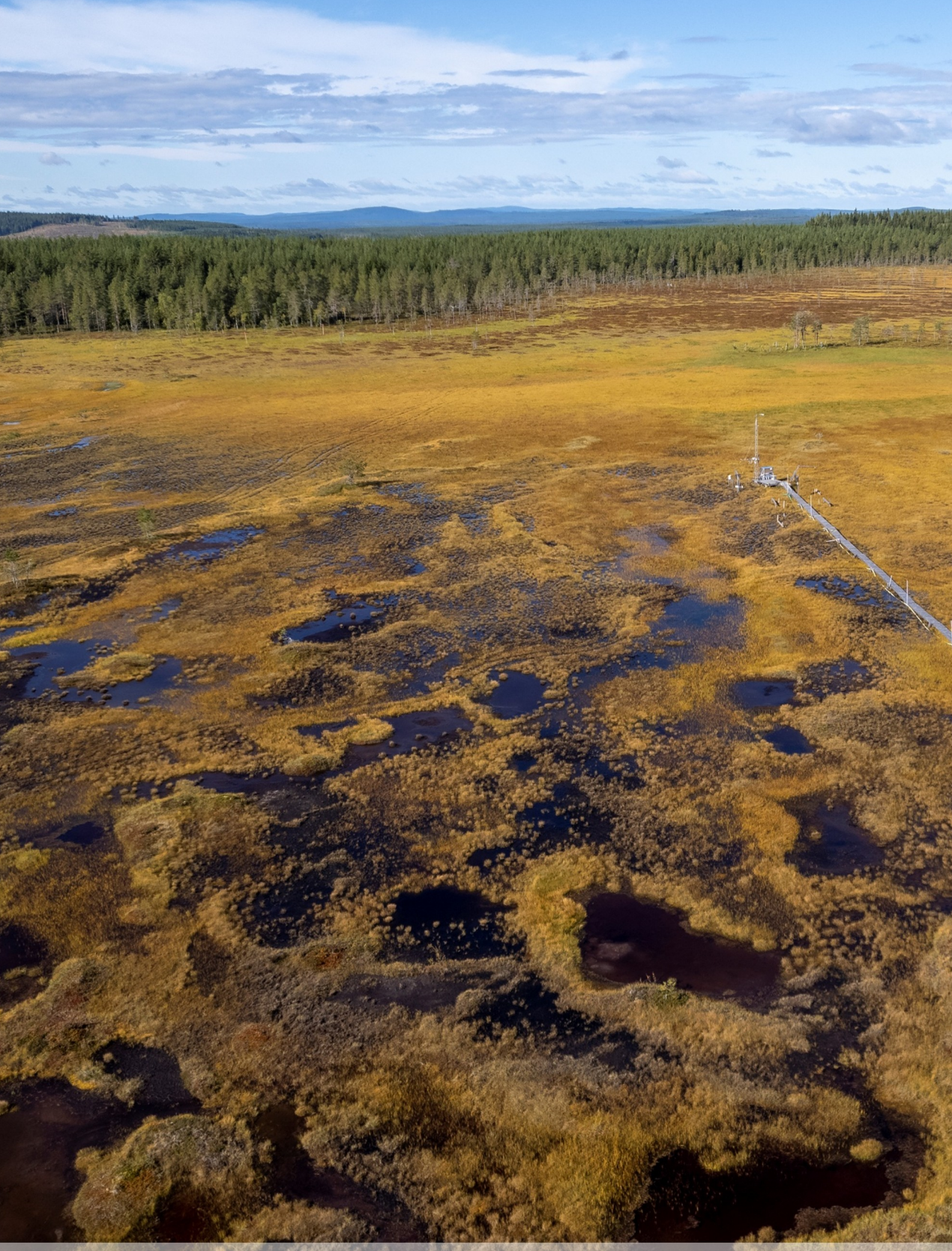

Photo: Andreas Palmén

5. Conclusions

This thesis investigated mesoscale variations in FCH_4 dynamics and their drivers across a boreal peatland complex using replicated ecosystem-scale measurements. Through four interconnected studies, this work developed new approaches for characterizing peatland surface structure, explored ecosystem-scale FCH_4 variations and their drivers, and developed a framework for comprehensive upscaling of single-site measurements to the mire complex scale. Results revealed substantial spatial variability in FCH_4 across the mire complex, with differences between sites comparable to those typically observed among geographically distant mire systems. These spatial variations were primarily controlled by peat properties (particularly C:N ratios) which set a baseline for FCH_4 across the mire complex, while temporal variations were driven by soil temperature and plant productivity. The Kulbäcksliden Research Infrastructure (KRI) with its replicated ecosystem-scale measurements enabled the development of data-driven approaches for estimating mire complex FCH_4, with implications for improving bottom-up regional emission estimates.

A specific summary of findings from each study is given below:

Paper I:

- A comprehensive description of the KRI was provided, including its unique configuration with replicated ecosystem-scale measurements, detailed mapping of vegetation, and research history across the peatland complex
- This research infrastructure enables new opportunities for understanding spatial heterogeneity in peatland biogeochemical processes, and for developing scaling approaches.

Paper II:

- The novel HuHoLa model was developed for classifying peatland microtopography based on DEMs
- The model advances beyond typical binary (hollow-hummock) classifications by identifying three microform types (lawns, hollows, and hummocks) and providing proxies for mapping WTD and Ts

- The model's hydrological basis makes it generalizable across different peatland systems with the potential for advancing our ability to characterize and understand peatland surface structure at landscape scales.

Paper III:

- The observed spatial variability in FCH_4 within the mire complex was comparable to the variability typically observed among geographically distant mire systems, suggesting that current bottom-up FCH_4 estimates based on single EC towers may have a high uncertainty
- Peat properties (particularly C:N ratio and bulk density) set the baseline for spatial variations in FCH_4, while Ts and GPP acted as inter-annual drivers of FCH_4. This suggests that incorporating peat properties into process-based models and upscaling approaches could capture mesoscale variability in FCH_4 and reduce uncertainties in regional and global methane budgets.

Paper IV:

- Data-driven machine learning approaches were developed to estimate mire complex FCH_4 based on single site EC measurements
- These approaches reduced uncertainty in mire complex FCH_4 estimates by more than 50% in a normal year, compared to when a single site measurement is considered representative of the mire complex
- These approaches provide a framework for improving FCH_4 estimates from large peatland complexes where measurements are limited to single locations.

6. Future perspectives and implications

The research presented in this thesis has enhanced our understanding of FCH_4 dynamics across peatland complexes through a unique dataset on mesoscale FCH_4 and drivers and the development of new approaches for characterizing peatland surface structure and upscaling FCH_4 measurements. However, several key questions and challenges remain.

As highlighted in **Paper I**, the Kulbäcksliden Research Infrastructure with replicated ecosystem-scale measurements provides unique insights into mesoscale variations in peatland processes. While the replication of such research infrastructure over many peatland complexes could improve bottom-up FCH_4 estimates, the high costs and logistical complexities of maintaining multiple eddy covariance systems limit the feasibility of replicating such setups widely. Exploring more cost-effective approaches to capture spatial heterogeneity in peatland complexes, such as mobile EC systems, could help address uncertainties in regional and global CH_4 budget estimates.

The HuHoLa model developed in **Paper II** is based on hydrological principles of surface flow that make it applicable across different peatland types, and advances beyond traditional binary hollow-hummock classifications. However, its secondary outputs providing proxies for WTD and Ts need to be validated at larger scales and in diverse peatland systems, to confirm their broader applicability.

The strong relationship between C:N ratios and FCH_4 observed across our study sites in **Paper III** suggests that this easily measurable indicator of peat properties could be valuable for predicting FCH_4 more broadly. Testing whether this relationship holds across other peatland complexes, particularly those with different nutrient status or peat formation histories, could provide a simple yet powerful tool for improving regional FCH_4 estimates. Furthermore, an exploration of how additional physical and chemical peat properties beyond C:N ratio (e.g., pH, redox potential, specific organic matter composition) and the relative abundance and activity of methanogens and methanotrophs influence FCH_4 could help identify additional drivers of the mesoscale variations in FCH_4.

The upscaling approaches developed in **Paper IV** demonstrated substantial improvement in mire complex FCH_4 estimates compared to the simple extrapolation of single site measurements to the mire complex.

However, their reduced performance during dry conditions highlights the need to better understand how FCH_4 patterns may shift under the extreme weather events which are predicted to become more frequent in northern regions under climate change. Furthermore, testing the transferability of these approaches at other peatland complexes would help evaluate how landscape position, catchment characteristics, and different peatland types influence upscaling effectiveness and further contribute to reducing uncertainty in global wetland FCH_4 estimates, and to reducing the discrepancy between bottom-up and top-down CH_4 budget estimates.

References

Ågren, A.M., Larson, J., Paul, S.S., Laudon, H., Lidberg, W., 2021. Use of multiple LIDAR-derived digital terrain indices and machine learning for high-resolution national-scale soil moisture mapping of the Swedish forest landscape. Geoderma 404, 115280. https://doi.org/10.1016/J.GEODERMA.2021.115280

Antezana-Vera, S.A., Marenco, R.A., 2022. Transpiration of Swartzia tomentifera in response to microclimatic variability in the central Amazon: the net effect of vapor pressure déficit. CERNE 27, e. https://doi.org/10.1590/01047760202127012999

Armstrong, A., Waldron, S., Ostle, N.J., Richardson, H., Whitaker, J., 2015. Biotic and Abiotic Factors Interact to Regulate Northern Peatland Carbon Cycling. Ecosystems 18, 1395–1409. https://doi.org/10.1007/s10021-015-9907-4

Arsenault, J., Talbot, J., Brown, L.E., Helbig, M., Holden, J., Hoyos-Santillan, J., Jolin, É., Mackenzie, R., Martinez-Cruz, K., Sepulveda-Jauregui, A., Lapierre, J.-F., 2023. Climate-driven spatial and temporal patterns in peatland pool biogeochemistry. Glob. Change Biol. 29, 4056–4068. https://doi.org/10.1111/gcb.16748

Baird, A.J., Beckwith, C.W., Waldron, S., Waddington, J.M., 2004. Ebullition of methane-containing gas bubbles from near-surface Sphagnum peat. Geophys. Res. Lett. 31, 21505. https://doi.org/10.1029/2004GL021157

Baldocchi, D., 2014. Measuring fluxes of trace gases and energy between ecosystems and the atmosphere - the state and future of the eddy covariance method. Glob. Change Biol. 20, 3600–3609. https://doi.org/10.1111/GCB.12649

Bellisario, L.M., Bubier, J.L., Moore, T.R., Chanton, J.P., 1999. Controls on CH4 emissions from a northern peatland. Glob. Biogeochem. Cycles 13, 81–91. https://doi.org/10.1029/1998GB900021

Belyea, L.R., Baird, A.J., 2006. Beyond "the limits to peat bog growth": cross-scale feedback in peatland development. Ecol. Monogr. 76, 299–322. https://doi.org/10.1890/0012-9615(2006)076[0299:BTLTPB]2.0.CO;2

Bergman, I., Svensson, B.H., Nilsson, M., 1998. Regulation of methane production in a Swedish acid mire by pH, temperature and substrate. Soil Biol. Biochem. 30, 729–741. https://doi.org/10.1016/S0038-0717(97)00181-8

Biester, H., Knorr, K.H., Schellekens, J., Basler, A., Hermanns, Y.M., 2014. Comparison of different methods to determine the degree of peat decomposition in peat bogs. Biogeosciences 11, 2691–2707. https://doi.org/10.5194/BG-11-2691-2014

Brubaker, K.M., Myers, W.L., Drohan, P.J., Miller, D.A., Boyer, E.W., 2013. The Use of LiDAR Terrain Data in Characterizing Surface Roughness and Microtopography. Appl. Environ. Soil Sci. 2013, 1–13. https://doi.org/10.1155/2013/891534

Bubier, J., Costello, A., Moore, T.R., Roulet, N.T., Savage, K., 1993. Microtopography and methane flux in boreal peatlands, northern Ontario, Canada. Can. J. Bot. 71, 1056–1063. https://doi.org/10.1139/b93-122

Bubier, J., Rock, B.N., Crill, P.M., 1997. Spectral reflectance measurements of boreal wetland and forest mosses. J. Geophys. Res. Atmospheres 102, 29483–29494. https://doi.org/10.1029/97JD02316

Bubier, J.L., Moore, T.R., Bellisario, L., Comer, N.T., Crill, P.M., 1995. Ecological controls on methane emissions from a Northern Peatland Complex in the zone of discontinuous permafrost, Manitoba, Canada. Glob. Biogeochem. Cycles 9, 455–470. https://doi.org/10.1029/95GB02379

Buck, A.L., 1981. New Equations for Computing Vapor Pressure and Enhancement Factor.

Burba, G., Anderson, D., 2010. A Brief Practical Guide to Eddy Covariance Flux Measurements: Principles and Workflow Examples for Scientific and Industrial Applications, LI-COR Biosciences. LI-COR Biosciences, Lincoln, NB, USA. https://doi.org/10.1890/06-1336.1

Campeau, A., Bishop, K.H., Billett, M.F., Garnett, M.H., Laudon, H., Leach, J.A., Nilsson, M.B., Öquist, M.G., Wallin, M.B., 2017. Aquatic export of young dissolved and gaseous carbon from a pristine boreal fen: Implications for peat carbon stock stability. Glob. Change Biol. 23, 5523–5536. https://doi.org/10.1111/GCB.13815

Campeau, A., He, H., Riml, J., Humphreys, E., Dalva, M., Roulet, N., 2024. Wind as a Driver of Peat CO2 Dynamics in a Northern Bog. Ecosystems 1–15. https://doi.org/10.1007/S10021-024-00904-1/FIGURES/6

Cazelles, B., Chavez, M., Berteaux, D., Ménard, F., Vik, J.O., Jenouvrier, S., Stenseth, N.C., 2008. Wavelet analysis of ecological time series. Oecologia 156, 287–304. https://doi.org/10.1007/S00442-008-0993-2/FIGURES/9

Chang, K.Y., Riley, W.J., Knox, S.H., Jackson, R.B., McNicol, G., Poulter, B., Aurela, M., Baldocchi, D., Bansal, S., Bohrer, G., Campbell, D.I., Cescatti, A., Chu, H., Delwiche, K.B., Desai, A.R., Euskirchen, E., Friborg, T., Goeckede, M., Helbig, M., Hemes, K.S., Hirano, T., Iwata, H., Kang, M., Keenan, T., Krauss, K.W., Lohila, A., Mammarella, I., Mitra, B., Miyata, A., Nilsson, M.B., Noormets, A., Oechel, W.C., Papale, D., Peichl, M., Reba, M.L., Rinne, J., Runkle, B.R.K., Ryu, Y., Sachs, T., Schäfer, K.V.R., Schmid, H.P., Shurpali, N., Sonnentag, O., Tang, A.C.I., Torn, M.S., Trotta, C., Tuittila, E.S., Ueyama, M., Vargas, R., Vesala, T., Windham-Myers, L., Zhang, Z., Zona, D., 2021. Substantial hysteresis in emergent temperature sensitivity of global wetland CH4 emissions. Nat. Commun. 12, 1–10. https://doi.org/10.1038/s41467-021-22452-1

Dean, J.F., Middelburg, J.J., Röckmann, T., Aerts, R., Blauw, L.G., Egger, M., Jetten, M.S.M., de Jong, A.E.E., Meisel, O.H., Rasigraf, O., Slomp, C.P., in't Zandt, M.H., Dolman, A.J., 2018. Methane Feedbacks to the Global Climate System in a Warmer World. Rev. Geophys. 56, 207–250. https://doi.org/10.1002/2017RG000559

Desai, A.R., Murphy, B.A., Wiesner, S., Thom, J., Butterworth, B.J., Koupaei-Abyazani, N., Muttaqin, A., Paleri, S., Talib, A., Turner, J., Mineau, J., Merrelli, A., Stoy, P., Davis, K., 2022. Drivers of Decadal Carbon Fluxes Across Temperate Ecosystems. J. Geophys. Res. Biogeosciences 127. https://doi.org/10.1029/2022JG007014

Diamond, J.S., McLaughlin, D.L., Slesak, R.A., Stovall, A., 2020. Microtopography is a fundamental organizing structure of vegetation and soil chemistry in black ash wetlands. Biogeosciences 17, 901–915. https://doi.org/10.5194/bg-17-901-2020

Duan, W., Wu, M., Peichl, M., He, H., Roulet, N., Noumonvi, K.D., Ratcliffe, J.L., Nilsson, M.B., Jansson, P.-E., 2025. Variations in ecosystem-scale methane fluxes across a boreal mire complex assessed by a network of flux towers.

Ehnvall, B., Ågren, A.M., Nilsson, M.B., Ratcliffe, J.L., Noumonvi, K.D., Peichl, M., Lidberg, W., Giesler, R., Mörth, C.M., Öquist, M.G., 2023. Catchment characteristics control boreal mire nutrient regime and vegetation patterns over ~5000 years of landscape development. Sci. Total Environ. 895, 165132. https://doi.org/10.1016/J.SCITOTENV.2023.165132

Eurola, S., Hicks, S., Kaakinen, E., 1984. Key to Finnish Mire Types, in: Moore, P.D. (Ed.), European Mires. Academic Press, pp. 11–117. https://doi.org/10.1016/B978-0-12-505580-2.50006-4

Eurola, S., Huttunen, A., Kaakinen, E., Kukko-oja, K., Saari, V., Salonen, V., 2015. Sata suotyyppiä : opas Suomen suokasvillisuuden tuntemiseen. University of Oulu; Thule Institute.

Eurola, S., Huttunen, A., Kukko-oja, K., 1995. Suokasvillisuusopas (Mire vegetation guide), Oulanka Reports. ed, Oulanka reports. Oulanka Biological Station, University of Oulu.

Euskirchen, E.S., Edgar, C.W., Kane, E.S., Waldrop, M.P., Neumann, R.B., Manies, K.L., Douglas, T.A., Dieleman, C., Jones, M.C., Turetsky, M.R., 2024. Persistent net release of carbon dioxide and methane from an Alaskan lowland boreal peatland complex. Glob. Change Biol. 30, e17139. https://doi.org/10.1111/GCB.17139

Feng, X., Deventer, M.J., Lonchar, R., Ng, G.H.C., Sebestyen, S.D., Roman, D.T., Griffis, T.J., Millet, D.B., Kolka, R.K., 2020. Climate Sensitivity of Peatland Methane Emissions Mediated by Seasonal Hydrologic Dynamics. Geophys. Res. Lett. 47, e2020GL088875. https://doi.org/10.1029/2020GL088875

Fratini, G., Ibrom, A., Arriga, N., Burba, G., Papale, D., 2012. Relative humidity effects on water vapour fluxes measured with closed-path eddy-covariance systems with short sampling lines. Agric. For. Meteorol. 165, 53–63. https://doi.org/10.1016/J.AGRFORMET.2012.05.018

Frolking, S., Talbot, J., Jones, M.C., Treat, C.C., Kauffman, J.B., Tuittila, E.-S., Roulet, N., 2011. Peatlands in the Earth's 21st century climate system. Environ. Rev. 19, 371–396. https://doi.org/10.1139/a11-014

GEE, 2024. Harmonized Sentinel-2 MSI: MultiSpectral Instrument, Level-2A, Earth Engine Data Catalog.

Goodrich, J.P., Campbell, D.I., Roulet, N.T., Clearwater, M.J., Schipper, L.A., 2015. Overriding control of methane flux temporal variability by water table dynamics in a Southern Hemisphere, raised bog. J. Geophys. Res. Biogeosciences 120, 819–831. https://doi.org/10.1002/2014JG002844

Gorham, E., 1957. The Development of Peat Lands. Q. Rev. Biol. 32, 145–166.

Graham, J.D., Glenn, N.F., Spaete, L.P., Hanson, P.J., 2020. Characterizing Peatland Microtopography Using Gradient and Microform-Based Approaches. Ecosystems 23, 1464–1480. https://doi.org/10.1007/s10021-020-00481-z

Granberg, G., Mikkelä, C., Sundh, I., Svensson, B.H., Nilsson, M., 1997. Sources of spatial variation in methane emission from mires in northern Sweden: A mechanistic approach in statistical modeling.

Glob. Biogeochem. Cycles 11, 135–150. https://doi.org/10.1029/96GB03352
Grinsted, A., Moore, J.C., Jevrejeva, S., 2004. Application of the cross wavelet transform and wavelet coherence to geophysical time series. Nonlinear Process. Geophys. 11, 561–566. https://doi.org/10.5194/npg-11-561-2004
Heffernan, L., Cavaco, M.A., Bhatia, M.P., Estop-Aragonés, C., Knorr, K.-H., Olefeldt, D., 2022. High peatland methane emissions following permafrost thaw: enhanced acetoclastic methanogenesis during early successional stages. Biogeosciences 19, 3051–3071. https://doi.org/10.5194/bg-19-3051-2022
Helbig, M., Waddington, J.M., Alekseychik, P., Amiro, B.D., Aurela, M., Barr, A.G., Black, T.A., Blanken, P.D., Carey, S.K., Chen, J., Chi, J., Desai, A.R., Dunn, A., Euskirchen, E.S., Flanagan, L.B., Forbrich, I., Friborg, T., Grelle, A., Harder, S., Heliasz, M., Humphreys, E.R., Ikawa, H., Isabelle, P.E., Iwata, H., Jassal, R., Korkiakoski, M., Kurbatova, J., Kutzbach, L., Lindroth, A., Löfvenius, M.O., Lohila, A., Mammarella, I., Marsh, P., Maximov, T., Melton, J.R., Moore, P.A., Nadeau, D.F., Nicholls, E.M., Nilsson, M.B., Ohta, T., Peichl, M., Petrone, R.M., Petrov, R., Prokushkin, A., Quinton, W.L., Reed, D.E., Roulet, N.T., Runkle, B.R.K., Sonnentag, O., Strachan, I.B., Taillardat, P., Tuittila, E.S., Tuovinen, J.P., Turner, J., Ueyama, M., Varlagin, A., Wilmking, M., Wofsy, S.C., Zyrianov, V., 2020. Increasing contribution of peatlands to boreal evapotranspiration in a warming climate. Nat. Clim. Change 10, 555–560. https://doi.org/10.1038/s41558-020-0763-7
Hersbach, H., Bell, B., Berrisford, P., Hirahara, S., Horányi, A., Muñoz-Sabater, J., Nicolas, J., Peubey, C., Radu, R., Schepers, D., Simmons, A., Soci, C., Abdalla, S., Abellan, X., Balsamo, G., Bechtold, P., Biavati, G., Bidlot, J., Bonavita, M., De Chiara, G., Dahlgren, P., Dee, D., Diamantakis, M., Dragani, R., Flemming, J., Forbes, R., Fuentes, M., Geer, A., Haimberger, L., Healy, S., Hogan, R.J., Hólm, E., Janisková, M., Keeley, S., Laloyaux, P., Lopez, P., Lupu, C., Radnoti, G., de Rosnay, P., Rozum, I., Vamborg, F., Villaume, S., Thépaut, J.N., 2020. The ERA5 global reanalysis. Q. J. R. Meteorol. Soc. 146, 1999–2049. https://doi.org/10.1002/QJ.3803
Hopple, A.M., Wilson, R.M., Kolton, M., Zalman, C.A., Chanton, J.P., Kostka, J., Hanson, P.J., Keller, J.K., Bridgham, S.D., 2020. Massive

peatland carbon banks vulnerable to rising temperatures. Nat. Commun. 11, 2373. https://doi.org/10.1038/s41467-020-16311-8

Ingle, R., Habib, W., Connolly, J., McCorry, M., Barry, S., Saunders, M., 2023. Upscaling methane fluxes from peatlands across a drainage gradient in Ireland using PlanetScope imagery and machine learning tools. Sci. Rep. 13, 11997. https://doi.org/10.1038/s41598-023-38470-6

IPCC, 2023. Climate Change 2022 – Impacts, Adaptation and Vulnerability: Working Group II Contribution to the Sixth Assessment Report of the Intergovernmental Panel on Climate Change. Cambridge University Press, Cambridge. https://doi.org/10.1017/9781009325844

Irvin, J., Zhou, S., McNicol, G., Lu, F., Liu, V., Fluet-Chouinard, E., Ouyang, Z., Knox, S.H., Lucas-Moffat, A., Trotta, C., Papale, D., Vitale, D., Mammarella, I., Alekseychik, P., Aurela, M., Avati, A., Baldocchi, D., Bansal, S., Bohrer, G., Campbell, D.I., Chen, J., Chu, H., Dalmagro, H.J., Delwiche, K.B., Desai, A.R., Euskirchen, E., Feron, S., Goeckede, M., Heimann, M., Helbig, M., Helfter, C., Hemes, K.S., Hirano, T., Iwata, H., Jurasinski, G., Kalhori, A., Kondrich, A., Lai, D.Y., Lohila, A., Malhotra, A., Merbold, L., Mitra, B., Ng, A., Nilsson, M.B., Noormets, A., Peichl, M., Rey-Sanchez, A.C., Richardson, A.D., Runkle, B.R., Schäfer, K.V., Sonnentag, O., Stuart-Haëntjens, E., Sturtevant, C., Ueyama, M., Valach, A.C., Vargas, R., Vourlitis, G.L., Ward, E.J., Wong, G.X., Zona, D., Alberto, M.C.R., Billesbach, D.P., Celis, G., Dolman, H., Friborg, T., Fuchs, K., Gogo, S., Gondwe, M.J., Goodrich, J.P., Gottschalk, P., Hörtnagl, L., Jacotot, A., Koebsch, F., Kasak, K., Maier, R., Morin, T.H., Nemitz, E., Oechel, W.C., Oikawa, P.Y., Ono, K., Sachs, T., Sakabe, A., Schuur, E.A., Shortt, R., Sullivan, R.C., Szutu, D.J., Tuittila, E.S., Varlagin, A., Verfaillie, J.G., Wille, C., Windham-Myers, L., Poulter, B., Jackson, R.B., 2021. Gap-filling eddy covariance methane fluxes: Comparison of machine learning model predictions and uncertainties at FLUXNET-CH4 wetlands. Agric. For. Meteorol. 308–309, 108528. https://doi.org/10.1016/J.AGRFORMET.2021.108528

Järveoja, J., Nilsson, M.B., Crill, P.M., Peichl, M., 2020. Bimodal diel pattern in peatland ecosystem respiration rebuts uniform temperature response. Nat. Commun. 2020 111 11, 1–9. https://doi.org/10.1038/s41467-020-18027-1

Järveoja, J., Nilsson, M.B., Gažovič, M., Crill, P.M., Peichl, M., 2018. Partitioning of the net CO2 exchange using an automated chamber

system reveals plant phenology as key control of production and respiration fluxes in a boreal peatland. Glob. Change Biol. 24, 3436–3451. https://doi.org/10.1111/GCB.14292

Joosten, Hans, Couwenberg, J., 2008. Peatlands and Carbon, in: Parish, F., Sirin, A., Charman, D., Joosten, H, Minayeva, T., Silvius, M., Stringer, L. (Eds.), Assessment on Peatlands, Biodiversity and Climate Change: Main Report. Global Environment Centre, Kuala Lumpur & Wetlands International, Wageningen, pp. 99–117.

Juottonen, H., Kotiaho, M., Robinson, D., Merilä, P., Fritze, H., Tuittila, E.-S., 2015. Microform-related community patterns of methane-cycling microbes in boreal Sphagnum bogs are site specific. FEMS Microbiol. Ecol. 91, fiv094. https://doi.org/10.1093/femsec/fiv094

Kalacska, M., Arroyo-Mora, J.P., Lucanus, O., 2021. Comparing UAS LiDAR and Structure-from-Motion Photogrammetry for Peatland Mapping and Virtual Reality (VR) Visualization. Drones 5, 36. https://doi.org/10.3390/drones5020036

Kämäräinen, M., Lintunen, A., Kulmala, M., Tuovinen, J., Mammarella, I., Aalto, J., Vekuri, H., Lohila, A., 2022. Evaluation of gradient boosting and random forest methods to model subdaily variability of the atmosphere – forest CO2 exchange. Biogeosciences Discuss. https://doi.org/10.5194/bg-2022-108

Kettridge, N., Tilak, A.S., Devito, K.J., Petrone, R.M., Mendoza, C.A., Waddington, J.M., 2016. Moss and peat hydraulic properties are optimized to maximize peatland water use efficiency. Ecohydrology 9, 1039–1051. https://doi.org/10.1002/eco.1708

Kleimeier, C., Rezanezhad, F., Cappellen, P.V., Lennartz, B., 2017. Influence of pore structure on solute transport in degraded and undegraded fen peat soils. Mires Peat 19, 9. https://doi.org/10.19189/MaP.2017.OMB.282

Kljun, N., Calanca, P., Rotach, M.W., Schmid, H.P., 2015. A simple two-dimensional parameterisation for Flux Footprint Prediction (FFP). Geosci. Model Dev. 8, 3695–3713. https://doi.org/10.5194/gmd-8-3695-2015

Kljun, N., Rotach, M.W., Schmid, H.P., 2002. A three-dimensional backward Lagrangian footprint model for a wide range of boundary-layer stratifications. Bound.-Layer Meteorol. 103, 205–226. https://doi.org/10.1023/A:1014556300021

Knox, S.H., Jackson, R.B., Poulter, B., McNicol, G., Fluet-Chouinard, E., Zhang, Z., Hugelius, G., Bousquet, P., Canadell, J.G., Saunois, M., Papale, D., Chu, H., Keenan, T.F., Baldocchi, D., Torn, M.S., Mammarella, I., Trotta, C., Aurela, M., Bohrer, G., Campbell, D.I.,

Cescatti, A., Chamberlain, S., Chen, J., Chen, W., Dengel, S., Desai, A.R., Euskirchen, E., Friborg, T., Gasbarra, D., Goded, I., Goeckede, M., Heimann, M., Helbig, M., Hirano, T., Hollinger, D.Y., Iwata, H., Kang, M., Klatt, J., Krauss, K.W., Kutzbach, L., Lohila, A., Mitra, B., Morin, T.H., Nilsson, M.B., Niu, S., Noormets, A., Oechel, W.C., Peichl, M., Peltola, O., Reba, M.L., Richardson, A.D., Runkle, B.R.K., Ryu, Y., Sachs, T., Schäfer, K.V.R., Schmid, H.P., Shurpali, N., Sonnentag, O., Tang, A.C.I., Ueyama, M., Vargas, R., Vesala, T., Ward, E.J., Windham-Myers, L., Wohlfahrt, G., Zona, D., 2019. FLUXNET-CH4 Synthesis Activity: Objectives, Observations, and Future Directions. Bull. Am. Meteorol. Soc. 100, 2607–2632. https://doi.org/10.1175/BAMS-D-18-0268.1

Koebsch, F., Jurasinski, G., Koch, M., Hofmann, J., Glatzel, S., 2015. Controls for multi-scale temporal variation in ecosystem methane exchange during the growing season of a permanently inundated fen. Agric. For. Meteorol. 204, 94–105. https://doi.org/10.1016/j.agrformet.2015.02.002

Koebsch, F., Sonnentag, O., Järveoja, J., Peltoniemi, M., Alekseychik, P., Aurela, M., Arslan, A.N., Dinsmore, K., Gianelle, D., Helfter, C., Jackowicz-Korczynski, M., Korrensalo, A., Leith, F., Linkosalmi, M., Lohila, A., Lund, M., Maddison, M., Mammarella, I., Mander, Ü., Minkkinen, K., Pickard, A., Pullens, J.W.M., Tuittila, E.S., Nilsson, M.B., Peichl, M., 2020. Refining the role of phenology in regulating gross ecosystem productivity across European peatlands. Glob. Change Biol. 26, 876–887. https://doi.org/10.1111/GCB.14905

Kowalska, N., Chojnicki, B.H., Rinne, J., Haapanala, S., Siedlecki, P., Urbaniak, M., 2013. Measurements of methane emission from a temperate wetland by the eddy covariance method. Int. Agrophysics 27, 283–290. https://doi.org/10.2478/v10247-012-0096-5

Krüger, J.P., Leifeld, J., Glatzel, S., Szidat, S., Alewell, C., 2015. Biogeochemical indicators of peatland degradation-a case study of a temperate bog in northern Germany. Biogeosciences 12, 2861–2871. https://doi.org/10.5194/bg-12-2861-2015

Lai, D.Y.F., 2009. Methane Dynamics in Northern Peatlands: A Review. Pedosphere 19, 409–421. https://doi.org/10.1016/S1002-0160(09)00003-4

Laitinen, J., Rehell, S., Huttunen, A., 2005. Vegetation-related hydrotopographic and hydrologic classification for aapa mires (Hirvisuo, Finland). Ann. Bot. Fenn. 42, 107–121.

Lees, K.J., Quaife, T., Artz, R.R.E., Khomik, M., Clark, J.M., 2018. Potential for using remote sensing to estimate carbon fluxes across northern peatlands – A review. Sci. Total Environ. 615, 857–874. https://doi.org/10.1016/J.SCITOTENV.2017.09.103

Leifeld, J., Klein, K., Wüst-Galley, C., 2020. Soil organic matter stoichiometry as indicator for peatland degradation. Sci. Rep. 10, 1–9. https://doi.org/10.1038/s41598-020-64275-y

Lhosmot, A., Jacotot, A., Steinmann, M., Binet, P., Toussaint, M.L., Gogo, S., Gilbert, D., Coffinet, S., Laggoun-Deffarge, F., Bertrand, G., 2023. Biotic and Abiotic Control Over Diurnal CH4 Fluxes in a Temperate Transitional Poor Fen Ecosystem. Ecosystems 26, 951–968. https://doi.org/10.1007/S10021-022-00809-X/FIGURES/9

LI-COR Biosciences, 2022. Eddy Covariance Processing Software (Version 7.0.9) [Software].

Limpens, J., Berendse, F., Blodau, C., Canadell, J.G., Freeman, C., Holden, J., Roulet, N., Rydin, H., Schaepman-Strub, G., 2008. Peatlands and the carbon cycle: from local processes to global implications – a synthesis. Biogeosciences 5, 1475–1491. https://doi.org/10.5194/bg-5-1475-2008

Lindsay, J.B., 2016. Whitebox GAT: A case study in geomorphometric analysis. Comput. Geosci. 95, 75–84. https://doi.org/10.1016/j.cageo.2016.07.003

Lovitt, J., Rahman, M., McDermid, G., 2017. Assessing the Value of UAV Photogrammetry for Characterizing Terrain in Complex Peatlands. Remote Sens. 9, 715. https://doi.org/10.3390/rs9070715

Määttä, T., Malhotra, A., 2023. Effects of spatial heterogeneity within the eddy covariance (EC) footprint on up-scaled methane fluxes across multiple wetland sites (No. EGU23-3338). Presented at the EGU23, Copernicus Meetings. https://doi.org/10.5194/egusphere-egu23-3338

Männistö, E., Korrensalo, A., Alekseychik, P., Mammarella, I., Peltola, O., Vesala, T., Tuittila, E.-S., 2019. Multi-year methane ebullition measurements from water and bare peat surfaces of a patterned boreal bog. Biogeosciences 16, 2409–2421. https://doi.org/10.5194/bg-16-2409-2019

Mauder, M., Foken, T., 2004. Documentation and Instruction Manual of the Eddy-Covariance Software Package TK3. Arbeitsergebnisse.

McEwing, K.R., Fisher, J.P., Zona, D., 2015. Environmental and vegetation controls on the spatial variability of CH4 emission from wet-sedge and tussock tundra ecosystems in the Arctic. Plant Soil 388, 37–52. https://doi.org/10.1007/S11104-014-2377-1/FIGURES/6

McNicol, G., Fluet-Chouinard, E., Ouyang, Z., Knox, S., Zhang, Z., Aalto, T., Bansal, S., Chang, K.Y., Chen, M., Delwiche, K., Feron, S., Goeckede, M., Liu, J., Malhotra, A., Melton, J.R., Riley, W., Vargas, R., Yuan, K., Ying, Q., Zhu, Q., Alekseychik, P., Aurela, M., Billesbach, D.P., Campbell, D.I., Chen, J., Chu, H., Desai, A.R., Euskirchen, E., Goodrich, J., Griffis, T., Helbig, M., Hirano, T., Iwata, H., Jurasinski, G., King, J., Koebsch, F., Kolka, R., Krauss, K., Lohila, A., Mammarella, I., Nilson, M., Noormets, A., Oechel, W., Peichl, M., Sachs, T., Sakabe, A., Schulze, C., Sonnentag, O., Sullivan, R.C., Tuittila, E.S., Ueyama, M., Vesala, T., Ward, E., Wille, C., Wong, G.X., Zona, D., Windham-Myers, L., Poulter, B., Jackson, R.B., 2023. Upscaling Wetland Methane Emissions From the FLUXNET-CH4 Eddy Covariance Network (UpCH4 v1.0): Model Development, Network Assessment, and Budget Comparison. AGU Adv. 4, e2023AV000956. https://doi.org/10.1029/2023AV000956

Moore, P.A., Lukenbach, M.C., Thompson, D.K., Kettridge, N., Granath, G., Waddington, J.M., 2019. Assessing the peatland hummock–hollow classification framework using high-resolution elevation models: implications for appropriate complexity ecosystem modeling. Biogeosciences 16, 3491–3506. https://doi.org/10.5194/bg-16-3491-2019

Nemitz, E., Mammarella, I., Ibrom, A., Aurela, M., Burba, G.G., Dengel, S., Gielen, B., Grelle, A., Heinesch, B., Herbst, M., Hörtnagl, L., Klemedtsson, L., Lindroth, A., Lohila, A., McDermitt, D.K., Meier, P., Merbold, L., Nelson, D., Nicolini, G., Nilsson, M.B., Peltola, O., Rinne, J., Zahniser, M., 2018. Standardisation of eddy-covariance flux measurements of methane and nitrous oxide. Int. Agrophysics 32, 517–549. https://doi.org/10.1515/INTAG-2017-0042

Newton, R.G., Spurrell, D.J., 1967. A development of multiple regression for the analysis of routine data. J. R. Stat. Soc. Ser. C Appl. Stat. 16, 51–64. https://doi.org/10.2307/2985237

Nijp, J.J., Metselaar, K., Limpens, J., Teutschbein, C., Peichl, M., Nilsson, M.B., Berendse, F., van der Zee, S.E.A.T.M., 2017. Including hydrological self-regulating processes in peatland models: Effects on peatmoss drought projections. Sci. Total Environ. 580, 1389–1400. https://doi.org/10.1016/J.SCITOTENV.2016.12.104

Nilsson, M., Sagerfors, J., Buffam, I., Laudon, H., Eriksson, T., Grelle, A., Klemedtsson, L., Weslien, P., Lindroth, A., 2008. Contemporary carbon accumulation in a boreal oligotrophic minerogenic mire – a

significant sink after accounting for all C-fluxes. Glob. Change Biol. 14, 2317–2332. https://doi.org/10.1111/J.1365-2486.2008.01654.X

Noumonvi, K.D., Ågren, A.M., Ratcliffe, J.L., Öquist, M.G., Ericson, L., Tong, C.H.M., Järveoja, J., Zhu, W., Osterwalder, S., Peng, H., Erefur, C., Bishop, K., Laudon, H., Nilsson, M.B., Peichl, M., 2023. The Kulbäcksliden Research Infrastructure: a unique setting for northern peatland studies. Front. Earth Sci. 11, 1194749. https://doi.org/10.3389/feart.2023.1194749

Noumonvi, K.D., Havertz, N.H., Bohlin, J., van der Linden, S., Nilsson, M.B., Peichl, M., 2025. HuHoLa: A novel Hummock-Hollow-Lawn mire microtopography modelling approach.

Öquist, M.G., Svensson, B.H., 2002. Vascular plants as regulators of methane emissions from a subarctic mire ecosystem. J. Geophys. Res. Atmospheres 107, 1–10. https://doi.org/10.1029/2001JD001030

Peichl, M., Gažovič, M., Vermeij, I., de Goede, E., Sonnentag, O., Limpens, J., Nilsson, M.B., 2018. Peatland vegetation composition and phenology drive the seasonal trajectory of maximum gross primary production. Sci. Rep. 8, 8012. https://doi.org/10.1038/s41598-018-26147-4

Peichl, M., Öquist, M., Ottosson Löfvenius, M., Ilstedt, U., Sagerfors, J., Grelle, A., Lindroth, A., Nilsson, M.B., 2014. A 12-year record reveals pre-growing season temperature and water table level threshold effects on the net carbon dioxide exchange in a boreal fen. Environ. Res. Lett. 9, 055006. https://doi.org/10.1088/1748-9326/9/5/055006

Peltola, O., Hensen, A., Belelli Marchesini, L., Helfter, C., Bosveld, F.C., van den Bulk, W.C.M., Haapanala, S., van Huissteden, J., Laurila, T., Lindroth, A., Nemitz, E., Röckmann, T., Vermeulen, A.T., Mammarella, I., 2015. Studying the spatial variability of methane flux with five eddy covariance towers of varying height. Agric. For. Meteorol. 214–215, 456–472. https://doi.org/10.1016/J.AGRFORMET.2015.09.007

Peltola, O., Vesala, T., Gao, Y., Räty, O., Alekseychik, P., Aurela, M., Chojnicki, B., Desai, A.R., Dolman, A.J., Euskirchen, E.S., Friborg, T., Göckede, M., Helbig, M., Humphreys, E., Jackson, R.B., Jocher, G., Joos, F., Klatt, J., Knox, S.H., Kowalska, N., Kutzbach, L., Lienert, S., Lohila, A., Mammarella, I., Nadeau, D.F., Nilsson, M.B., Oechel, W.C., Peichl, M., Pypker, T., Quinton, W., Rinne, J., Sachs, T., Samson, M., Schmid, H.P., Sonnentag, O., Wille, C., Zona, D., Aalto, T., 2019. Monthly gridded data product of northern wetland

methane emissions based on upscaling eddy covariance observations. Earth Syst. Sci. Data 11, 1263–1289. https://doi.org/10.5194/essd-11-1263-2019

Perryman, C.R., McCalley, C.K., Ernakovich, J.G., Lamit, L.J., Shorter, J.H., Lilleskov, E., Varner, R.K., 2022. Microtopography Matters: Belowground CH4 Cycling Regulated by Differing Microbial Processes in Peatland Hummocks and Lawns. J. Geophys. Res. Biogeosciences 127, e2022JG006948. https://doi.org/10.1029/2022JG006948

Rantanen, M., Karpechko, A.Y., Lipponen, A., Nordling, K., Hyvärinen, O., Ruosteenoja, K., Vihma, T., Laaksonen, A., 2022. The Arctic has warmed nearly four times faster than the globe since 1979. Commun. Earth Environ. 3, 1–10. https://doi.org/10.1038/s43247-022-00498-3

Reichstein, M., Falge, E., Baldocchi, D.D., Papale, D., Aubinet, M., Berbigier, P., Bernhofer, C., Buchmann, N., Gilmanov, T., Granier, A., Grunwald, T., Havrankova, K., Ilvesniemi, H., Janous, D., Knohl, A., Laurila, T., Lohila, A., Loustau, D., Matteucci, G., Meyers, T., Miglietta, F., Ourcival, J.-M., Pumpanen, J., Rambal, S., Rotenberg, E., Sanz, M., Tenhunen, J., Seufert, G., Vaccari, F., Vesala, T., Yakir, D., Valentini, R., 2005. On the separation of net ecosystem exchange into assimilation and ecosystem respiration: review and improved algorithm. Glob. Change Biol. 11, 1424–1439. https://doi.org/10.1111/j.1365-2486.2005.001002.x

Richardson, A.D., Hollinger, D.Y., 2007. A method to estimate the additional uncertainty in gap-filled NEE resulting from long gaps in the CO2 flux record. Agric. For. Meteorol. 147, 199–208. https://doi.org/10.1016/J.AGRFORMET.2007.06.004

Rinne, J., Łakomiec, P., Vestin, P., White, J.D., Weslien, P., Kelly, J., Kljun, N., Ström, L., Klemedtsson, L., 2022. Spatial and temporal variation in $\delta^{13}C$ values of methane emitted from a hemiboreal mire: methanogenesis, methanotrophy, and hysteresis. Biogeosciences 19, 4331–4349. https://doi.org/10.5194/bg-19-4331-2022

Rinne, J., Riutta, T., Pihlatie, M., Aurela, M., Haapanala, S., Tuovinen, J.-P., Tuittila, E.-S., Vesala, T., 2007. Annual cycle of methane emission from a boreal fen measured by the eddy covariance technique. Tellus B 59, 449–457. https://doi.org/10.1111/j.1600-0889.2007.00261.x

Rinne, J., Tuovinen, J.-P., Klemedtsson, L., Aurela, M., Holst, J., Lohila, A., Weslien, P., Vestin, P., Łakomiec, P., Peichl, M., Tuittila, E.S., Heiskanen, L., Laurila, T., Li, X., Alekseychik, P., Mammarella, I.,

Ström, L., Crill, P., Nilsson, M.B., 2020. Effect of the 2018 European drought on methane and carbon dioxide exchange of northern mire ecosystems. Philos. Trans. R. Soc. B 375. https://doi.org/10.1098/RSTB.2019.0517

Roulet, N.T., Lafleur, P.M., Richard, P.J.H., Moore, T.R., Humphreys, E.R., Bubier, J., 2007. Contemporary carbon balance and late Holocene carbon accumulation in a northern peatland. Glob. Change Biol. 13, 397–411. https://doi.org/10.1111/j.1365-2486.2006.01292.x

Rydin, H., Jeglum, J.K., 2013. The Biology of Peatlands. Oxford University Press. https://doi.org/10.1093/acprof:osobl/9780199602995.001.0001

Sabbatini, S., Mammarella, I., Arriga, N., Fratini, G., Graf, A., Hörtnagl, L., Ibrom, A., Longdoz, B., Mauder, M., Merbold, L., Metzger, S., Montagnani, L., Pitacco, A., Rebmann, C., Sedlák, P., Šigut, L., Vitale, D., Papale, D., 2018. Eddy covariance raw data processing for CO2 and energy fluxes calculation at ICOS ecosystem stations. Int. Agrophysics 32, 495–515. https://doi.org/10.1515/intag-2017-0043

Salmon, E., Jégou, F., Guenet, B., Jourdain, L., Qiu, C., Bastrikov, V., Guimbaud, C., Zhu, D., Ciais, P., Peylin, P., Gogo, S., Laggoun-Défarge, F., Aurela, M., Bret-Harte, M.S., Chen, J., Chojnicki, B.H., Chu, H., Edgar, C.W., Euskirchen, E.S., Flanagan, L.B., Fortuniak, K., Holl, D., Klatt, J., Kolle, O., Kowalska, N., Kutzbach, L., Lohila, A., Merbold, L., Pawlak, W., Sachs, T., Ziemblińska, K., 2022. Assessing methane emissions for northern peatlands in ORCHIDEE-PEAT revision 7020. Geosci. Model Dev. 15, 2813–2838. https://doi.org/10.5194/GMD-15-2813-2022

Saunois, M., Stavert, A.R., Poulter, B., Bousquet, P., Canadell, J.G., Jackson, R.B., Raymond, P.A., Dlugokencky, E.J., Houweling, S., Patra, P.K., Ciais, P., Arora, V.K., Bastviken, D., Bergamaschi, P., Blake, D.R., Brailsford, G., Bruhwiler, L., Carlson, K.M., Noce, S., O'doherty, S., Parker, R.J., Peng, C., Peng, S., Peters, G.P., Prigent, C., Prinn, R., Ramonet, M., Regnier, P., Riley, W.J., Rosentreter, J.A., Segers, A., Simpson, I.J., Shi, H., Smith, S.J., Steele, L.P., Thornton, B.F., Tian, H., Tohjima, Y., Tubiello, F.N., Tsuruta, A., Viovy, N., Voulgarakis, A., Weber, T.S., Van Weele, M., Van Der Werf, G.R., Weiss, R.F., Worthy, D., Wunch, D., Yin, Y., Yoshida, Y., Zhang, W., Zhang, Z., Zhao, Y., Zheng, B., Zhu, Qing, Zhu, Qiuan, Zhuang, Q., 2020. The Global Methane Budget 2000–2017. Earth Syst. Sci. Data 12, 1561–1623. https://doi.org/10.5194/essd-12-1561-2020

Šimanauskienė, R., Linkevičienė, R., Bartold, M., Dąbrowska-Zielińska, K., Slavinskienė, G., Veteikis, D., Taminskas, J., 2019. Peatland degradation: The relationship between raised bog hydrology and normalized difference vegetation index. Ecohydrology 12, e2159. https://doi.org/10.1002/eco.2159

Srinivasan, R., Ramachandran, G.N., El-Manzalawy, Y., Honavar, V., 2013. Bonferroni Correction. Encycl. Syst. Biol. 154–154. https://doi.org/10.1007/978-1-4419-9863-7_1213

Stovall, A.E.L., Diamond, J.S., Slesak, R.A., McLaughlin, D.L., Shugart, H., 2019. Quantifying wetland microtopography with terrestrial laser scanning. Remote Sens. Environ. 232, 111271. https://doi.org/10.1016/j.rse.2019.111271

Streiner, D.L., 2005. Finding Our Way: An Introduction to Path Analysis. Can. J. Psychiatry 50, 115–122.

Ström, L., Falk, J.M., Skov, K., Jackowicz-Korczynski, M., Mastepanov, M., Christensen, T.R., Lund, M., Schmidt, N.M., 2015. Controls of spatial and temporal variability in CH4 flux in a high arctic fen over three years. Biogeochemistry 125, 21–35. https://doi.org/10.1007/S10533-015-0109-0/FIGURES/4

Tokida, T., Miyazaki, T., Mizoguchi, M., Nagata, O., Takakai, F., Kagemoto, A., Hatano, R., 2007. Falling atmospheric pressure as a trigger for methane ebullition from peatland. Glob. Biogeochem. Cycles 21. https://doi.org/10.1029/2006GB002790

Tuovinen, J.P., Aurela, M., Hatakka, J., Räsänen, A., Virtanen, T., Mikola, J., Ivakhov, V., Kondratyev, V., Laurila, T., 2019. Interpreting eddy covariance data from heterogeneous Siberian tundra: Land-cover-specific methane fluxes and spatial representativeness. Biogeosciences 16, 255–274. https://doi.org/10.5194/BG-16-255-2019

Turetsky, M.R., Kotowska, A., Bubier, J., Dise, N.B., Crill, P., Hornibrook, E.R.C., Minkkinen, K., Moore, T.R., Myers-Smith, I.H., Nykänen, H., Olefeldt, D., Rinne, J., Saarnio, S., Shurpali, N., Tuittila, E.S., Waddington, J.M., White, J.R., Wickland, K.P., Wilmking, M., 2014. A synthesis of methane emissions from 71 northern, temperate, and subtropical wetlands. Glob. Change Biol. 20, 2183–2197. https://doi.org/10.1111/GCB.12580

Turner, J.C., Moorberg, C.J., Wong, A., Shea, K., Waldrop, M.P., Turetsky, M.R., Neumann, R.B., 2020. Getting to the Root of Plant-Mediated Methane Emissions and Oxidation in a Thermokarst Bog. J. Geophys. Res. Biogeosciences 125, e2020JG005825. https://doi.org/10.1029/2020JG005825

Vesala, T., Kljun, N., Rannik, Ü., Rinne, J., Sogachev, A., Markkanen, T., Sabelfeld, K., Foken, T., Leclerc, M.Y., 2008. Flux and concentration footprint modelling: State of the art. Environ. Pollut. 152, 653–666. https://doi.org/10.1016/j.envpol.2007.06.070

Waddington, J.M., Roulet, N.T., 1996. Atmosphere-wetland carbon exchanges: Scale dependency of CO2 and CH4 exchange on the developmental topography of a peatland. Glob. Biogeochem. Cycles 10, 233–245. https://doi.org/10.1029/95GB03871

Walsh, J.E., 2014. Intensified warming of the Arctic: Causes and impacts on middle latitudes. Glob. Planet. Change 117, 52–63. https://doi.org/10.1016/j.gloplacha.2014.03.003

Wang, J.M., Murphy, J.G., Geddes, J.A., Winsborough, C.L., Basiliko, N., Thomas, S.C., 2013. Methane fluxes measured by eddy covariance and static chamber techniques at a temperate forest in central Ontario, Canada. Biogeosciences 10, 4371–4382. https://doi.org/10.5194/bg-10-4371-2013

Watmough, S., Gilbert-Parkes, S., Basiliko, N., Lamit, L.J., Lilleskov, E.A., Andersen, R., del Aguila-Pasquel, J., Artz, R.E., Benscoter, B.W., Borken, W., Bragazza, L., Brandt, S.M., Bräuer, S.L., Carson, M.A., Chen, X., Chimner, R.A., Clarkson, B.R., Cobb, A.R., Enriquez, A.S., Farmer, J., Grover, S.P., Harvey, C.F., Harris, L.I., Hazard, C., Hoyt, A.M., Hribljan, J., Jauhiainen, J., Juutinen, S., Kane, E.S., Knorr, K.H., Kolka, R., Könönen, M., Laine, A.M., Larmola, T., Levasseur, P.A., McCalley, C.K., McLaughlin, J., Moore, T.R., Mykytczuk, N., Normand, A.E., Rich, V., Robinson, B., Rupp, D.L., Rutherford, J., Schadt, C.W., Smith, D.S., Spiers, G., Tedersoo, L., Thu, P.Q., Trettin, C.C., Tuittila, E.S., Turetsky, M., Urbanová, Z., Varner, R.K., Waldrop, M.P., Wang, M., Wang, Z., Warren, M., Wiedermann, M.M., Williams, S.T., Yavitt, J.B., Yu, Z.G., Zahn, G., 2022. Variation in carbon and nitrogen concentrations among peatland categories at the global scale. PLOS ONE 17, e0275149. https://doi.org/10.1371/JOURNAL.PONE.0275149

Webster, K.L., Bhatti, J.S., Thompson, D.K., Nelson, S.A., Shaw, C.H., Bona, K.A., Hayne, S.L., Kurz, W.A., 2018. Spatially-integrated estimates of net ecosystem exchange and methane fluxes from Canadian peatlands. Carbon Balance Manag. 13, 16. https://doi.org/10.1186/s13021-018-0105-5

Welpelo, C., Dubbert, M., Tiemeyer, B., Voigt, C., Piayda, A., 2024. Effects of birch encroachment, water table and vegetation on methane emissions from peatland microforms in a rewetted bog. Sci. Rep. 14, 2533. https://doi.org/10.1038/s41598-024-52349-0

Weng, H., Lau, K.-M., 1994. Wavelets, Period Doubling, and Time–Frequency Localization with Application to Organization of Convection over the Tropical Western Pacific. J. Atmospheric Sci. 51, 2523–2541. https://doi.org/10.1175/1520-0469(1994)051

Wilczak, J.M., Oncley, S.P., Stage, S.A., 2001. Sonic anemometer tilt correction algorithms. Bound.-Layer Meteorol. 99, 127–150. https://doi.org/10.1023/A:1018966204465/METRICS

Wutzler, T., Lucas-Moffat, A., Migliavacca, M., Knauer, J., Sickel, K., Šigut, L., Menzer, O., Reichstein, M., 2018. Basic and extensible post-processing of eddy covariance flux data with REddyProc. Biogeosciences 15, 5015–5030. https://doi.org/10.5194/bg-15-5015-2018

Yuan, K., Li, F., McNicol, G., Chen, M., Hoyt, A., Knox, S., Riley, W.J., Jackson, R., Zhu, Q., 2024. Boreal–Arctic wetland methane emissions modulated by warming and vegetation activity. Nat. Clim. Change 2024 143 14, 282–288. https://doi.org/10.1038/s41558-024-01933-3

Yuan, K., Zhu, Q., Li, F., Riley, W.J., Torn, M., Chu, H., McNicol, G., Chen, M., Knox, S., Delwiche, K., Wu, H., Baldocchi, D., Ma, H., Desai, A.R., Chen, J., Sachs, T., Ueyama, M., Sonnentag, O., Helbig, M., Tuittila, E.S., Jurasinski, G., Koebsch, F., Campbell, D., Schmid, H.P., Lohila, A., Goeckede, M., Nilsson, M.B., Friborg, T., Jansen, J., Zona, D., Euskirchen, E., Ward, E.J., Bohrer, G., Jin, Z., Liu, L., Iwata, H., Goodrich, J., Jackson, R., 2022. Causality guided machine learning model on wetland CH4 emissions across global wetlands. Agric. For. Meteorol. 324, 109115. https://doi.org/10.1016/J.AGRFORMET.2022.109115

Zhang, H., Tuittila, E.S., Korrensalo, A., Laine, A.M., Uljas, S., Welti, N., Kerttula, J., Maljanen, M., Elliott, D., Vesala, T., Lohila, A., 2021. Methane production and oxidation potentials along a fen-bog gradient from southern boreal to subarctic peatlands in Finland. Glob. Change Biol. 27, 4449–4464. https://doi.org/10.1111/GCB.15740

Zhang, H., Tuittila, E.-S., Korrensalo, A., Räsänen, A., Virtanen, T., Aurela, M., Penttilä, T., Laurila, T., Gerin, S., Lindholm, V., Lohila, A., 2020. Water flow controls the spatial variability of methane emissions in a northern valley fen ecosystem. Biogeosciences 17, 6247–6270. https://doi.org/10.5194/bg-17-6247-2020

Zhang, Z., Poulter, B., Melton, J.R., Riley, W.J., Allen, G.H., Beerling, D.J., Bousquet, P., Canadell, J.G., Fluet-Chouinard, E., Ciais, P., Gedney, N., Hopcroft, P.O., Ito, A., Jackson, R.B., Jain, A.K., Jensen, K.,

Joos, F., Kleinen, T., Knox, S.H., Li, T., Li, X., Liu, X., McDonald, K., McNicol, G., Miller, P.A., Müller, J., Patra, P.K., Peng, C., Peng, S., Qin, Z., Riggs, R.M., Saunois, M., Sun, Q., Tian, H., Xu, X., Yao, Y., Xi, Y., Zhang, W., Zhu, Qing, Zhu, Qiuan, Zhuang, Q., 2025. Ensemble estimates of global wetland methane emissions over 2000–2020. Biogeosciences 22, 305–321. https://doi.org/10.5194/bg-22-305-2025

Zhu, Q., Jacob, D.J., Yuan, K., Li, F., Runkle, B.R.K., Chen, M., Bloom, A.A., Poulter, B., East, J.D., Riley, W.J., McNicol, G., Worden, J., Frankenberg, C., Halabisky, M., 2025. Advancements and opportunities to improve bottom–up estimates of global wetland methane emissions. Environ. Res. Lett. 20, 023001. https://doi.org/10.1088/1748-9326/adad02

Zhuang, Q., Melillo, Jerry M, Sarofim, Marcus C, Kicklighter, David W, Mcguire, A David, Felzer, Benjamin S, Sokolov, Andrei, Prinn, Ronald G, Steudler, Paul A, Hu, Shaomin, Zhuang, C.:, Melillo, J M, Sarofim, M C, Kicklighter, D W, Mcguire, A D, Felzer, B S, Sokolov, A, Prinn, R G, Steudler, P A, Hu, S, 2006. CO2 and CH4 exchanges between land ecosystems and the atmosphere in northern high latitudes over the 21st century. Geophys. Res. Lett. 33, 17403. https://doi.org/10.1029/2006GL026972

Photo: Andreas Palmén

Popular science summary

Global warming and associated climate change due to increasing greenhouse gas concentrations in the atmosphere is one of the major crises for humans to solve in the coming decades. Methane (CH_4) is a powerful greenhouse gas that, over a 20-year time frame, traps 86 times more heat in the atmosphere relative to carbon dioxide.

Northern peatlands are a major natural source of CH_4 and therefore play a crucial role in our climate system. Emissions of CH_4 from peatlands occur because microbial communities in the deeper water-saturated oxygen-free peat layer produce more CH_4 than is consumed in the upper oxygen-rich peat layers. Currently, however, we face considerable challenges in accurately estimating how various factors regulate these CH_4 production and consumption processes across space and time. These factors include water table depth, soil temperature, and plant productivity. Due to the complex interactions between these factors and their high spatial variability, estimates of total CH_4 emissions from northern peatlands, and their associated climate impact, are highly uncertain.

One main constraint for estimating the total CH_4 emissions from northern peatlands is that we typically rely on measurements from small areas (typically < 5 ha) which provide limited understanding of the extent of their variations across large mires (mire complexes). This is problematic because peatland characteristics and CH_4 emissions can vary considerably across even relatively small distances.

To better understand these variations, we used a unique research setup in northern Sweden, where four measurement towers were installed across a peatland complex covering about 7.6 km². Each tower is equipped with sensors that continuously measured CH_4 emissions within a distance of typically less than 200 meters.

To understand the drivers of the variations in these measurements, we created detailed maps of the peatland's surface features, including different vegetation types and microtopography, that is, small-scale elevation differences. We developed a new microtopography model called HuHoLa that not only helped with mapping the microtopography but also provided information about spatial variations in the water table depth and soil temperature across the peatland.

Using these multiple measurement towers, we discovered that some areas consistently released more CH_4 than others even within a single mire complex, with the highest-emitting site releasing about 50% more CH_4 than the lowest-emitting site. Interestingly, we reveal that these differences were mainly linked to the underlying peat properties, as areas with higher carbon-to-nitrogen ratios and less decomposed peat consistently produced more CH_4. We conclude that these peat properties set the baseline for spatial differences in CH_4 emissions, whereas day-to-day variations were mainly controlled by soil temperature and plant activity.

Building on these findings, we developed approaches to estimate peatland complex CH_4 emissions using measurements from a single tower. These methods significantly improved our estimates compared to assuming that measurements from one location represent the entire peatland, reducing uncertainty by up to 50%. This offers a practical way to better estimate CH_4 emissions from large peatland areas where measurements are limited to single locations.

Overall, findings from this research help us better understand how CH_4 emissions vary across peatlands and provide practical tools for scientists to improve regional estimates of peatland CH_4 emissions. This is particularly important as we work to understand how these ecosystems might respond to climate change and how they influence our global climate system.

Populärvetenskaplig sammanfattning

Global uppvärmning och klimatförändringar som följd av ökande koncentrationer av växthusgaser i atmosfären är ett av de största hoten mänskligheten måste lösa under de kommande årtiondena. Metan (CH_4) är en kraftfull växthusgas, som över en 20-årsperiod, fångar 86 gånger mer värme i atmosfären jämfört med koldioxid.

Nordliga myrar är en stor naturlig metankälla och spelar därför en avgörande roll i jordens klimatsystem. Utsläpp av CH_4 från myrar sker i huvudsak då mikroorganismer i de djupare, vattenmättade och syrefria, torvlagren producerar mer CH_4 än vad som konsumeras i de övre syrerika torvlagren. För närvarande står vi dock inför betydande utmaningar när det gäller att korrekt uppskatta hur olika faktorer reglerar produktion och konsumtion av CH_4 i tid och rum. Dessa faktorer är bland annat grundvattennivå, marktemperatur och växtproduktivitet. På grund av de komplexa interaktionerna mellan dessa faktorer och deras höga rumsliga variation är uppskattningar av totala CH_4-utsläpp från nordliga myrar, och deras tillhörande klimatpåverkan, mycket osäkra.

En central begränsning för att uppskatta de totala CH_4-utsläppen från nordliga myrar är att vi vanligtvis förlitar oss på mätningar från små områden (vanligtvis < 5 ha) vilket ger begränsad förståelse för omfattningen av variationer över större områden. Detta är problematiskt då myregenskaper och CH_4-utsläpp kan variera avsevärt även över relativt korta avstånd.

För att bättre förstå dessa variationer använde vi en unik forskningsinfrastruktur i norra Sverige, där fyra mätstationer installerades över ett torvmarkskomplex, som täcker cirka 7.6 km². Varje station utrustades med sensorer som kontinuerligt mätte CH_4-utsläpp inom ett avstånd på vanligtvis mindre än 200 meter.

För att förstå drivkrafterna bakom variationerna i dessa mätningar skapade vi detaljerade kartor över myrens ytegenskaper, inklusive olika vegetationstyper och mikrotopografi, det vill säga småskaliga höjdskillnader. Vi utvecklade en ny mikrotopografimodell kallad HuHoLa som inte bara hjälpte till med kartläggning av mikrotopografin, utan också gav information om rumsliga variationer i grundvattennivån och marktemperaturen över myrkomplexets yta.

Då vi kunde jämföra flera mätstationer nära varandra upptäckte vi att vissa områden i myrkomplexet konsekvent släppte ut mer CH_4 än andra.

Platsen med högst utsläpp släppte ut cirka 50% mer CH_4 än platsen med lägst utsläpp. Vi kan visa att dessa skillnader huvudsakligen var kopplade till de underliggande torvegenskaperna, eftersom områden inom ett myrkomplex med högre kol-till-kväveförhållanden och mindre nedbruten torv konsekvent producerade mer CH_4. Vi drar slutsatsen att dessa torvegenskaper är utgångspunkten för rumsliga skillnader i CH_4-utsläpp, medan dag-till-dag-variationer huvudsakligen styrdes av marktemperatur och växtaktivitet.

Baserat på dessa resultat utvecklade vi metoder för att uppskatta CH_4-utsläpp från myrkomplex baserat på mätningar från endast en mätstation. Dessa metoder förbättrade avsevärt våra uppskattningar jämfört med att anta att mätningar från en plats representerar hela torvmarken, vilket minskade osäkerheten i beräkningarna med upp till 50%. Detta erbjuder ett praktiskt sätt att bättre uppskatta CH_4-utsläpp från stora myrområden där mätningar är begränsade till enstaka platser.

Resultaten från denna forskning har gett oss en bättre förståelse av hur CH_4-utsläpp varierar över myrmarker och har lett till utvekclingen av praktiska verktyg som forskare kan använda för att förbättra regionala uppskattningar av CH_4-utsläpp från myrar. Detta är särskilt viktigt i arbetet att förstå hur myrar både kan reagera på klimatförändringar och hur de påverkar jordens klimatsystem.

Acknowledgements

First and foremost, I thank God for providing me with strength, wisdom, and perseverance throughout this challenging journey. There were moments when I questioned whether I could finish this race, but my faith sustained me and gave me the courage to continue.

My deepest gratitude goes to my supervisors who guided me through this journey with patience, knowledge, and unwavering support. **Matthias**, thank you for your exceptional availability and support. Even during times of sickness or parental leave, you made yourself accessible, and I never had to remind you of any unaddressed questions. Our weekly meetings were moments of learning and enlightenment, where I could bring problems I couldn't solve, and you would provide brilliant suggestions almost immediately. **Mats N.**, starting this journey with you during the pandemic was truly memorable. I appreciated the freedom to explore datasets and your quick, insightful feedback via email and during our supervision meetings. Your immense knowledge in the field makes you a valuable resource I always feel comfortable approaching for assistance. **Mats Ö.**, thank you for your excellent support with fieldwork preparation, especially during the peat pore water sampling. I cherish the memories of our fieldwork with **Jacob**, learning first-hand from you how to conduct proper sampling. Your insights helped me better understand key biogeochemical processes. Thanks for the translations of my abstract and popular science into Swedish. **Natascha Kljun**, it is an honor to have you as a supervisor. Despite the distance, your feedback and availability when I needed clarifications related to your footprint model were invaluable. **Johan**, it has been a pleasure to interact with you. Your expertise in remote sensing significantly shaped those aspects of the project. **Joss**, while you may be an unofficial supervisor, your feedback makes me consider you just as important as the official ones. Thank you for introducing me to the field sites with **Lukas**, teaching me the basics of Eddy covariance data processing, and always providing prompt and encouraging feedback.

I extend my sincere thanks to all the research engineers working behind the scenes to ensure we have high-quality data. Special thanks to **Tommy**, **Rowan**, **Eric**, and **Per** for your assistance with UAV flights, and to all of you plus **Joss**, **Pernilla**, and others for equipment maintenance and data collection. To all lab personnel, though I haven't interacted with everyone,

thank you for preparing the equipment needed for sampling. Your work forms the foundation upon which our research is built.

I am fortunate to have collaborated with so many brilliant minds: **Joss**, **Matthias**, **Järvi**, **Marcus**, **Gillian**, **Natascha**, **Johan**, **Hjalmar**, **Anders**, **Lars**, **Mats N.**, **Mats Ö.**, **Betty**, **Jacob**, **Anneli**, **Jonas B.**, **Nils**, **Sebastian**, **Wei**, **Haijun**, **Charlotta**, **Kevin**, **Stefan**, and **Bwalya**. Thank you for your contributions both to my thesis and in your individual work. It has been a privilege to share these collaborative efforts with you.

Lei, **Järvi**, **Antonia**, **Alex**, and **Sijia**, thank you for proofreading my Kappa and noticing details that I would have missed even if I had looked specifically for them. Your careful attention helped polish my work.

Ulf, thank you for always being available to answer any administrative questions and for quickly addressing any issues that arose. Our interactions have always been a pleasure.

Marcus, thank you for being both a wonderful brother and colleague. I will treasure our time spent at work and church, playing games, reflecting on data processing, and co-authoring papers. **Aswin**, I cherished our time together at the round fika table and beyond, and memories from your help in the field. It was comforting to share similar challenges, and I appreciated being able to learn from your experiences. **Antonia**, thank you for the shared experience of having the same supervisor. I value the memories from fieldwork with you, driving to the field, playing games, and engaging in interesting conversations. **Daniel**, thank you for the fun conversations every time we meet and for the free laughter you bring. **Lukas**, it was great to have started this journey with you. Although we didn't continue together to the end, I am happy for the time we spent together, and happy that you could start over in Germany. **Jacob**, thank you for the interesting fieldwork together. It was great to have started together and, for different reasons, be finishing our PhDs around the same time. **Tong**, thank you for the wonderful memories from fieldwork, carrying liquid nitrogen through the peatlands like in that game you enjoy. **Lei** and **Ruirui**, thank you for being my go-to corridor neighbor-colleagues for lunches together in the fika room in recent months. **Ritwika**, thank you for the shared moments with me and my family, and for the attentions to my sons. It was always interesting to spend time with you. **Shirin**, thank you for the great time at SLU, solving problems together. **Lina**, it's wonderful to see you again here at SLU after meeting in

Padova years ago. I'm glad you could witness the first days of my first son. Thank you for being such a pleasant person.

Thank you **Gillian**, **Alisa**, **Alex**, **Sijia**, **Järvi**, **Antonia**, **Marcus**, and **Matthias** for the engaging Thursday scientific group discussions and fika over the years.

Thanks to **Aswin**, **Betty**, **Vicky**, **Alejandro**, **Kohsuke**, **Marcus K.**, **Lin**, **Mariana**, **Anne**, **Magda**, **Olivia**, **Cedric**, **Samiul**, **Jasmin**, **Shandry**, **Annrose**, **Johannes**, **Alex A.**, **Ritwika**, **Lina**, **Shirin**, **Viktor B.**, **Kishore**, **Maja**, **José**, **Aniceto**, **Marija**, **Jenny**, **Lei**, **Sijia**, **Ruirui**, **Isaac**, **Alisa**, **Bowen**, **William**, **Arvid**, **Jonas**, **Meredith**, **Eliza**, **Joss**, **Barry**, **Alex P.**, **Gillian**, **Martin**, **Ilse**, **Wei**, **Francesco**, **Peta**, **Johan**, **Max, Gillian, Valeria, Desi,** and **Paula** (…) for various reasons I cannot list exhaustively. Above all, thank you for being good friends, good colleagues, and wonderful people. I appreciate every moment shared around the lunch table or during different activities and occasions.

Atif, **Mario**, **Chuxian**, and **Kyohsuke**, thank you for being considerate officemates, making our shared space harmonious.

I am deeply grateful for the family I found in church. **Crosby** and family, thank you for the wonderful fellowship and home group. **Pastor Gustaf** and **Lena**, **Håkan** and **Erika**, **Daniel**, **Pepe**, **Ida**, **Joshua**, **Ida**, **Selina**, some for your leadership, others for the meaningful conversations, others for inspiration and encouragement, and others for the enjoyable times playing music. With a family like you, my time here was much easier, and I always looked forward to our next meeting. Your support, kindness, and the moments we shared refuelled me and sustained me intellectually, emotionally, and spiritually during these intense years.

Thank you to the international Christian home group, particularly **Marcus**, **Thomas**, **Nelson**, **Tinkara**, **Samuel**, **Svenja**, and **Bwalya**, to name just a few. I appreciate our great discussions and communion times.

Thanks to friends I have made along the ALX software engineering path, particularly **Patience**, **Isiaq**, **Seth** and **Stephen**. Your grit encouraged me to do hard things. It was tough combining software engineering with my PhD, but working with such motivated people as you guys was all it took to persevere and gain experience that has been also useful for my PhD journey.

Thanks to friends that checked in often, and encouraged me along the journey: **Julien**, **Modeste**, **Collins**, **George**, **Stéphane**, **Amidou**, **Etienne**, **Samari**, **Hugo**, **Iztok & family**, **Eliza & Flavio** (…). Thanks to those who

are making it all the way from other countries to share the final moments of my PhD time with me: **Samari & Bella**, **Hugo**, and **Célia**.

Thank you to my family, who have always supported me. My Mother **Houndémé** and late father **Kodédjro**, thank you for your unconditional love, and for raising me to be a serious and hardworking person, and for encouraging me and believing in me. Thanks to my brothers and sisters, who, despite the distance, remain close to my heart and remind me how far we have come.

To my wonderful wife **Angèle**, thank you for your support throughout these PhD years. It would have been difficult without you by my side during these challenging times, especially during the long and sometimes depressing winters. To my sons **Geordy** and **Djidula**, who made these years challenging but incredibly fun. Your smiles and laughter always helped keep me going.

A PhD is a bumpy road that requires perseverance and hard work, but above all, it needs companionship, encouragement, and support. It takes a tribe to help one fulfil this commitment. I was immensely fortunate to find the perfect tribe for my journey. Umeå, SLU, and the FEM department provided everything I needed, and for that, I am eternally grateful.

I

frontiers | Frontiers in Earth Science

TYPE Review
PUBLISHED 31 May 2023
DOI 10.3389/feart.2023.1194749

OPEN ACCESS

EDITED BY
Dominic E. L. Ong,
Griffith University, Australia

REVIEWED BY
Mashal Alawi,
Dr. Brill + Partner GmbH, Germany
Xiangjin Shen,
Chinese Academy of Sciences, China

*CORRESPONDENCE
Koffi Dodji Noumonvi,
koffi.noumonvi@slu.se

RECEIVED 27 March 2023
ACCEPTED 05 May 2023
PUBLISHED 31 May 2023

CITATION
Noumonvi KD, Ågren AM, Ratcliffe JL, Öquist MG, Ericson L, Tong CHM, Järveoja J, Zhu W, Osterwalder S, Peng H, Erefur C, Bishop K, Laudon H, Nilsson MB and Peichl M (2023), The Kulbäcksliden Research Infrastructure: a unique setting for northern peatland studies.
Front. Earth Sci. 11:1194749.
doi: 10.3389/feart.2023.1194749

The Kulbäcksliden Research Infrastructure: a unique setting for northern peatland studies

Koffi Dodji Noumonvi[1]*, Anneli M. Ågren[1], Joshua L. Ratcliffe[2], Mats G. Öquist[1], Lars Ericson[3], Cheuk Hei Marcus Tong[1], Järvi Järveoja[1], Wei Zhu[1], Stefan Osterwalder[4], Haijun Peng[1], Charlotta Erefur[2], Kevin Bishop[5], Hjalmar Laudon[1], Mats B. Nilsson[1] and Matthias Peichl[1]

[1]Department of Forest Ecology and Management, Swedish University of Agricultural Sciences, Umeå, Sweden, [2]Unit for Field-based Forest Research, Swedish University of Agricultural Sciences, Umeå, Sweden, [3]Department of Ecology and Environmental Science, Umeå University, Umeå, Sweden, [4]Department of Environmental Systems Science D-USYS, ETH Zurich, Zurich, Switzerland, [5]Department of Aquatic Sciences and Assessment, Swedish University of Agricultural Sciences, Uppsala, Sweden

Boreal peatlands represent a biogeochemically unique and diverse environment in high-latitude landscape. They represent a long-term globally significant sink for carbon dioxide and a source of methane, hence playing an important role in regulating the global climate. There is an increasing interest in deciphering peatland biogeochemical processes to improve our understanding of how anthropogenic and climate change effects regulate the peatland biogeochemistry and greenhouse gas balances. At present, most studies investigating land-atmosphere exchanges of peatland ecosystems are commonly based on single-tower setups, which require the assumption of homogeneous conditions during upscaling to the landscape. However, the spatial organization of peatland complexes might feature large heterogeneity due to its varying underlying topography and vegetation composition. Little is known about how well single site studies represent the spatial variations of biogeochemical processes across entire peatland complexes. The recently established Kulbäcksliden Research Infrastructure (KRI) includes five peatland study sites located less than 3 km apart, thus providing a unique opportunity to explore the spatial variation in ecosystem-scale processes across a typical boreal peatland complex. All KRI sites are equipped with eddy covariance flux towers combined with installations for detailed monitoring of biotic and abiotic variables, as well as catchment-scale hydrology and hydrochemistry. Here, we review studies that were conducted in the Kulbäcksliden area and provide a description of the site characteristics as well as the instrumentation available at the KRI. We highlight the value of long-term infrastructures with ecosystem-scale and replicated experimental sites to advance our understanding of peatland biogeochemistry, hydrology, ecology, and its feedbacks on the environment and climate system.

KEYWORDS

greenhouse gas fluxes, global change, manipulation experiments, mercury, stream carbon export, boreal biome, biogeochemistry, wetland

1 Introduction

Boreal peatlands represent a biogeochemically unique and diverse environment providing a long-term globally significant carbon (C) sink and an important methane (CH_4) source (Frolking and Roulet, 2007). Specifically, they are the most C dense terrestrial ecosystem in the world (Joosten and Couwenberg, 2008; Dunn and Freeman, 2014). Covering less than 3% of land area (Limpens et al., 2008; Frolking et al., 2011), boreal peatlands store C in excess of all the fossil fuels burnt since 1870 (Le Quéré et al., 2018; Ratcliffe et al., 2020). Peatlands are characterized by a high water table which strongly regulates their ecology and biogeochemistry (Mulqueen, 1986), including the production and consumption of greenhouse gases (GHG) such as carbon dioxide (CO_2) and CH_4 (Moore and Dalva, 1993; Shen et al., 2022). The current C and GHG balances of peatlands are however susceptible to ongoing climate change and our knowledge on their responses to these perturbations remains limited.

Peatlands are natural examples of complex adaptive systems (Rydin and Jeglum, 2013). Peatland types show both a latitudinal (zonal) and longitudinal (azonal) differentiation (Ruuhijärvi, 1960; Rydin et al., 1999; Masing et al., 2010) indicating that they respond to thermic and hygric changes in the climate. However, the relative importance of the various components combined with the role of local topographical conditions has demonstrated that responses to climate or nutrient forcing may be elusive (Belyea and Baird, 2006). Peatlands have spatially variable feedbacks which contribute to their iconic 'surface patterning' but importantly also results in a spatial heterogeneity of response to climate and nutrients changes (Eppinga et al., 2007), potentially confounding up-scaling of studies performed at only plot-scales. The response of peatlands to external forcing can also be slow, potentially over the course of centuries (Swindles et al., 2012), as seen in peatlands which have undergone spontaneous recovery after mining or drainage many centuries earlier (Swindles et al., 2016). The considerable complexity of the peatland response to external perturbations necessitates both a long-term and spatially inclusive approach to research.

One common feature of most peatland research settings is that they are focused either on the small-scale variation between different microforms, i.e., hummocks, lawns and hollows (Bubier et al., 1993; Granberg et al., 1997; Korrensalo et al., 2018), or on large-scale variations between clearly distinct peatland systems (Turetsky et al., 2014; Abdalla et al., 2016; Peltola et al., 2019). However, northern peatlands often occur as an ensemble of patches which form heterogeneous peatland complexes, with distinct and yet hydrologically connected units (Pakarinen, 1995; Laitinen et al., 2007). These complexes represent an intermediate spatial scale which is almost completely overlooked in current peatland research. Instead, peatlands are often implicitly studied as homogeneous entities, i.e., assuming that a small area is representative of the entire peatland complex. Specifically, micrometeorological studies of land-atmosphere exchanges (e.g., from eddy covariance, or EC, towers) are often limited to a single site assuming that the footprint of a single flux tower represents large areas surrounding the tower, with little or no validation (Desai et al., 2022). However, upscaling of flux measurements should be done with footprint awareness, i.e., considering the local conditions such as vegetation type and microtopography, that affect the representativeness of EC measurements at the surrounding areas (Chu et al., 2021). Across an entire peatland complex, local conditions on vegetation type, microtopography and hydrology are prone to variation and thus can be expected to affect biogeochemical processes.

At present, only few studies have explored the effects from varying local conditions across peatland complexes. For instance, research in the Siikaneva mire complex in Finland revealed that its fen and bog sections had similar net ecosystem exchange (NEE), but the fen section exhibited higher gross primary production (GPP) and ecosystem respiration (Reco), as well as higher CH_4 emissions compared to the bog section (Alekseychik et al., 2021). A study in a freshwater wetland in California United States combining a stationary and a roving EC tower to compare CH_4 fluxes at three sites within the same wetland system, found substantial heterogeneity in CH_4 fluxes due to spatial variations in air temperature (Ta), friction velocity, and vegetation composition (Matthes et al., 2014). The spatial variability of CH_4 emissions in an agricultural peatland was also observed through the use of EC towers installed at different heights in the Netherlands, which integrated different local conditions as the footprint increased from short towers (6 m height) to taller towers (20 and 60 m height) (Peltola et al., 2015). Different non-coordinated EC towers are in operation in the sub-arctic Stordalen Palsa bog in Abisko, Sweden, with more focus on C fluxes in link with permafrost thawing (Jammet et al., 2017; Łakomiec et al., 2021). Other efforts exist, but mostly limited to short-term infrastructures and other land uses, such as the CHEESEHEAD19 cluster of 20 EC towers investigating the variability of a forested landscape in the upper Midwest United States during 2019 (Desai et al., 2022).

To our knowledge, no coordinated research infrastructures with the aim of investigating ecosystem-scale processes at multiple sites within the same peatland complex in the boreal biome exist. Despite the need for establishing replication, the complex nature and limited accessibility of peatlands encourages the concentration of research within relatively small, dedicated areas, resulting in confined peatland research hubs around the globe. One of these peatland research hubs with long-term records is Degerö Stormyr, Northern Sweden (64° 10′ 55.3″ N, 19° 33′ 23.5″ E) where research on peatland biogeochemistry has been carried out since 1909, with intense contemporary research since 1995 including ongoing EC measurements since 2001. Building on this experimental site, the Kulbäcksliden Research Infrastructure (KRI) was established, including today five peatland study sites located less than 3 km apart within the same peatland complex, to facilitate replicated studies of ecosystem-scale processes. Here, we first present a review of the research history at Degerö Stormyr starting in the early 1900s followed by a comprehensive description of the site characteristics and instrumentation at KRI. We further emphasize the relevance of such replicated ecosystem-scale infrastructures for a better understanding of the biogeochemistry of peatland systems and how they interact with the environment and climate.

2 Review of the infrastructure research history

The research history at Kulbäcksliden is more than a century old, starting in the beginning of the 19th century with the overall aim to provide science-based knowledge on how to manage forests in Sweden. At that time, forest products were one of the fundaments of the Swedish economy. One of the believed major threats to forest growth was paludification, i.e., vertical expansion of mires with the peat mosses

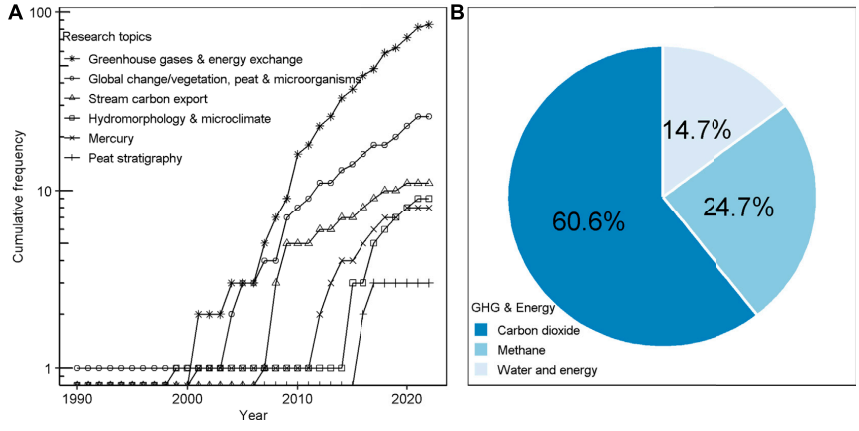

FIGURE 1
Research topics covered at Degerö Stormyr from 1990 to present **(A)** Cumulative frequencies per research topic, note the logarithmic *Y*-axis; and **(B)** relative share in the research topic "greenhouse gases and energy exchange".

transforming soils to conditions that are unsuitable for tree growth. To investigate if this assumption had any scientific support, a study on general mire hydroecology was started in 1909 at Degerö Stormyr, Kulbäcksliden. This study resulted in one of the very first doctoral thesis on general mire ecology and concluded that paludification has halted and that the peat-forming vegetation was mostly connected to sites with shallow groundwater during most of the year (Malmström, 1923). In 1923, Kulbäcksliden was incorporated as part of the Vindeln Experimental Forests, where research has continued until today (Grip, 2015; Laudon et al., 2021).

Most of the historic research was carried out at Degerö Stormyr, the primary hub of the present KRI. After a temporary halt in research activities following these initial investigations during the early 20th century, active research resumed in the late 1990s and has steadily grown until today. A keyword search ("Degerö", "Degerö Stormyr", "Kulbäcksliden", "Krycklan+C18") both on the Web of Knowledge and Google Scholar (on 2 February 2022) generated a database of 142 peer-reviewed articles based on research at Degerö Stormyr either as a single-site study, regional projects or within global synthesis studies. These research articles can be broadly classified into six research topics: peat stratigraphy; mercury; hydromorphology and microclimate; stream C export; global change (mainly temperature, nitrogen, N, and sulphur, S) impact on vegetation development, peat stoichiometry and microbiology; greenhouse gases and energy exchange (Figure 1). A list of all papers included in this review as well as their categorization can be found at https://slughg.github.io/Kulbacksliden-Publications.

Since 2001, research in the area is dominated by studies of the C and greenhouse gas balances (Figure 1A). The number of investigations of the impact of global change on vegetation development, peat stoichiometry and microorganisms has been growing as well, while peat stratigraphy has, to date, been limited to three studies. Within the topic "greenhouse gases and energy exchange", CO_2 exchange was the most studied gas species (61%), followed by CH_4 emissions (25%) (Figure 1B).

2.1 Peat stratigraphy

An early description of peat stratigraphy at Degerö Stormyr was made through multiple cores from a 1,200 m long transect in the direction North-South (Malmström, 1923; Kulczyński, 1949) which were dated using the spruce pollen horizon. However, it was only in 2009 that a high-resolution peat composition and age were investigated with the collection and analysis of a 314 cm long peat core for elemental composition and ^{14}C-dating (Larsson et al., 2017). It was found that organic matter started accumulating prior to 8,300 calendar years BP (i.e. 8300 years before 1950 AD), which was in agreement with the earlier conclusions of Malmström (1923) and Kulczyński (1949). The long-term accumulation rates for C and N were 13.7 ± 5.5 and 0.28 ± 0.14 g m^{-2} yr^{-1}, respectively. ^{13}C content increased with depth and the content in ^{15}N was higher at lower C:N ratios, likely due to preferential utilization of lighter isotope compounds during decomposition (^{12}C) and plant nutrient uptake (^{14}N). It was also apparent that changes in vegetation species composition over time were reflected in the peat C and N content and had a major impact on the degree of organic matter decomposition, thereby also affecting peat growth and decay (Larsson et al., 2017).

2.2 Mercury

Peatlands are considered as hotspots of methylmercury (MeHg) production due to their low redox status and high C content (St. Louis et al., 1996; Bishop and Lee, 1997; Hu et al., 2020). Highly toxic MeHg can be transported to lakes that are hydrologically connected to peatlands (Bergman et al., 2012) and bioaccumulate in its foodwebs (Åkerblom et al., 2014). Given that sulphate-reducing bacteria are one of the primary methylators of reactive mercury (Hg^{II}), investigations of the effect of long-term S deposition on the

methylation of Hg^{II} revealed a linear relationship between MeHg content in pore water and sulphate additions (Branfireun et al., 2001; Åkerblom et al., 2020). However, the effect of increased S loading on MeHg net production was counteracted by increased temperature, most likely due to increased loss of S at higher temperature (Åkerblom et al., 2013). The availability of Hg^{II} in peat that potentially transforms to MeHg also depends on the input of atmospherically deposited Hg by rain (Hg^{II}) and vegetation uptake (Hg^0) as well as the output of Hg via re-emission (Hg^0) (Bishop et al., 2020). Full-year land-atmosphere emission of Hg^0 from Degerö Stormyr was 2.4 times greater than inputs by rain and 7.2 times greater than output with runoff (Osterwalder et al., 2017). This finding indicates that Hg^0 re-emissions from peatlands prolongs the cycling of anthropogenic Hg in the environment, but will decrease Hg contamination of downstream aquatic ecosystems locally. In another study, dynamic flux chambers measurements helped investigate the effect of S and N deposition as well as greenhouse treatments on the net Hg^0 flux (Fritsche et al., 2014). The data revealed that net Hg^0 re-emission was significantly reduced by long-term sulphate additions. These recent investigations on Hg cycling at Degerö Stormyr have important implications for future human consumption of freshwater fish in the region.

2.3 Hydromorphology and microclimate

When research started at Degerö Stormyr in order to investigate the possible paludification of northern Sweden, it consisted of soil sampling for groundwater particle flow (tracer experiment), porosity, hydraulic conductivity, water permeability in undisturbed soil cores, mechanical and chemical analysis. In addition, dissolved compounds (including oxygen) were analysed on groundwater samples (Malmström, 1923). During the last two decades, hydromorphology studies mainly investigated topics such as hydraulic conductivity (Nijp et al., 2017a), peat volume change in relation to microtopography (Nijp et al., 2017b; 2019), and N cycling from mires to surface waters (Sponseller et al., 2018). Efforts have been made also towards modelling (Nijp et al., 2017b), gapfilling and upscaling meteorological variables like water table level (WTL) (Granberg et al., 1999) using remote sensing (Bechtold et al., 2019; Burdun et al., 2020) but also soil temperature (Ts) (Granberg et al., 1999; Vuichard and Papale, 2015; Lembrechts et al., 2021).

2.4 Stream carbon export

Part of the large C stock in mires (Yu, 2012) is continuously transported in different aquatic forms (e.g., dissolved organic or inorganic C) by streams to nearby lakes and other freshwaters. The extent of this phenomenon and its controls have been investigated at Degerö Stormyr and its main draining stream (Ågren et al., 2008; Berggren et al., 2009; Giesler et al., 2009; Campeau et al., 2017), suggesting total C exports in the range from 6 to 18 g C m^{-2} yr^{-1} with a 12 years (2003–2014) average of 12.2 g C m^{-2} yr^{-1} (Leach et al., 2016). Stream and freshwater C support for bacterial growth has also been studied (Berggren et al., 2007; 2009).

2.5 Global change impacts on vegetation development, peat stoichiometry and microorganisms

Response data from plot scale N and S amendments and temperature treatments (Granberg et al., 2001) have been used in several studies which were unanimous on the substantial change in growth, production and competition of plants in response to changes in environmental conditions. One such change is the progressive replacement of the moss carpet by vascular plants with increased N deposition and warming (Gunnarsson et al., 2004; Wiedermann et al., 2007; 2009b; 2009a; Limpens et al., 2011; 2012; Wiedermann and Nilsson, 2020). In the long-term, C input and accumulation was increased by N addition, reduced by S addition, and significant interactions were found between the different factors, i.e., N, S and temperature (Nilsson and Eriksson, 2011; Olid et al., 2014).

The water regime of different mires was found to regulate nutrient allocation, with more nutrients being available in hollows than in hummocks in discharge-dominated mires, compared to evapotranspiration-dominated mires (Eppinga et al., 2010). Increasing Ta and N and S deposition was found to alter the peat geochemistry with an increased retention of Ca, Fe, P, and Zn in the surface peat (Olid et al., 2017).

Microclimate and microtopography control plant (Wiedermann and Nilsson, 2020) and microbial community composition (Økland, 1990; Nilsson et al., 2011; Robroek et al., 2014). Consequently, changes in the local conditions could induce substantial changes in the abundance and activity of microorganisms as observed for the altered activity of methanogens with increased temperature, N and S (Martí et al., 2015; 2019) or the dominance of fungal or bacterial activity depending on the management regime of peatlands (Groß-Schmölders et al., 2020). Increased vascular plant disease occurrence due to parasitic fungi has been observed with increased N deposition which may have important implications for CO_2 and CH_4 exchange between mires and the atmosphere (Wiedermann et al., 2007).

2.6 Greenhouse gas and energy land-atmosphere exchanges

The long-term EC measurements at Degerö Stormyr since 2001 show that the peatland is an annual CO_2 sink with a 12-year mean of 58 ± 21 g C m^{-2} yr^{-1} (Peichl et al., 2014). However, during the unusual drought year of 2018, the mire acted as a net C source (15.2 g C m^{-2} yr^{-1}) for the first time in the measurement record (Rinne et al., 2020). Accounting also for C fluxes via CH_4, total organic C in precipitation and stream C export to estimate the net ecosystem C balance (NECB), suggested a net C sink of 24 ± 4.9 g C m^{-2} yr^{-1} during 2004 and 2005 (Nilsson et al., 2008). Early studies suggested that among the abiotic variables, Ta and WTL explain most of the variance in NEE (Yi et al., 2010), GPP and Reco (Lindroth et al., 2007; Yurova et al., 2007). The length of the growing season (Lund et al., 2010) and light availability (Nijp et al., 2015) are important variables driving summertime GPP and Reco.

Several studies demonstrated that plant development is the dominant control of C fluxes (Järveoja et al., 2018; Peichl et al., 2018; Koebsch et al., 2020). Some cross-seasonal biotic effects have been observed as well, as reflected for instance by strong correlations

between growing season GPP and subsequent winter CH_4 emissions (Zhao et al., 2016b). Continuous automated chamber measurements revealed a divergent diel temperature sensitivity of Reco (Järveoja et al., 2020). A synthesis study found that higher heterotrophic respiration will occur with increased temperature, decreased precipitation and lower WTL as observed during a severe drought in 2018 (Fu et al., 2020). Another global synthesis also reported that their CO_2 sink strength shows a seasonal divergence to increasing temperature, with warmer early summers causing an increased net CO_2 uptake and warmer late summers connected to decreased net CO_2 uptake (Helbig et al., 2022).

Lab incubations have revealed that microbial activity in the peat proceed also when the peat is frozen (Segura et al., 2019). The photosynthesizing biomass of different plant functional types was also important to consider in NEE (Laine et al., 2012). This motivated the use of different satellite-derived vegetation indices (Schubert et al., 2010; Wißkirchen et al., 2013; Zhou S. et al., 2016) or digital repeat photography based chromatic coordinates (Peichl et al., 2015) to explain phenology effects on C fluxes. Remote sensing land surface temperature products were also used to estimate Reco (Ai et al., 2018). Some modelling exercises simulated the sensitivity of Degerö Stormyr and other mires to global change (Wania et al., 2009; Wu et al., 2012; Wu and Roulet, 2014; Metzger et al., 2016).

CH_4 fluxes across global peatlands (including Degerö Stormyr) have been reported to be mainly controlled by WTL, peat temperature and atmospheric pressure (Knox et al., 2021). Investigations of the short- and long-term effects of plot-scale N addition and increased temperature on CH_4 emission at Degerö Stormyr revealed a positive effect of temperature and a negative effect of N addition in the short-term with the opposite effects in the long-term (Granberg et al., 2001; Eriksson et al., 2010a). S pollution was found to reduce CH_4 emissions in peatlands (Gauci et al., 2004). In fact, S treatment seemingly altered the vertical distribution of methanogens and sulfate-reducing bacteria, hence inhibiting CH_4 production only close to the surface while no effect was observed at the depth of maximum production (Eriksson et al., 2010b). CH_4 oxidation has been measured with two new *in situ* approaches at Degerö Stormyr, one using a two-source isotope mixing model (Nielsen et al., 2019), the other based on passive $^{13}CH_4$-pulse labelling through diffuse chambers (Dorodnikov et al., 2022). Several studies modelled CH_4 emissions (Zhu et al., 2014; Zhou

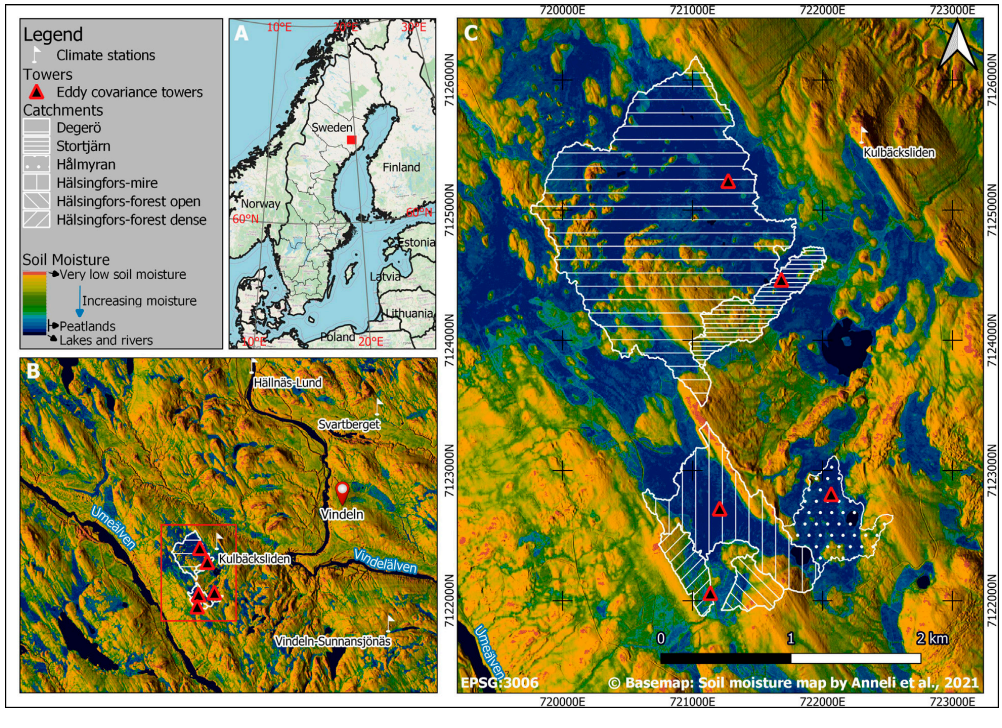

FIGURE 2
Kulbäcksliden Research Infrastructure sites location and its different catchments **(A)** Geographic location within Sweden **(B)** Situation of the catchments between two major rivers, i.e., Umeälven and Vindelälven, with a view of the nearest climate stations (white flags); black and red triangles indicate eddy covariance installations **(C)** Catchments with a soil moisture map (Ågren et al., 2021) background blended with a hillshade derived from a 2 m resolution digital elevation model.

TABLE 1 Coordinates and altitudes of the EC towers and catchment areas for the Kulbäcksliden Research Infrastructure sites.

Site attributes	Degerö	Stortjärn	Hålmyran	Hälsingfors-mire	Hälsingfors-forest
Longitude (E)	19.556543	19.563810	19.569240	19.551496	19.549071
Latitude (N)	64.182029	64.174977	64.159996	64.159555	64.153794
Altitude (m a.s.l.)	265.659	268.890	290.117	291.752	287.137
Area (ha)	273	30	33	65	14 + 12[a]

[a]The area for Hälsingfors-forest is decomposed into areas of the dense section (14 ha) and the open section (12 ha).

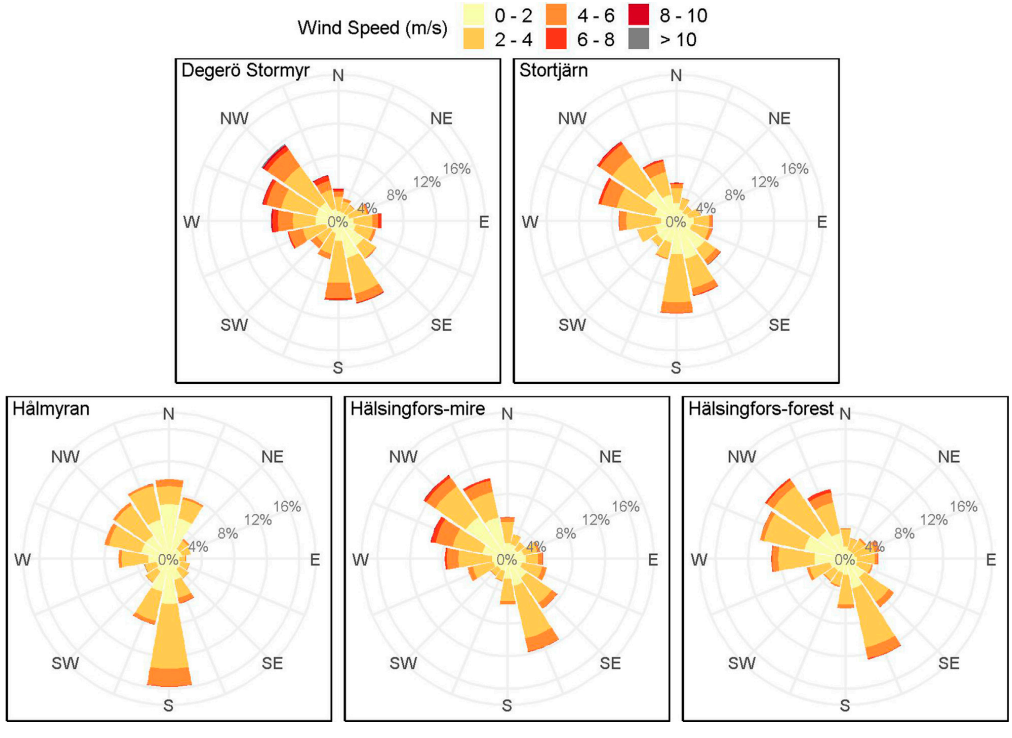

FIGURE 3
Windrose at the different peatland sites, i.e., Degerö Stormyr, Stortjärn, Hålmyran, Hälsingfors-mire and Hälsingfors-forest. The windrose is based on one year wind speed and direction data from May 2020 to April 2021.

Y. et al., 2016; Peltola et al., 2019; Ueyama et al., 2023), making use of global flux datasets (Delwiche et al., 2021).

Studies on the exchanges of water and energy revealed that plant functional type composition, precipitation, radiation amount and timing were the major drivers of the partitioning of mire energy and water budgets at Degerö Stormyr (Peichl et al., 2013). Peatlands have a great climate warming mitigation potential due to some of their biophysical properties such as their relatively higher growing season albedo compared to forests (Helbig et al., 2020a). It has also been reported that the increased sensitivity of peatland evapotranspiration and vapour pressure deficit, relative to boreal forests, puts them at particular risk to increasing air dryness (Helbig et al., 2020b).

3 Description of the Kulbäcksliden Research Infrastructure (KRI) sites

3.1 Geographical situation

In 2018, Degerö Stormyr was extended with 3 more mire sites and a drained peatland forest site to form the KRI. The KRI is

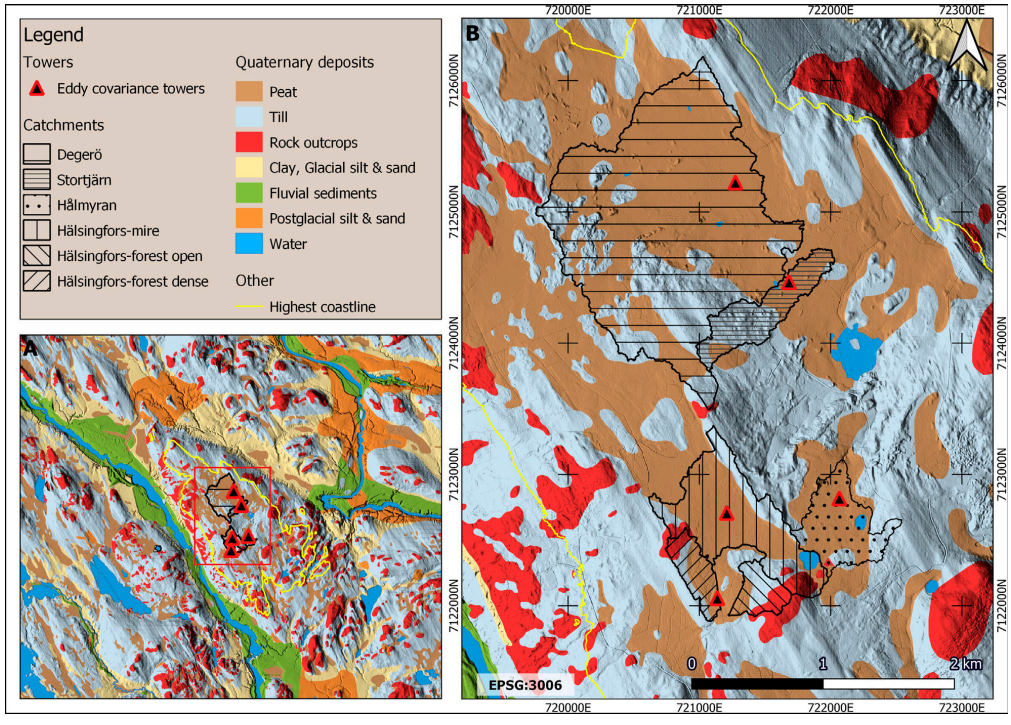

FIGURE 4
Quaternary deposits map of KRI blended with a hillshade derived from a 2 m resolution digital elevation model **(A)** Zoomed-out view of the quaternary deposits map showing the catchments and the highest postglacial coastline **(B)** zoomed-in view of the catchments with their relative share of different quaternary deposits.

located near the municipality of Vindeln, northern Sweden (Figure 2A), on an elevation between two major rivers: Umeälven and Vindelälven (Figure 2B). The research infrastructure at the peatland complex includes four natural mire catchments (Degerö Stormyr, Stortjärn, Hålmyran and Hälsingfors) and a drained peatland forest site (Hälsingfors-forest), the latter divided into two sub-catchments encompassing an open and a dense tree canopy section (Figure 2C). To limit the EC footprint to the mires, the natural mire sites were selected based on the size of the open areas in the mire complex. The few large open areas were examined to verify that they belonged to the same fen system, and that there were no apparent disparities in vegetation type or local conditions. Wind direction was considered while determining the tower location at each site, ensuring that flux measurements originate only from the mire and not the neighbouring forests. The footprints of the EC towers altogether cover comprehensively any heterogeneity in the mire complex.

The Degerö Stormyr and Stortjärn sites are located at slightly lower altitudes (265 and 268 m a.s.l., respectively) compared to Hålmyran, Hälsingfors-mire and Hälsingfors-forest (290, 291 and 287 m a.s.l., respectively). The catchment areas range from 25 ha for Hälsingfors-forest to 273 ha for Degerö Stormyr (Table 1). The prevalent winds originate from the north-west, the south and south-southeast except at Hålmyran, where the predominant wind direction is from the south, reflecting the north-south orientation of the open area created by the forested ridges at the east and west (Figure 3).

3.2 Geology, soils and historic land use

The bedrock consists of paragneiss resulting from the Svecokarelian orogeny (1.92–1.87 billion years ago) (SGU, 1963; Ladenberger et al., 2013). Soils formed from this parent material are often among the most nutrient poor in Fennoscandia (Ivarsson and Bjarnason, 2009; Ruuhola et al., 2016). The peatland complex is situated above the highest postglacial coastline in the area, ~257–259 m above current sea level (Laudon et al., 2021) (Figure 4) and has therefore never been inundated by the sea. However, the highest coastline is located near the edge of the peatland complex and it has been hypothesised that sea level retreat, associated with isostatic rebound, influenced the

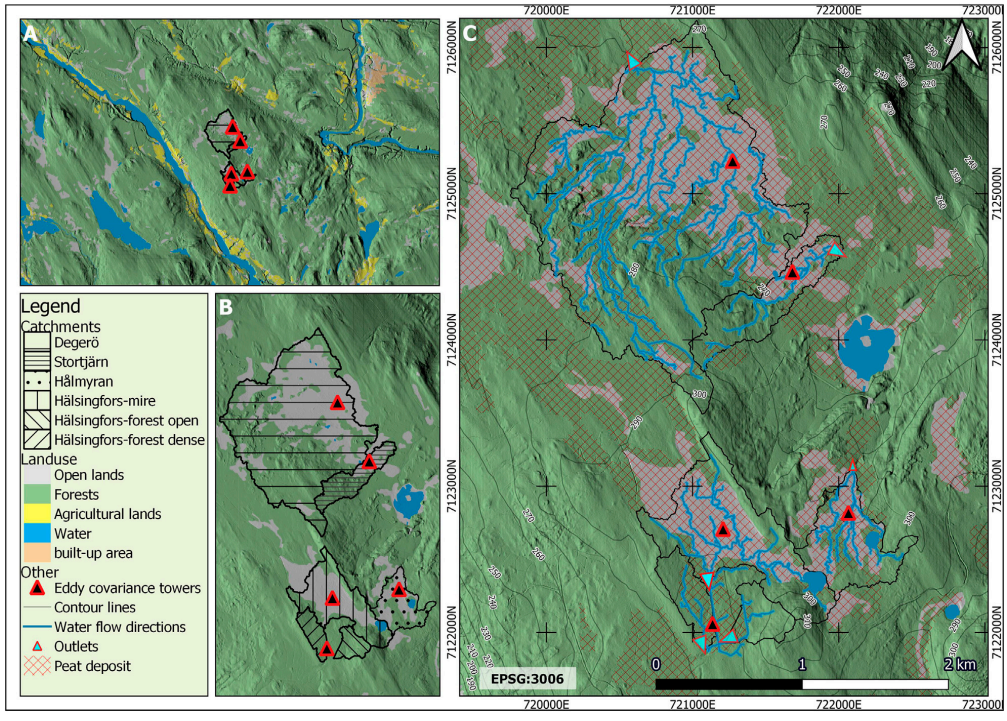

FIGURE 5
Land use and hydrology of the Kulbäcksliden Research Infrastructure **(A)** Zoomed-out view of the land use map **(B)** zoomed-in view showing the different catchments **(C)** zoomed-in view of the land use map indicating in blue the modelled flow direction in the different catchments.

TABLE 2 Fractional cover (%) of the quaternary deposits and land uses at the different catchments. Areal covers of the different combinations of quaternary deposits and land use are available in Supplementary Table S1, APPENDIX A.

		Degerö	Stortjärn	Hålmyran	Hälsingfors- mire	Hälsingfors-forest	
						Dense section	Open section
Quaternary deposits	Till	28	54	20	24	26	47
	Rock outcrops	0	0	1	9	17	31
	Peat	72	46	76	65	58	22
Land use	Forests	58	72	49	47	100	100
	Open lands	42	28	48	50	0	0
	Lakes	0.2	0.1	3	3	0	0

hydrology of the peatland in its early development phase, possibly resulting in erosion (Kulczyński, 1949). The quaternary deposits are dominated by till forming ridges of moraine, on which peat has formed for significant areas of the different catchments filling up many of the small depressions (SGU, 1990).

Soil types are dominated by histosols and podzols (depending on the hydrology) on the till deposits. Forests cover between 47% and 72% of each mire catchment (Figure 5; Table 2). All open lands in the catchments are peatlands, whereas forests have developed on the till and to some extent on the peat covered areas (e.g., at Hälsingfors-

TABLE 3 Thirty years average temperature and precipitation sums for two selected stations of the Swedish Meteorological and Hydrological Institute (Vindeln-Sunnansjönäs station and Hällnäs-Lund station, 11 and 11.3 km away from the study sites respectively) and two reference stations of the Swedish University of Agricultural Sciences (Kulbäcksliden and Svartberget, 1.8 and 13.1 km away from the study sites respectively).

Month	Temperature (°C)				Precipitation (mm)			
	Hällnäs-lund (1961–1989)	Vindeln-sunnansjönäs (1991–2020)	Kulbäcksliden (1991–2020)	Svartberget (1991–2020)	Hällnäs-lund (1961–1989)	Vindeln-sunnansjönäs (1991–2020)	Kulbacksliden (1991–2020)	Svartberget (1991–2020)
1	−12.3	−7.4	−7.2	−8.4	34.1	43.4	44.3	44.1
2	−10.8	−7.4	−7.3	−8.2	26.7	36.5	36.9	36.0
3	−5.7	−3.3	−3.6	−3.9	32.0	34.0	32.8	32.5
4	0.4	1.8	1.5	1.3	29.1	31.2	29.0	30.5
5	7.0	7.7	7.6	7.2	41.1	41.4	41.8	42.0
6	12.7	12.6	12.6	12.3	51.0	59.4	57.7	58.9
7	14.4	15.4	15.4	15.0	70.8	88.9	89.0	88.4
8	12.4	13.6	13.5	13.0	79.9	76.3	83.7	75.6
9	7.3	8.6	8.5	8.0	64.9	57.5	59.2	60.4
10	2.0	2.4	2.2	1.8	56.5	58.5	59.4	60.3
11	−5.2	−2.4	−2.4	−3.1	47.8	54.1	55.8	53.5
12	−10.0	−5.4	−5.3	−6.4	39.4	53.7	56.0	55.0
Annual	1.02	3.02	2.96	2.38	573.3	634.9	645.6	637.2

10.3389/feart.2023.1194749

forest) (Figure 5). Detailed fractional covers of the quaternary deposits and land use classes for the different catchments are presented in Table 2.

Drainage history at the peatland complex is limited to spatially restricted attempts at the edge of Degerö Stormyr back in the end of the 19th century (Malmström, 1923), in addition to the Hälsingfors-forest site which was drained by a network of ditches (still visible today) estimated to ~130 years ago based on unpublished tree ring analysis data.

3.3 Hydrology

Flow accumulation modelling based on a digital elevation model (DEM) provided detailed output information on modelled flow directions at KRI (Figure 5C). More details on the flow accumulation modelling can be found in APPENDIX B of Supplementary Materials. Apart from a few ditches and small streams, most of the water movements in the catchments are surficial groundwater movements in the upper parts of the soil where the peat is less decomposed or where the till is less compacted (Ågren et al., 2008). As the peatland complex is situated at the apex of a wide and shallow ridge between two rivers, the different parts drain in different directions; Degerö and Hålmyran drain to the north, Stortjärn to the north-east, while Hälsingfors (mire and forest) drains south/south-west.

3.4 Climate

Several meteorological stations exist in the vicinity of the study area (Supplementary Table S2, Supplementary Materials APPENDIX C). A selection of the four closest stations (Figure 2B) give a representation of the span of temperature and precipitations (Table 3) in the surroundings of the study area (SLU, 2021; SMHI, 2021). Locally, topography can have a strong influence on microclimate with large differences between south and north slopes and cooler heavier air draining into the valleys and hollows.

The climate in the area can be defined as subarctic (Dfc) after Köppen-Geiger (Peel et al., 2007), or more specifically a cold temperate humid climate with mean annual precipitation and temperature of 645 mm and +3°C, respectively, with the mean temperatures in July and January being +15.4°C and −7.4°C, respectively (Figure 6). These climate descriptors are 30 years average (1991–2020) from the SLU reference climate station Kulbäcksliden.

3.5 Vegetation classification

The vegetation at the mire sites can be grouped into six broad categories (group I to VI) depending on the microtopography (hummocks, lawns, carpets, loose-bottoms and pools) and vegetation types (Table 4). Detailed information on vegetation types as well as the classification methodology and results are available in Supplementary Materials APPENDIX D.

The percentage share for each of the different groups per catchment and footprint area (Table 5) shows that their cover vary considerably from one catchment to the other. Within the 90% footprint area, there is almost no forest on mineral soils (group VI) at any of the sites. It is also noticeable that the wettest vegetation groups (groups III and II) represent the dominant vegetation at Degerö Stormyr and Hälsingfors in the 90% footprint area whereas the drier lawn communities (group I) prevail at Stortjärn and Hålmyran.

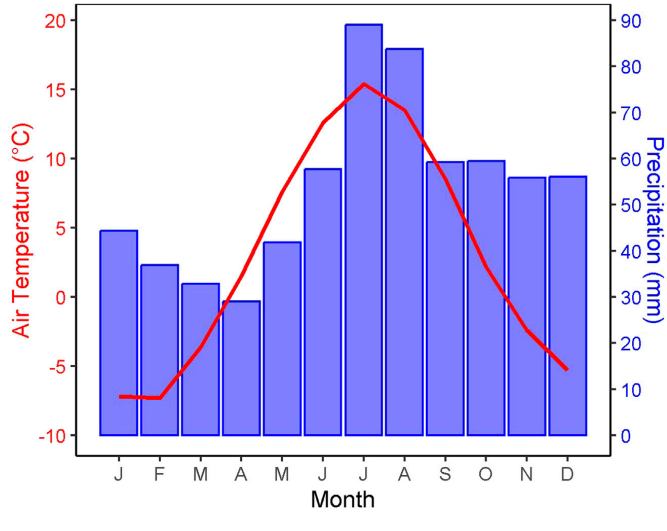

FIGURE 6
Climograph from the SLU reference climate station Kulbäcksliden (1991–2020).

TABLE 4 Vegetation groups (visualized in Figure 7), vegetation types, important plant species, and some comments on ecology (see APPENDIX D for details).

Group	Dominant species	Comments
I: Lawns dominated by short sedges and Sphagna	*Eriophorum vaginatum, Trichophorum cespitosum, Carex pauciflora, Andromeda polifolia, Oxycoccus palustris, Sphagnum angustifolium, S. balticum, S. medium, S. rubellum, S. compactum, S. papillosum*	Dominant in the peripheral areas of the open mire
		The *Trichophorum-S. compactum* type indicates unstable hydrology. Other short sedge-*S. papillosum* types indicate stable hydrology
		Includes both ombrotrophic (*S. papillosum* absent) and minerotrophic (oligotrophic) vegetation types
II: Carpets dominated by short sedges and *Sphagnum* subg. *Cuspidata*	*Eriophorum vaginatum, Trichophorum cespitosum, Scheuchzeria palustris, Andromeda polifolia, Oxycoccus palustris*	Characterize string flark fens in central patterned aapa mires, and flarks in string mixed mires
	A closed carpet of *Sphagnum* subg. *Cuspidata* (*S. balticum, S. majus, S. lindbergii, S. jensenii*) + *S. papillosum* or *S. compactum*	For *S. compactum* and *S. papillosum* types see I. Only oligotrophic types
III: Mud/loose bottoms, tall sedge fens	*Scheuchzeria palustris, Carex limosa, Trichophorum cespitosum* (tussocky), *Drosera longifolia, Sphagnum* subg. *Cuspidata*	Characterize extensive wet flarks in central string-flark (*Sphagnum* flark fen) and flark fens (*S. majus* flark fen)
	Cladopodiella fluitans	Declining Sphagna and *Trichophorum* tussocks replaced by liverworts indicate unstable hydrology
	Menyanthes trifoliata	The *Menyanthes* type border ponds with stable hydrology
	Carex rostrata, Sphagnum fallax, Warnstorfia spp.	*C. rostrata-S. fallax* type extensive stands in central stringless fens (Hälsingfors, Degerö), also slightly mesotrophic (*Warnstorfia*-type)
IV: Hummocks and sparsely treed mires	*Pinus sylvestris, Betula nana, Andromeda polifolia, Calluna vulgaris, Empetrum nigrum. E. hermaphroditum, Oxycoccus microcarpus, Vaccinium uliginosum, V. vitis-idaea, Eriophorum vaginatum, Rubus chamaemorus, Sphagnum angustifolium, S. fuscum, S. medium, S. rubellum, Pleurozium schreberi, Cladonia mitis, C. stygia*	Various *Sphagnum fuscum* bogs (*Andromeda-*, *Calluna-*, *Empetrum nigrum-*, *E. hermaphroditum*-types) as islands in island mixed mires and strings in string mixed mires
		The dominance of *Calluna* types are characteristic for the area
		Combination types, short-sedge pine fens, dominate the transition from open mire to mire forest, due to outflow of minerogenic groundwater
V: Mire forests including high hummocks	*Pinus sylvestris, Betula pubescens, Picea abies, Betula nana, Andromeda polifolia, Empetrum hermaphroditum, Ledum palustre, Oxycoccus* spp., *Vaccinium myrtillus, V. uliginosum, V. vitis-idaea, Eriophorum vaginatum, Carex globularis, Dactylorhiza maculata, Rubus chamaemorus, Sphagnum angustifolium, S. divinum, S. giergensohnii, S. russowii, Polytrichum commune, Pleurozium schreberi, Hylocomium splendens, Dicranum* spp., *Cladonia* spp.	Various pine- and spruce mires characterized by minerotrophic influence.
		Pine-birch fens (*Eriophorum* and *C. globularis* types) characteristic for areas with stronger groundwater influence.
		Ombrotrophic areas of limited importance except for the higher strings in mixed mires.
	Carex rostrata, Sphagnum angustifolium, S. fallax, S. flexuosum, S. riparium	Wet combination types with tall sedges, *Carex rostrata*, and covering Sphagna in areas with groundwater outflow, in outlet areas and at brooks, both oligo- and mesotrophic
VI: Forests on mineral soils	*Pinus sylvestris, Betula pubescens, Picea abies, Calluna vulgaris, Empetrum hermaphroditum, Linnaea borealis, Vaccinium vitis-idaea, V. myrtillus, V. uliginosum, Deschampsia flexuosa, Dicranum* spp., *Polytrichum* spp., *Hylocomium splendens, Pleurozium schreberi, Ptilium crista-castrensis, Barbilophozia lycopodioides, Cladonia* spp.	Situated outside the mire system although within the catchment area
		Species poor heath forests of *Cladina* type, *Empetrum-Calluna* type, *Empetrum-Vaccinium* type, *Vaccinium-Myrtillus* type
		Only a few low-herb species do occur

Vegetation classification based on the previous grouping illustrates the spatial distribution of the vegetation types in a radius of 300 m from each eddy covariance tower (Figure 7). A higher resolution map is available at https://gis-slu.maps.arcgis.com/apps/View/index.html?appid=7d485f469233422aa98a5d49e031fd44.

At the forested site (Hälsingfors-forest), *Pinus sylvestris* is dominant (90%) in the open forest section, while *Picea abies* and *Betula pubescens* are dominant (37% and 56%, respectively) in the dense forest section. The understorey in the open section is composed of dwarf-shrub species such as *Andromeda polifolia*, *Calluna vulgaris*, *Empetrum hermaphroditum*, *Oxycoccus microcarpus*, the graminoid *Eriophorum vaginatum* and *Sphagnum* spp. (*Sphagnum angustifolium, Sphagnum fuscum*) together with *Pleurozium schreberi*. The understorey in the dense forest section, a mesic-moist dwarf-shrub type, is dominated by *Vaccinium myrtillus* and *Vaccinium vitis-idaea* together with *Rubus chamaemorus* and forest mosses *Hylocomium splendens*, *P. schreberi* and *Dicranum* spp.

4 Instrumentation and experiments

The main instrument installations at KRI (Supplementary Table S4, Supplementary Materials APPENDIX E) are almost all located within the 90% footprint of the EC towers (Figure 8).

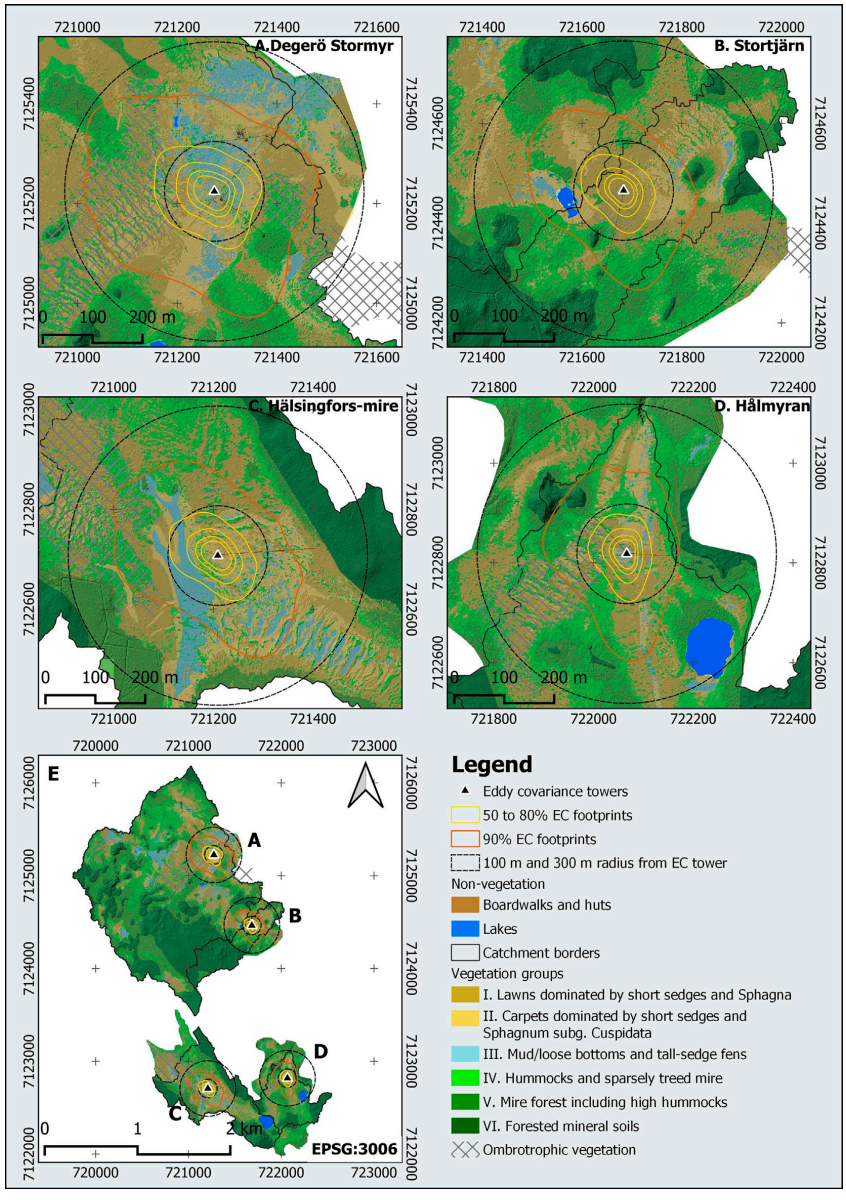

FIGURE 7
Vegetation classification map of the mire sites of the Kulbäcksliden peatland research infrastructure with a focus on a 300 m radius from EC towers at **(A)** Degerö Stormyr, **(B)** Stortjärn, **(C)** Hälsingfors-mire, **(D)** Hålmyran, and **(E)** an overview of all four catchments. The footprint climatologies were calculated from 1-year data wind speed and wind direction (May 2020 to April 2021) based on Kljun et al. (2015). The vegetation groups layer is blended with a hillshade derived from a 0.5 m resolution digital elevation model.

TABLE 5 Percentage share of the different groups of vegetation per catchment, 80% and 90% footprint climatology area. The same information for 50%, 60% and 70% footprint climatology areas is available in Supplementary Table S3 of Supplementary Materials APPENDIX D.

Zone	Mire site	Total area (ha)	Percentage (%) of total area							
			Group I	Group II	Group III	Group IV	Group V	Group VI	Board-walks	Water
Catchments	Degerö Stormyr	273	16	8	4	23	21	28	0.2	0.2
	Stortjärn	30	14	7	0.6	11	10	58	0.1	0.1
	Hålmyran	33	23	7	2	31	14	21	0.1	3
	Hälsingfors	65	20	11	5	18	13	32	0	3
Footprint 90%	Degerö Stormyr	15	33	31	12	20	4	0	0.5	0.1
	Stortjärn	8	48	21	2	21	5	1	0.2	2
	Hålmyran	7	34	18	4	34	7	2	0.2	0
	Hälsingfors	10	27	35	19	20	0.7	0	0.1	0

4.1 Eddy covariance flux towers for monitoring land-atmosphere exchanges of CO2, CH4, water vapour, energy and Hg^0

An EC flux tower is located in the centre of each of the sites within KRI (Figure 8). The EC tower at Degerö Stormyr was established in 2001, and has since then provided near-continuous measurements of CO_2 and water vapour (H_2O) (Nilsson et al., 2022). The EC towers at the remaining sites were established during 2019 and are in operation since 2020. The instrumental setup is consistent at the new sites, whereas the need for standardisation across the Integrated Carbon Observation System (ICOS) was considered at the ICOS Degerö station. Specifically, the EC setup at Degerö initially included a LI-6262 gas analyser which was replaced by a LI-7200 gas analyser in 2014. Since 2013 an additional combined CO_2/H_2O and CH_4 analyser (Los Gatos Research, LGR FGGA 911-0010) was added to the EC system at Degerö Stormyr. The three new mire stations Stortjärn, Hålmyran and Hälsingfors-mire are equipped with a CO_2-CH_4-H_2O Picarro G2311-f analyser. At the Hälsingfors-forest site, the EC system includes a LGR CO_2-CH_4-H_2O analyser (LGR FGGA 908-0010). As part of the above described EC systems, a 3D ultrasonic anemometer has been installed at each site to measure wind speed and wind direction. Current installations consist of a Gill HS-50 anemometer installed at a height of 3.07 m at Degerö Stormyr in conformity with ICOS standards, and a Metek uSonic-3 Class A anemometer was mounted at the other KRI sites, at 2.75 m height at the other three mire sites and at 20.2 m height at the Hälsingfors-forest. The current installations are closed path systems so the air inlet is mounted at the same height as the anemometer at each site.

The land-atmosphere exchange of gaseous elemental mercury (Hg^0) is measured using the EC technique at Degerö Stormyr and Hälsingfors-forest sites with two new Eddy Mercury 2.0 systems installed in October 2021. The systems were developed based on the first Eddy Mercury system that measured grassland-atmosphere exchange of Hg^0 at the Swiss FluxNet site Chamau (CH-CHA) in 2018 (Osterwalder et al., 2020). In short, the Eddy Mercury 2.0 consists of a Metek uSonic-3 Class A MP anemometer to record wind data and of a Lumex RA-915 a.m. mercury monitor (Lumex Ltd.) to measure ambient Hg^0 concentration. The uSonics and air inlets for both closed-path systems were mounted at 2.75 m height at Degerö Stormyr and at 20.2 m height at Hälsingfors-forest. Specific software was implemented to measure the Hg^0 concentrations at a frequency of 16 Hz and to achieve real-time merging of high resolution data from both the uSonic and the RA-915 am. The Hg^0 fluxes are calculated into 30 min averages and flux data quality control procedures are established based on data quality control information from the concurrently running CO_2-CH_4-H_2O EC system to retain or reject Hg^0 fluxes. In addition, long-term ambient Hg^0 concentration measurements using Mercury Passive Air Sampler (MerPAS, Tekran Instruments Corporation) were initiated at Degerö Stormyr in 2022. At Degerö Stormyr, ambient Hg^0 concentration and peatland-atmosphere exchange of Hg^0 have been measured intermittently with diverse methods since 2009 (Fritsche et al., 2014; Osterwalder et al., 2016; 2017; 2018).

4.2 Ancillary meteorological and soil environmental measurements

Each flux tower is equipped with a standard suite of instrumentation for measuring meteorological variables to support the EC data. At the Hälsingfors-forest site, meteorological sensors are installed on the flux tower as well as on a separate flagpole to monitor the dense and open forest parts of the study site, respectively. At each site, the current instrumentation includes.

- Ta and humidity sensors (Rotronic MP102H-331000 at Degerö Stormyr and HC2S3 at the other sites),
- Rain gauges (Lambrecht Rain [e]H3 at Degerö Stormyr and ARG100 at the other sites except Hälsingfors-forest which has no precipitation sensor),
- Global radiation sensors (CMP21, Kipp and Zonen only at Degerö Stormyr),

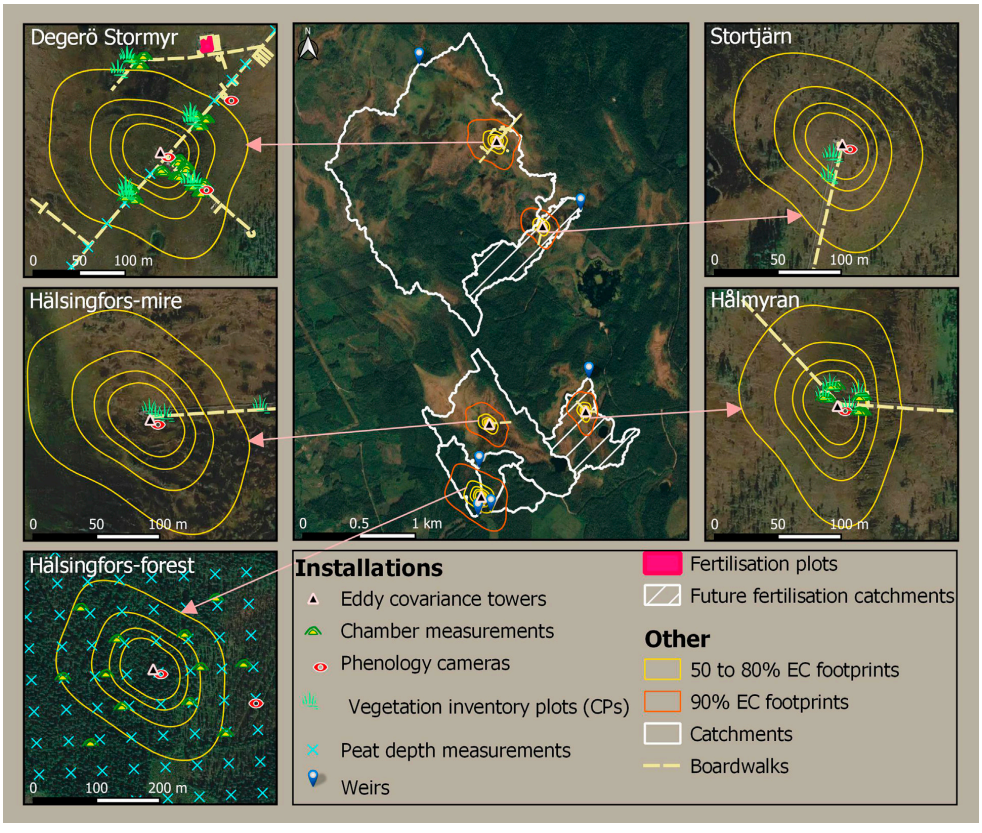

FIGURE 8
Location of the main installations and experiments at the Kulbäcksliden Research Infrastructure (KRI). The footprint climatologies were calculated from one year data wind speed and wind direction (May 2020 to April 2021) based on Kljun et al. (2015).

- Incoming and outgoing shortwave/longwave radiation sensors (CNR4, Kipp and Zonen at Degerö Stormyr and NR01 Campbell Scientific (CS) at the other sites),
- Photosynthetically active radiation (PAR) sensors (LI-190 at all sites).

In addition, Ts at 2, 10, 15, 30, and 50 cm depth and WTL measurements are carried out at replicated plots (six at Degerö Stormyr, two at each of the other sites). The instrumentation includes Ts sensors (Fischer Pt 100 at Degerö Stormyr and TR03 TOJO Skogsteknik at the other sites) and WTL sensors (CS450 at Degerö Stormyr and CS451 at the other sites).

4.3 Phenology observations

To monitor the phenology of the vegetation at each of the peatland sites, digital repeat photography is applied through the installation of phenology cameras (Figure 8). At Degerö Stormyr, a Canon A480 operated from 2011 to 2014, substituted by a Canon PowerShot A810 between 2014 and 2022, itself replaced in 2022 by a Mobotix Mx-M26B-6D. In addition since 2016, a Stardot Netcam SC camera was in operation at Degerö Stormyr as part of ICOS and a Mobotix Mx-M26B-6D061 as part of the Swedish Infrastructure for Ecosystem Sciences (SITES)-Spectral. SITES-Spectral also supports the monitoring of plant vegetation indices (NDVI, SWIR, PRI) as a proxy for vegetation development using fixed spectral sensors (SKYE; SK-1860) mounted to a 20 m flagpole. At each of the other mire sites, a Canon PowerShot A810 camera was in operation since 2020, replaced by Stardot Netcam SC cameras in 2022. At Hälsingfors-forest, two Wingscapes Timelapse cameras were in operation from 2020 to 2022, monitoring each the dense and open areas of the forest. In 2022, they were replaced with Stardot Netcam SC cameras. The phenology cameras record images with a 1-h time resolution and oversee the northern parts of the main EC footprint. In addition to the phenology cameras, NDVI is also

monitored using fixed-spectral sensors (Decagon SRS) at the new KRI sites.

4.4 Multispectral UAV images at the mire sites

Since 2021, aerial images were collected over the four mire sites, covering at least the 80% footprint of the EC tower at each site. The campaigns were conducted towards the end of each month, from May to September. In 2021, a MAIA multispectral camera mounted on a DJI matrice UAV was used at a flight height of 60 m for the campaigns except in July when a Parrot Sequoia multispectral camera mounted on a 3DR Solo UAV was used instead at a height of 30 m. In 2022, a DJI Phantom 4 multispectral UAV was flown at ~55 m height. In either case, the resulting orthomosaics had ~3 cm pixel resolution on the ground.

4.5 Continuous vegetation inventory plots

In order to assess the growth of vascular plants and mosses, continuous measurement plots (CP) have been installed at each of the mire sites (Figure 8), consisting of 60 × 60 cm squares. In total, 16 CPs were installed at Degerö Stormyr and four CPs at each of the other three mires, spanning both lawn and hummock locations. At each CP, five subplots of 8 × 8 cm are marked in which vegetation height is measured every second week at the CP level, i.e., the average height of the ten tallest individuals in the CP. Green area index and above ground biomass are also estimated at the species level in the subplots using a combination of non-destructive methods within the subplots and destructive methods outside the CP, with specific approaches depending on the plant functional type. More specifically, for mosses a brush wire is inserted into the peat, and moss growth is derived from the height difference of the visible part of the brush at beginning and end of the growing season. In addition, the number of living moss stems (moss stem density) is counted per species in the subplots at the end of the growing season, and samples of the moss carpet that have grown out of a mesh placed at the beginning of the growing season are taken for dry weight calculation. For vascular plants, the number of leaves and stems of individuals is counted inside the CP and the average leaf area and dry weight are calculated on the samples collected outside the CP. All measurements are carried out following the ICOS protocol for mire vegetation monitoring (ICOS, 2020).

4.6 Manual and automated chambers for measuring CH_4 and CO_2 land-atmosphere exchanges

Fluxes of CH_4 and CO_2 have been measured using manual chambers (Figure 8) at Degerö Stormyr between 2004 and 2014 at the original six CPs, as well as at experimental N-S-addition, warming and snow exclusion plots (Eriksson et al., 2010a; Zhao et al., 2016a). The CO_2 fluxes were quantified *in situ* with a custom-made portable infrared gas analyzer system (with a PP Systems measurement cell), while repeated air samples drawn with a syringe were analyzed in a gas chromatograph in the lab to determine CH_4 fluxes. Between 2014 and 2018, a LGR UGGA analyzer was used to measure both CH_4 and CO_2 fluxes in the field.

Since 2018, forest floor CO_2 and CH_4 fluxes have been measured every second week at Hälsingfors-forest with the closed dynamic chamber technique during snow-free seasons. Measurements are taken at 12 spatially equally distributed plots (Figure 8) in the open and dense forest sections, where two measurement frames (48.5 × 48.5 cm) were inserted into the soil, one in a natural setting and the other in an area where all aboveground plant and moss vegetation was clipped and removed within the measurement frame in order to estimate heterotrophic respiration. The fluxes were determined with a LGR UGGA (model 915-0011) in 2018 and with a Picarro GasScouter™ G4301 since 2019.

A custom-made automated chamber system has been in operation at Degerö Stormyr since 2014 (Järveoja et al., 2018; 2020; Nielsen et al., 2019). This system includes 12 chambers connected in a closed loop to originally a CO_2-CH_4 LGR analyzer (model GGA-24 E P). The chambers are located within the EC footprint (Figure 8) and distributed in four replicate groups over natural and trenching/vegetation removal plots to partition the hourly to 2-hourly resolution NEE into GPP, net primary production, and Reco, i.e., both autotrophic respiration and heterotrophic respiration, using a mass balance approach (Järveoja et al., 2018). In 2017, the LGR analyzer was replaced by a Picarro isotope analyzer (Picarro G1101-I.) that also determines the $^{12/13}C$ stable isotope ratios for both CO_2 and CH_4. Combined with the experimental plot setup, this allows for quantifying CH_4 oxidation (Nielsen et al., 2019). In 2020, additional moss-only plots were established by clipping all vascular plants to separate the contributions from vascular plants and mosses. At each chamber, headspace Ta and PAR, Ts (2 and 10 cm depth) and WTL are recorded. Additionally, vegetation inventory conducted every second week and seasonal brush wire measurements deliver chamber-specific information on plant and moss production, respectively.

In 2022, a second automated chamber system was installed at the Hålmyran mire within the EC flux footprint. This system also includes 12 chambers (Figure 8) and mirrors the latest experimental set up at Degerö Stormyr to estimate NEE, GPP and Reco at natural and moss-only plots, and Rh at vegetation removal plots. Additionally, the same abiotic (Ta, Ts, PAR and WTL) and vegetation data (vascular plants and moss growth) are collected at each chamber. In contrast to the custom-built Degerö Stormyr system, the Hålmyran system is equipped with Eosense chambers (model eosAC-LT/LO) and the CO_2-CH_4 concentrations are determined with a LGR UGGA analyzer (model 915-0011).

4.7 Continuous measurements of water discharge and water chemistry

A weir has been installed at the outlet of each catchment and equipped with sensors for recording hourly average water height, partial pressure of CO_2 (pCO_2), water and Ta (Figure 5). The weir at Degerö Stormyr is located inside a small house set-up on a flume and heated during winter, hence allowing for year-round measurements. The weirs at the other sites are a V-Notch type set-up in open-air, causing discontinuous measurements during winter and so the wintertime data is derived through regressions with the nearby heated and non-

heated weirs. In addition to the sensor measurements at the weirs, water samples are collected once to three times a week during the freshet, i.e., spring flood, once a month during winter and every second week the rest of the time. The collected samples are analyzed for pH, total organic C (TOC), dissolved inorganic C (DIC), CH_4-C, ^{18}O, nutrients, anions, cations, methylmercury, total mercury and the dissolved organic C absorbance and fluorescence properties (Leach et al., 2016).

4.8 Warming, nitrogen and sulphur addition and snow exclusion plot-scale experiments

In order to investigate the response of mire vegetation to global changes, a 21-plots factorial experiment with warming effect (greenhouse treatment) as well as N (as ammonium nitrate, i.e., NH_4NO_3) and S (as sodium sulfate, i.e., Na_2SO_4) additions was set up in 1995, and is still maintained at Degerö Stormyr. The greenhouse enclosure increases the average yearly temperature by 3.6 °C. N and S are added at rates of 30 and 20 kg ha^{-1} yr^{-1}, respectively as compared to their background levels or controls of 2 and 3 kg ha^{-1} yr^{-1} for N and S, respectively. The full experimental setting was described by Granberg et al. (2001).

Snow exclusion plots were set up since 2003 in order to study the effects of an enhanced soil frost regime (which could happen naturally as a consequence of snow reduction induced by the ongoing climate change) on different biogeochemical processes. In total, six plots (3 × 3 m each) separated by a 1.5 m buffer zone were created and snow is excluded via a temporary enclosure every winter from three of the plots, while the other three plots remain uncovered and serve as controls (Zhao et al., 2016a).

4.9 Replicated ecosystem-scale N addition experiment

Starting in 2024, a unique ecosystem-scale N-fertilization experiment will be carried out at the Stortjärn and Hålmyran catchment sites. Specifically, N in the form of pellets will be spread via helicopter over the entire catchment and EC footprint areas once per year before mid-summer, at a rate of ~10 kg ha^{-1} yr^{-1}. Dedicated subplots will be covered during the helicopter N application and manually fertilized to ensure consistent N addition rate for experimental plot-scale studies. This experiment will provide an exceptional opportunity to study the ecosystem-scale responses of the water and energy balances to N addition, and how these interact with changes in mire biogeochemistry and land-atmosphere exchanges of GHGs, water and energy.

4.10 LiDAR data

The Kulbäcksliden area has been scanned with LiDAR repeatedly, twice in the national LiDAR scans by Lantmäteriet; in 2010 with a point density of 0.5 points m^{-2} and in 2019 with a point density of one to two points m^{-2}. In addition, the area has been scanned twice during different research campaigns, allowing for high resolution DEMs down to 0.5 m resolution and providing detailed ground- and tree-level data. The first specific scanning was conducted in 2006 by Blom Geomatics at a flight elevation of 1,100 m with a point density of up to 10 points m^{-2}. In 2019, the area was scanned with a Riegl VQ-1560i-DW 532 nm (green) and 1,064 nm (NIR) with an average point density of 20 points m^{-2}.

4.11 Ground penetrating radar (GPR) data and other peat depth measurements

During winter in 2016, a campaign was conducted to measure peat thickness at Degerö Stormyr using a MALÅ ground-penetrating radar (MALÅ Geosciences, Sweden) with a 100 MHz shielded antenna towed using a snowmobile. Traces (16 stacks each) were spaced 0.1 m and a time window of 790 ns provided a maximum detection depth of 13 m, and a resolution of ~25 cm. In total, twenty parallel transects (each 500–2,500 m long) with 100 m spacing were surveyed, making it a total length of 25 km. Prior to the GPR campaign, 15 manual peat depth measurement points along the main boardwalk were surveyed as well, and 250 additional control points were manually measured with a probe to validate the GPR data. The peat depth at Degerö Stormyr ranges between 3 and 4 m in average, with some areas having up to 8 m peat thickness. At the Hälsingfors-forest site, peat depth was measured manually with a probe at 81 locations organised in a regular grid of 9 × 9 points with 50 m spacing showing a mean depth of 142 ± 13 cm and 65 ± 7 cm in the open and dense sections of the forest, respectively (C.H.M. Tong, personal communication, 12 April 2022).

4.12 Forest inventory at Hälsingfors-forest

A forest inventory was conducted within a 10 m radius around each of the 12 chamber measurement plots at the Hälsingfors-forest in May 2018. The average stem volume was 52 m^3 ha^{-1} in the open section and 131 m^3 ha^{-1} in the dense section of the forest. In November 2020, increment cores collected from 147 sample trees across the range of tree diameters at Hälsingfors-forest were examined to reconstruct annual series of the individual tree growth using standard dendrochronological methods (Cook and Kairiukstis, 1990). The average biomass production was 55 g C m^{-2} yr^{-1} in the open section and 114 g C m^{-2} yr^{-1} in the dense section of the forest during the years 2019 and 2020.

5 Global relevance of KRI

Degerö Stormyr is one of the most studied mires in the boreal biome, and its global relevance has grown during the last decade (Figure 9). The increasing importance further results from the labelling of Degerö Stormyr as an ICOS ecosystem station in 2019, and from contributing data to several international flux networks and databases: FLUXNET (Papale et al., 2012), the COSORE soil respiration and other soil-atmosphere fluxes database (Bond-Lamberty et al., 2020), FLUXNET-CH_4 (Delwiche et al., 2021), the arctic-boreal CO_2-flux (ABC-flux) database (Virkkala et al., 2022).

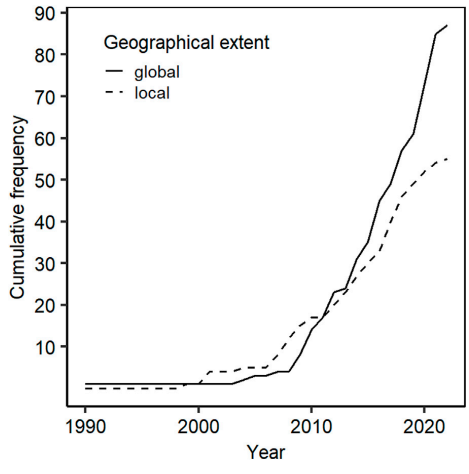

FIGURE 9
Evolution of the cumulative frequency of local vs global studies involving Degerö Stormyr throughout years.

The recently established KRI extends Degerö Stormyr with four additional peatland research sites which creates a unique setting for replicated plot-to ecosystem-scale studies of biogeochemistry and hydrology, including their responses to global changes across northern peatland complexes. Thus, this setup overcomes the traditional spatial limitations in field-based studies, thereby enabling investigations of key drivers regulating the observed spatial differences in processes and refining budget estimates for heterogeneous peatland landscapes.

We hypothesize that the nutrient status of the different sites within the peatland complex would be influenced by their catchment sizes and how much nutrient come from the surrounding mineral soils. Additionally, the orientation of the peatland complex in the landscape and the distinct hydrological pathways around each site would affect water table dynamics and lead to unique vegetation communities, resulting in differences in biogeochemical processes at each site, despite their apparent similarities. Measurements at the research infrastructure will facilitate the investigation of any eventual differences between sites.

The location of KRI, i.e., in the middle boreal zone in a transition area where more southern peatland types are gradually replaced by and co-exist with northern types (Ruuhijärvi, 1983; Laitinen et al., 2007) further provides an attractive platform for northern peatland studies. In fact, within KRI, different mire types (aapa mires, bogs and intermediate types) co-occur in a sort of dynamic equilibrium with the prevailing abiotic conditions (i.e., climate, geology, nutrient levels), and the sites are easily accessible within a limited area. Supported by long-term data records, the KRI therefore offers unique possibilities to study how global changes in, e.g., temperature, precipitation and nutrient availability as well as their interactions may affect species composition and ecosystem processes related to peatland biogeochemistry and hydrology. The KRI is embedded in the national infrastructures of ICOS and SITES which support several of the routine data collection activities as well as the general site maintenance (i.e., physical and technical infrastructure components). Thus, the KRI provides a research hub to support collaborations and interdisciplinary research in order to advance our understanding of northern peatland functioning and feedbacks with the environment and climate.

Apart from the advantages offered by the KRI, its main limitation is the considerable effort in terms of funding and labour that are required to coordinate and maintain such a research infrastructure. The general support from national infrastructures (SITES, ICOS) helps to overcome this challenge. In addition, while the KRI settings are typical for boreal nutrient-poor fen systems, the spatial variability within the KRI peatland complex system could still be specific and thus difficult to generalize across other forms of peatland complexes within the boreal biome. This highlights the need for more peatland complex infrastructures, which will reduce the uncertainties related to upscaling of fluxes from single towers or plot level measurements.

Author contributions

KN, JR, AÅ, MÖ, MN, and MP conceived and designed the study. KN, AÅ, MN, LE, CT, JJ, WZ, SO, HP, JR, MÖ, and MP contributed to gathering required information for drafting the manuscript. KN synthesized the information and drafted the manuscript. All authors contributed to the article and approved the submitted version.

Funding

Research and instrumentation at the Kulbäcksliden Research Infrastructure sites have been funded by project grants from the Swedish Research Council (VR, grant no. 2018-03966) and the Swedish Research Council for Spatial Planning (FORMAS, grant no. 2016-01289), as well as by infrastructure grants from the Kempe Foundation (grant no. JCK-1712) and the Swedish University of Agricultural Sciences (SLU). The sites contribute to the Swedish Infrastructure for Ecosystem Science (SITES) and Degerö Stormyr is part of the Swedish Integrated carbon Observation System (ICOS-Sweden) research infrastructure. Financial support from the Swedish Research Council and contributing research institutes to both SITES and ICOS-Sweden are acknowledged.

Acknowledgments

We thank the state-owned forest company Sveaskog for allowing for research to be carried out at Kulbäcksliden. We thank the engineers and technicians from the SLU Unit for Field-based Forest research for maintenance and operation of equipment and experiments at the Kulbäcksliden Research Infrastructure.

Conflict of interest

The co-author JJ is also co-editor of the special issue "Wetland Ecology and Biogeochemistry Under Natural and Human Disturbance-Volume II".

Publisher's note

All claims expressed in this article are solely those of the authors and do not necessarily represent those of their affiliated organizations, or those of the publisher, the editors and the reviewers. Any product that may be evaluated in this article, or claim that may be made by its manufacturer, is not guaranteed or endorsed by the publisher.

Supplementary material

The Supplementary Material for this article can be found online at: https://www.frontiersin.org/articles/10.3389/feart.2023.1194749/full#supplementary-material

References

Abdalla, M., Hastings, A., Truu, J., Espenberg, M., Mander, Ü., and Smith, P. (2016). Emissions of methane from northern peatlands: A review of management impacts and implications for future management options. *Ecol. Evol.* 6 (19), 7080–7102. doi:10.1002/ece3.2469

Ågren, A. M., Buffam, I., Berggren, M., Bishop, K., Jansson, M., Laudon, H., et al. (2008). Dissolved organic carbon characteristics in boreal streams in a forest-wetland gradient during the transition between winter and summer. *J. Geophys. Res. Biogeosciences* 113 (G3), G03031. doi:10.1029/2007jg000674

Ågren, A. M., Larson, J., Paul, S. S., Laudon, H., and Lidberg, W. (2021). Use of multiple LIDAR-derived digital terrain indices and machine learning for high-resolution national-scale soil moisture mapping of the Swedish forest landscape. *Geoderma* 404, 115280. doi:10.1016/j.geoderma.2021.115280

Ai, J., Jia, G., Epstein, H. E., Wang, H., Zhang, A., and Hu, Y. (2018). MODIS-based estimates of global terrestrial ecosystem respiration. *J. Geophys. Res. Biogeosciences* 123 (2), 326–352. doi:10.1002/2017jg004107

Åkerblom, S., Bignert, A., Meili, M., Sonesten, L., and Sundbom, M. (2014). Half a century of changing mercury levels in Swedish freshwater fish. *Ambio* 43 (1), 91–103. doi:10.1007/s13280-014-0564-1

Åkerblom, S., Bishop, K., Björn, E., Lambertsson, L., Eriksson, T., and Nilsson, M. B. (2013). Significant interaction effects from sulfate deposition and climate on sulfur concentrations constitute major controls on methylmercury production in peatlands. *Geochimica Cosmochimica Acta* 102, 1–11. doi:10.1016/j.gca.2012.10.025

Åkerblom, S., Nilsson, M. B., Skyllberg, U., Björn, E., Jonsson, S., Ranneby, B., et al. (2020). Formation and mobilization of methylmercury across natural and experimental sulfur deposition gradients. *Environ. Pollut.* 263, 114398. doi:10.1016/j.envpol.2020.114398

Alekseychik, P., Korrensalo, A., Mammarella, I., Launiainen, S., Tuittila, E. S., Korpela, I., et al. (2021). Carbon balance of a Finnish bog: Temporal variability and limiting factors based on 6 years of eddy-covariance data. *Biogeosciences* 18 (16), 4681–4704. doi:10.5194/bg-18-4681-2021

Bechtold, M., De Lannoy, G. J. M., Koster, R. D., Reichle, R. H., Mahanama, S. P., Bleuten, W., et al. (2019). PEAT-CLSM: A specific treatment of peatland hydrology in the nasa catchment land surface model. *J. Adv. Model. Earth Syst.* 11 (7), 2130–2162. doi:10.1029/2018ms001574

Belyea, L. R., and Baird, A. J. (2006). Beyond "the limits to peat bog growth": Cross-scale feedback in peatland development. *Ecol. Monogr.* 76 (3), 299–322. doi:10.1890/0012-9615(2006)076[0299:btltpb]2.0.co;2

Berggren, M., Laudon, H., and Jansson, M. (2009). Hydrological control of organic carbon support for bacterial growth in boreal headwater streams. *Microb. Ecol.* 57 (1), 170–178. doi:10.1007/s00248-008-9423-6

Berggren, M., Laudon, H., and Jansson, M. (2007). Landscape regulation of bacterial growth efficiency in boreal freshwaters. *Glob. Biogeochem. Cycles* 21 (4). doi:10.1029/2006gb002844

Bergman, I., Bishop, K., Tu, Q., Frech, W., Åkerblom, S., and Nilsson, M. (2012). The influence of sulphate deposition on the seasonal variation of peat pore water methyl Hg in a boreal mire. *PLoS ONE* 7 (9), e45547. doi:10.1371/journal.pone.0045547

Bishop, H. K., and Lee, Y.-H. (1997). "Catchments as a source of mercury/methylmercury in boreal surface waters," in *Metal ions in biological systems*. Editors A. Sigel and H. Sigel (Basel: Marcel Dekker), 34, 113–130. Retrieved from https://books.google.se/books?hl=sv&lr=&id=VCRxnObbsSIC&oi=fnd&pg=PA113&ots=s1FOo58B2x&sig=ZspCsyNVP-2ON3k9Dsb95_MUy2s&redir_esc=y#v=onepage&q&f=false.

Bishop, K., Shanley, J. B., Riscassi, A., de Wit, H. A., Eklöf, K., Meng, B., et al. (2020). Recent advances in understanding and measurement of mercury in the environment: Terrestrial Hg cycling. *Sci. Total Environ.* 721, 137647. doi:10.1016/j.scitotenv.2020.137647

Bond-Lamberty, B., Christianson, D. S., Malhotra, A., Pennington, S. C., Sihi, D., AghaKouchak, A., et al. (2020). Cosore: A community database for continuous soil respiration and other soil-atmosphere greenhouse gas flux data. *Glob. Change Biol.* 26 (12), 7268–7283. doi:10.1111/gcb.15353

Branfireun, B. A., Bishop, K., Roulet, N. T., Granberg, G., and Nilsson, M. (2001). Mercury cycling in boreal ecosystems: The long-term effect of acid rain constituents on peatland pore water methylmercury concentrations. *Geophys. Res. Lett.* 28 (7), 1227–1230. doi:10.1029/2000gl011867

Bubier, J., Costello, A., Moore, T. R., Roulet, N. T., and Savage, K. (1993). Microtopography and methane flux in boreal peatlands, northern Ontario, Canada. *Can. J. Bot.* 71 (8), 1056–1063. doi:10.1139/b93-122

Burdun, I., Bechtold, M., Sagris, V., Lohila, A., Humphreys, E., Desai, A. R., et al. (2020). Satellite determination of peatland water table temporal dynamics by localizing representative pixels of A SWIR-based moisture index. *Remote Sens.* 12 (18), 2936. doi:10.3390/rs12182936

Campeau, A., Bishop, K. H., Billett, M. F., Garnett, M. H., Laudon, H., Leach, J. A., et al. (2017). Aquatic export of young dissolved and gaseous carbon from a pristine boreal fen: Implications for peat carbon stock stability. *Glob. Change Biol.* 23 (12), 5523–5536. doi:10.1111/gcb.13815

Chu, H., Luo, X., Ouyang, Z., Chan, W. S., Dengel, S., Biraud, S. C., et al. (2021). Representativeness of Eddy-Covariance flux footprints for areas surrounding AmeriFlux sites. *Agric. For. Meteorology* 301–302, 108350. doi:10.1016/j.agrformet.2021.108350

Delwiche, K. B., Helen Knox, S., Malhotra, A., Fluet-Chouinard, E., McNicol, G., Feron, S., et al. (2021). FLUXNET-CH₄: A global, multi-ecosystem dataset and analysis of methane seasonality from freshwater wetlands. *Earth Syst. Sci. Data* 13, 3607–3689. doi:10.5194/essd-13-3607-2021

Desai, A. R., Murphy, B. A., Wiesner, S., Thom, J., Butterworth, B. J., Koupaei-Abyazani, N., et al. (2022). Drivers of decadal carbon fluxes across temperate ecosystems. *J. Geophys. Res. Biogeosciences* 127 (12). doi:10.1029/2022jg007014

Dorodnikov, M., Knorr, K.-H., Fan, L., Kuzyakov, Y., and Nilsson, M. B. (2022). A novel belowground *in-situ* gas labeling approach: CH4 oxidation in deep peat using passive diffusion chambers and 13C excess. *Sci. Total Environ.* 806, 150457. doi:10.1016/j.scitotenv.2021.150457

Dunn, C., and Freeman, C. (2014). Peatlands: Our greatest source of carbon credits? *Carbon Manag.* 2 (3), 289–301. doi:10.4155/Cmt.11.23

Eppinga, M. B., Rietkerk, M., Belyea, L. R., Nilsson, M. B., De Ruiter, P. C., and Wassen, M. J. (2010). Resource contrast in patterned peatlands increases along a climatic gradient. *Ecology* 91 (8), 2344–2355. doi:10.1890/09-1313.1

Eppinga, M. B., Rietkerk, M., Wassen, M. J., and De Ruiter, P. C. (2007). Linking habitat modification to catastrophic shifts and vegetation patterns in bogs. *Plant Ecol.* 200 (1), 53–68. doi:10.1007/s11258-007-9309-6

E. R. Cook and L. A. Kairiukstis (Eds.). (1990). *Methods of dendrochronology*. Dordrecht: Springer, Netherlands.

Eriksson, T., Öquist, M. G., and Nilsson, M. B. (2010a). Effects of decadal deposition of nitrogen and sulfur, and increased temperature, on methane emissions from a boreal peatland. *J. Geophys. Res. Biogeosciences* 115 (G4), G04036. doi:10.1029/2010jg001285

Eriksson, T., Öquist, M. G., and Nilsson, M. B. (2010b). Production and oxidation of methane in a boreal mire after a decade of increased temperature and nitrogen and sulfur deposition. *Glob. Change Biol.* 16 (7), 2130–2144. doi:10.1111/j.1365-2486.2009.02097.x

Fritsche, J., Osterwalder, S., Nilsson, M. B., Sagerfors, J., Åkerblom, S., Bishop, K., et al. (2014). Evasion of elemental mercury from a boreal peatland suppressed by long-term sulfate addition. *Environ. Sci. Technol. Lett.* 1 (10), 421–425. doi:10.1021/ez500223a

Frolking, S., and Roulet, N. T. (2007). Holocene radiative forcing impact of northern peatland carbon accumulation and methane emissions. *Glob. Change Biol.* 13 (5), 1079–1088. doi:10.1111/j.1365-2486.2007.01339.x

Frolking, S., Talbot, J., Jones, M. C., Treat, C. C., Kauffman, J. B., Tuittila, E.-S., et al. (2011). Peatlands in the Earth's 21st century climate system. *Environ. Rev.* 19, 371–396. doi:10.1139/a11-014

Fu, Z., Ciais, P., Bastos, A., Stoy, P. C., Yang, H., Green, J. K., et al. (2020). *Sensitivity of gross primary productivity to climatic drivers during the summer drought of 2018 in Europe*. Philosophical Transactions of the Royal Society B, 375.

Gauci, V., Matthews, E., Dise, N., Walter, B., Koch, D., Granberg, G., et al. (2004). Sulfur pollution suppression of the wetland methane source in the 20th and 21st centuries. *Proc. Natl. Acad. Sci.* 101 (34), 12583–12587. doi:10.1073/pnas.0404412101

Giesler, R., Björkvald, L., Laudon, H., and Mörth, C. M. (2009). Spatial and seasonal variations in stream water δ34S-dissolved organic matter in Northern Sweden. *Environ. Sci. Technol.* 43 (2), 447–452. doi:10.1021/es8017946

Granberg, G., Grip, H., Löfvenius, M. O., Sundh, I., Svensson, B. H., and Nilsson, M. B. (1999). A simple model for simulation of water content, soil frost, and soil temperatures in boreal mixed mires. *Water Resour. Res.* 35 (12), 3771–3782. doi:10.1029/1999wr900216

Granberg, G., Mikkelä, C., Sundh, I., Svensson, B. H., and Nilsson, M. (1997). Sources of spatial variation in methane emission from mires in northern Sweden: A mechanistic approach in statistical modeling. *Glob. Biogeochem. Cycles* 11 (2), 135–150. doi:10.1029/96gb03352

Granberg, G., Sundh, I., Svensson, B. H., and Nilsson, M. (2001). Effects of temperature, and nitrogen and sulfur deposition, on methane emission from a boreal mire. *Ecology* 82 (7), 1982–1998. doi:10.1890/0012-9658(2001)082[1982:eotana]2.0.co;2

Grip, H. (2015). Sweden's first forest hydrology field study 1905–1926: Contemporary relevance of inherited conclusions and data from the rokliden hillslope. *Hydrol. Process.* 29 (16), 3616–3631. doi:10.1002/hyp.10420

Groß-Schmölders, M., Von Sengbusch, P., Paul Krüger, J., Klein, K., Birkholz, A., Leifeld, J., et al. (2020). Switch of fungal to bacterial degradation in natural, drained and rewetted oligotrophic peatlands reflected in <i>δ</i>¹⁵N and fatty acid composition. *SOIL* 6 (2), 299–313. doi:10.5194/soil-6-299-2020

Gunnarsson, U., Granberg, G., and Nilsson, M. (2004). Growth, production and interspecific competition in Sphagnum: Effects of temperature, nitrogen and sulphur treatments on a boreal mire. *New Phytol.* 163 (2), 349–359. doi:10.1111/j.1469-8137.2004.01108.x

Helbig, M., Waddington, J. M., Alekseychik, P., Amiro, B. D., Aurela, M., Barr, A. G., et al. (2020a). The biophysical climate mitigation potential of boreal peatlands during the growing season. *Environ. Res. Lett.* 15 (10), 104004. doi:10.1088/1748-9326/abab34

Helbig, M., Waddington, J. M., Alekseychik, P., Amiro, B. D., Aurela, M., Barr, A. G., et al. (2020b). Increasing contribution of peatlands to boreal evapotranspiration in a warming climate. *Nat. Clim. Change* 10 (6), 555–560. doi:10.1038/s41558-020-0763-7

Helbig, M., Živković, T., Alekseychik, P., Aurela, M., El-Madany, T. S., Euskirchen, E. S., et al. (2022). Warming response of peatland CO2 sink is sensitive to seasonality in warming trends. *Nat. Clim. Change* 12 (8), 743–749. doi:10.1038/s41558-022-01428-z

Hu, H., Wang, B., Bravo, A. G., Björn, E., Skyllberg, U., Amouroux, D., et al. (2020). Shifts in mercury methylation across a peatland chronosequence: From sulfate reduction to methanogenesis and syntrophy. *J. Hazard. Mater.* 387, 121967. doi:10.1016/j.jhazmat.2019.121967

ICOS (2020). *Ancillary vegetation measurements in mires*. Retrieved from https://fileshare.icos-cp.eu/s/9E3bEdrNtsoQDTH.

Ivarsson, K., and Bjarnason, S. (2009). The long-term soil fertility experiments in southern Sweden. *Acta Agric. Scand.* 38 (2), 137–143. doi:10.1080/00015128809438477

Jammet, M., Dengel, S., Kettner, E., Parmentier, F. J. W., Wik, M., Crill, P., et al. (2017). Year-round CH₄ and CO₂ flux dynamics in two contrasting freshwater ecosystems of the subarctic. *Biogeosciences* 14 (22), 5189–5216. doi:10.5194/bg-14-5189-2017

Järveoja, J., Nilsson, M. B., Crill, P. M., and Peichl, M. (2020). Bimodal diel pattern in peatland ecosystem respiration rebuts uniform temperature response. *Nat. Commun.* 11 (1), 4255–4259. doi:10.1038/s41467-020-18027-1

Järveoja, J., Nilsson, M. B., Gažovič, M., Crill, P. M., and Peichl, M. (2018). Partitioning of the net CO2 exchange using an automated chamber system reveals plant phenology as key control of production and respiration fluxes in a boreal peatland. *Glob. Change Biol.* 24 (8), 3436–3451. doi:10.1111/gcb.14292

Joosten, H., and Couwenberg, J. (2008). "Peatlands and carbon," in *Assessment on peatlands, biodiversity and climate change: Main report*. Editors F. Parish, A. Sirin, D. Charman, H. Joosten, T. Minayeva, M. Silvius, et al. (Wageningen: Global Environment Centre, Kuala Lumpur and Wetlands International), 99–117. Retrieved from www.peat-portal.net.

Kljun, N., Calanca, P., Rotach, M. W., and Schmid, H. P. (2015). A simple two-dimensional parameterisation for Flux Footprint Prediction (FFP). *Geosci. Model Dev.* 8 (11), 3695–3713. doi:10.5194/gmd-8-3695-2015

Knox, S. H., Bansal, S., McNicol, G., Schafer, K., Sturtevant, C., Ueyama, M., et al. (2021). Identifying dominant environmental predictors of freshwater wetland methane fluxes across diurnal to seasonal time scales. *Glob. Change Biol.* 27 (15), 3582–3604. doi:10.1111/gcb.15661

Koebsch, F., Sonnentag, O., Järveoja, J., Peltoniemi, M., Alekseychik, P., Aurela, M., et al. (2020). Refining the role of phenology in regulating gross ecosystem productivity across European peatlands. *Glob. Change Biol.* 26 (2), 876–887. doi:10.1111/gcb.14905

Korrensalo, A., Männistö, E., Alekseychik, P., Mammarella, I., Rinne, J., Vesala, T., et al. (2018). Small spatial variability in methane emission measured from a wet patterned boreal bog. *Biogeosciences* 15 (6), 1749–1761. doi:10.5194/bg-15-1749-2018

Kulczyński, S. (1949). *Peat bogs of polesie*. Kraków: Polish Academy of Arts and Sciences.

Ladenberger, A., Andersson, M., Reimann, C., Tarvainen, T., Filzmoser, P., Uhlbäck, J., et al. (2013). *Geochemical mapping of agricultural soils and grazing land (GEMAS) in Norway, Finland and Sweden-regional report*. Uppsala. Retrieved from http://resource.sgu.se/produkter/sgurapp/s1217-rapport.pdf.

Laine, A. M., Bubier, J., Riutta, T., Nilsson, M. B., Moore, T. R., Vasander, H., et al. (2012). Abundance and composition of plant biomass as potential controls for mire net ecosytem CO2 exchange. *Botany* 90 (1), 63–74. doi:10.1139/b11-068

Laitinen, J., Rehell, S., Huttunen, A., Tahvanainen, T., Heikkilä, R., and Lindholm, T. (2007). Mire systems in Finland-special view to aapa mires and their water-flow pattern. *Suo* 58 (1), 1–26.

Łakomiec, P., Holst, J., Friborg, T., Crill, P., Rakos, N., Kljun, N., et al. (2021). Field-scale CH₄ emission at a subarctic mire with heterogeneous permafrost thaw status. *Biogeosciences* 18 (20), 5811–5830. doi:10.5194/bg-18-5811-2021

Larsson, A., Segerström, U., Laudon, H., and Nilsson, M. B. (2017). Holocene carbon and nitrogen accumulation rates in a boreal oligotrophic fen. *Holocene* 27 (6), 811–821. doi:10.1177/0959683616675936

Laudon, H., Hasselquist, E. M., Peichl, M., Lindgren, K., Sponseller, R. A., Lidman, F., et al. (2021). Northern landscapes in transition: Evidence, approach and ways forward using the Krycklan Catchment Study. *Hydrol. Process.* 35 (4), e14170. doi:10.1002/hyp.14170

Le Quéré, C., Andrew, R., Friedlingstein, P., Sitch, S., Hauck, J., Pongratz, J., et al. (2018). Global carbon budget 2018. *Earth Syst. Sci. Data* 10 (4), 2141–2194. doi:10.5194/essd-10-2141-2018

Leach, J. A., Larsson, A., Wallin, M. B., Nilsson, M. B., and Laudon, H. (2016). Twelve year interannual and seasonal variability of stream carbon export from a boreal peatland catchment. *J. Geophys. Res. Biogeosciences* 121 (7), 1851–1866. doi:10.1002/2016jg003357

Lembrechts, J. J., Hoogen, J. V. D., Aalto, J., Ashcroft, M. B., Frenne, P. D., Kemppinen, J., et al. (2021). Global maps of soil temperature. *Glob. Change Biol.* 28, 3110–3144. doi:10.1111/gcb.16060

Limpens, J., Berendse, F., Blodau, C., Canadell, J. G., Freeman, C., Holden, J., et al. (2008). Peatlands and the carbon cycle: From local processes to global implications – a synthesis. *Biogeosciences* 5 (5), 1475–1491. doi:10.5194/bg-5-1475-2008

Limpens, J., Granath, G., Aerts, R., Heijmans, M. M. P. D., Sheppard, L. J., Bragazza, L., et al. (2012). Glasshouse vs field experiments: Do they yield ecologically similar results for assessing N impacts on peat mosses? *New Phytol.* 195 (2), 408–418. doi:10.1111/j.1469-8137.2012.04157.x

Limpens, J., Granath, G., Gunnarsson, U., Aerts, R., Bayley, S., Bragazza, L., et al. (2011). Climatic modifiers of the response to nitrogen deposition in peat-forming Sphagnum mosses: A meta-analysis. *New Phytol.* 191 (2), 496–507. doi:10.1111/j.1469-8137.2011.03680.x

Lindroth, A., Lund, M., Nilsson, M., Aurela, M., Christensen, T. R., Laurila, T., et al. (2007). Environmental controls on the CO 2 exchange in north European mires. *Tellus B Chem. Phys. Meteorology* 59 (5), 812–825. doi:10.3402/tellusb.v59i5.17061

Lund, M., Lafleur, P. M., Roulet, N. T., Lindroth, A., Christensen, T. R., Aurela, M., et al. (2010). Variability in exchange of CO2 across 12 northern peatland and tundra sites. *Glob. Change Biol.* 16 (9), 2436–2448.

Malmström, C. (1923). Degerö Stormyr. En botanisk, hydrologisk och utvecklingshistorisk undersökning över ett nordsvenskt myrkomplex *(Meddelanden från Statens Skogsförsöksanstalt No. 20)*. Stockholm. Retrieved from https://pub.epsilon.slu.se/10091/1/medd_statens_skogsforskningsanst_020_01.pdf.

Martí, M., Juottonen, H., Robroek, B. J. M., Yrjälä, K., Danielsson, Å., Lindgren, P. E., et al. (2015). Nitrogen and methanogen community composition within and among three Sphagnum dominated peatlands in Scandinavia. *Soil Biol. Biochem.* 81, 204–211. doi:10.1016/j.soilbio.2014.11.016

Martí, M., Nilsson, M. B., Danielsson, Å., Lindgren, P.-E., and Svensson, B. H. (2019). Strong long-term interactive effects of warming and enhanced nitrogen and sulphur deposition on the abundance of active methanogens in a boreal oligotrophic mire. *Mires Peat* 24, 1–14.

Masing, V., Botch, M., and Läänelaid, A. (2010). Mires of the former soviet union. *Wetl. Ecol. Manag.* 18 (4), 397–433. doi:10.1007/s11273-008-9130-6

Matthes, J. H., Sturtevant, C., Verfaillie, J., Knox, S., and Baldocchi, D. (2014). Parsing the variability in CH4 flux at a spatially heterogeneous wetland: Integrating multiple eddy covariance towers with high-resolution flux footprint analysis. *J. Geophys. Res. Biogeosciences* 119 (7), 1322–1339. doi:10.1002/2014jg002642

Metzger, C., Nilsson, M. B., Peichl, M., and Jansson, P. E. (2016). Parameter interactions and sensitivity analysis for modelling carbon heat and water fluxes in a natural peatland, using CoupModel v5. *Geosci. Model Dev.* 9 (12), 4313–4338. doi:10.5194/gmd-9-4313-2016

Moore, T. R., and Dalva, M. (1993). The influence of temperature and water table position on carbon dioxide and methane emissions from laboratory columns of peatland soils. *J. Soil Sci.* 44 (4), 651–664. doi:10.1111/j.1365-2389.1993.tb02330.x

Mulqueen, J. (1986). Hydrology and drainage of peatland. *Environ. Geol. Water Sci.* 9 (1), 15–22. doi:10.1007/bf02439882

Nielsen, C. S., Hasselquist, N. J., Nilsson, M. B., Öquist, M., Järveoja, J., and Peichl, M. (2019). A novel approach for high-frequency *in-situ* quantification of methane oxidation in peatlands. *Soil Syst.* 3 (1), 4. doi:10.3390/soilsystems3010004

Nijp, J. J., Limpens, J., Metselaar, K., Peichl, M., Nilsson, M. B., van der Zee, S. E. A. T. M., et al. (2015). Rain events decrease boreal peatland net CO2 uptake through reduced light availability. *Glob. Change Biol.* 21 (6), 2309–2320. doi:10.1111/gcb.12864

Nijp, J. J., Metselaar, K., Limpens, J., Bartholomeus, H. M., Nilsson, M. B., Berendse, F., et al. (2019). High-resolution peat volume change in a northern peatland: Spatial variability, main drivers, and impact on ecohydrology. *Ecohydrology* 12 (6), e2114. doi:10.1002/eco.2114

Nijp, J. J., Metselaar, K., Limpens, J., Gooren, H. P. A., and van der Zee, S. E. A. T. M. (2017a). A modification of the constant-head permeameter to measure saturated hydraulic conductivity of highly permeable media. *MethodsX* 4, 134–142. doi:10.1016/j.mex.2017.02.002

Nijp, J. J., Metselaar, K., Limpens, J., Teutschbein, C., Peichl, M., Nilsson, M. B., et al. (2017b). Including hydrological self-regulating processes in peatland models: Effects on peatmoss drought projections. *Sci. Total Environ.* 580, 1389–1400. doi:10.1016/j.scitotenv.2016.12.104

Nilsson, B. M., Ottosson Lofvenius, M., Peichl, M., and Holst, J.ICOS Ecosystem Thematic Center (2022). *Warm winter 2020 ecosystem eddy covariance flux product from Degerö*. (Version 1.0) [dataset].

Nilsson, M. B., Baath, E., and Soderstrom, B. (2011). The microfungal communities of a mixed mire in northern Sweden. *Can. J. Bot.* 70 (2), 272–276. doi:10.1139/b92-037

Nilsson, M., and Eriksson, T. (2011). Boreal mire carbon exchange-long term effects of climate change and nitrogen and sulphur additions. *Geophys. Res. Abstr.* 13, 2011–8602.

Nilsson, M., Sagerfors, J., Buffam, I., Laudon, H., Eriksson, T., Grelle, A., et al. (2008). Contemporary carbon accumulation in a boreal oligotrophic minerogenic mire – A significant sink after accounting for all C-fluxes. *Glob. Change Biol.* 14 (10), 2317–2332. doi:10.1111/j.1365-2486.2008.01654.x

Økland, R. (1990). Regional variation in SE Fennoscandian mire vegetation. *Nordic J. Bot.* 10 (3), 285–310. doi:10.1111/j.1756-1051.1990.tb01774.x

Olid, C., Bindler, R., Nilsson, M. B., Eriksson, T., and Klaminder, J. (2017). Effects of warming and increased nitrogen and sulfur deposition on boreal mire geochemistry. *Appl. Geochem.* 78, 149–157. doi:10.1016/j.apgeochem.2016.12.015

Olid, C., Nilsson, M. B., Eriksson, T., and Klaminder, J. (2014). The effects of temperature and nitrogen and sulfur additions on carbon accumulation in a nutrient-poor boreal mire: Decadal effects assessed using 210Pb peat chronologies. *J. Geophys. Res. Biogeosciences* 119 (3), 392–403. doi:10.1002/2013jg002365

Osterwalder, S., Bishop, K., Alewell, C., Fritsche, J., Laudon, H., Åkerblom, S., et al. (2017). Mercury evasion from a boreal peatland shortens the timeline for recovery from legacy pollution. *Sci. Rep.* 7 (1), 16022–16029. doi:10.1038/s41598-017-16141-7

Osterwalder, S., Eugster, W., Feigenwinter, I., and Jiskra, M. (2020). Eddy covariance flux measurements of gaseous elemental mercury over a grassland. *Atmos. Meas. Tech.* 13 (4), 2057–2074. doi:10.5194/amt-13-2057-2020

Osterwalder, S., Fritsche, J., Alewell, C., Schmutz, M., Nilsson, M. B., Jocher, G., et al. (2016). A dual-inlet, single detector relaxed eddy accumulation system for long-term measurement of mercury flux. *Atmos. Meas. Tech.* 9 (2), 509–524. doi:10.5194/amt-9-509-2016

Osterwalder, S., Sommar, J., Åkerblom, S., Jocher, G., Fritsche, J., Nilsson, M. B., et al. (2018). Comparative study of elemental mercury flux measurement techniques over a Fennoscandian boreal peatland. *Atmos. Environ.* 172, 16–25. doi:10.1016/j.atmosenv.2017.10.025

Pakarinen, P. (1995). "Classification of boreal mires in Finland and scandinavia: A review," in *Classification and inventory of the world's wetlands. Advances in vegetation science*. Editors C. M. Finlayson and A. G. van der Valk (Springer Netherlands), 16, 29–38.

Papale, D., Agarwal, D. A., Baldocchi, D., Cook, R. B., Fisher, J. B., and Ingen, C. van. (2012). "Database maintenance, data sharing policy, collaboration," in *Eddy covariance*. Editors M. Aubinet, T. Vesala, and D. Papale (Dordrecht: Springer Atmospheric Sciences, Springer), 399–424.

Peel, M. C., Finlayson, B. L., and McMahon, T. A. (2007). Updated world map of the Köppen-Geiger climate classification. *Hydrology Earth Syst. Sci.* 11 (5), 1633–1644. doi:10.5194/hess-11-1633-2007

Peichl, M., Gažovič, M., Vermeij, I., de Goede, E., Sonnentag, O., Limpens, J., et al. (2018). Peatland vegetation composition and phenology drive the seasonal trajectory of maximum gross primary production. *Sci. Rep.* 8 (1), 8012. doi:10.1038/s41598-018-26147-4

Peichl, M., Öquist, M., Ottosson Löfvenius, M., Ilstedt, U., Sagerfors, J., Grelle, A., et al. (2014). A 12-year record reveals pre-growing season temperature and water table level threshold effects on the net carbon dioxide exchange in a boreal fen. *Environ. Res. Lett.* 9 (5), 055006. doi:10.1088/1748-9326/9/5/055006

Peichl, M., Sagerfors, J., Lindroth, A., Buffam, I., Grelle, A., Klemedtsson, L., et al. (2013). Energy exchange and water budget partitioning in a boreal minerogenic mire. *J. Geophys. Res. Biogeosciences* 118 (1), 1–13. doi:10.1029/2012jg002073

Peichl, M., Sonnentag, O., and Nilsson, M. B. (2015). Bringing color into the picture: Using digital repeat photography to investigate phenology controls of the carbon dioxide exchange in a boreal mire. *Ecosystems* 18 (1), 115–131. doi:10.1007/s10021-014-9815-z

Peltola, O., Hensen, A., Belelli Marchesini, L., Helfter, C., Bosveld, F. C., van den Bulk, W. C. M., et al. (2015). Studying the spatial variability of methane flux with five eddy covariance towers of varying height. *Agric. For. Meteorology* 214–215, 456–472. doi:10.1016/j.agrformet.2015.09.007

Peltola, O., Vesala, T., Gao, Y., Räty, O., Alekseychik, P., Aurela, M., et al. (2019). Monthly gridded data product of northern wetland methane emissions based on upscaling eddy covariance observations. *Earth Syst. Sci. Data* 11 (3), 1263–1289. doi:10.5194/essd-11-1263-2019

Ratcliffe, J. L., Lowe, D. J., Schipper, L. A., Gehrels, M. J., French, A. D., and Campbell, D. I. (2020). Rapid carbon accumulation in a peatland following Late Holocene tephra deposition, New Zealand. *Quat. Sci. Rev.* 246, 106505. doi:10.1016/j.quascirev.2020.106505

Rinne, J., Tuovinen, J.-P., Klemedtsson, L., Aurela, M., Holst, J., Lohila, A., et al. (2020). *Effect of the 2018 European drought on methane and carbon dioxide exchange of northern mire ecosystems*. Philosophical Transactions of the Royal Society B, 375.1810

Robroek, B. J. M., Wubs, E. R. J., Martí, M., Zając, K., Andersen, J. P., Andersson, A., et al. (2014). Microclimatological consequences for plant and microbial composition in Sphagnum-dominated peatlands. *Boreal Environ. Res.* 19 (3), 195–208. Retrieved from https://www.dora.lib4ri.ch/wsl/islandora/object/wsl%3A9545/.

Ruuhijärvi, R. (1960). "Über die regionale Einteilung der nordfinnischen Moore," in *Annales botanici societas zoologica botanica fennica "vanamo*, 31. Retrieved from https://books.google.se/books/about/Über_die_regionale_Einteilung_der_nordf.html?id=i7VQAAAAYAAJ&redir_esc=y.1

Ruuhijärvi, R. (1983). "The Finnish mire types and their regional distribution," in *Ecosystems of the world, 4 B. Mires: Swamp, bog, fen and moor. Regional studies*. Editor A. G. P. Gore (Amsterdam: Elsevier), 47–49.

Ruuhola, T., Nikula, A., Nivala, V., Nevalainen, S., and Matala, J. (2016). Effects of bedrock and surficial deposit composition on moose damage in young forest stands in Finnish Lapland. *Silva Fenn.* 50 (3). doi:10.14214/sf.1565

Rydin, H., and Jeglum, J. K. (2013). *The biology of peatlands* 2nd ed. Oxford University Press.

Rydin, H., Sjörs, H., and Löfroth, M. (1999). Mires. *Acta Phytogeogr. Suec.* 84, 91–112. Retrieved from https://www.researchgate.net/publication/286628326_7_Mires.

Schubert, P., Eklundh, L., Lund, M., and Nilsson, M. (2010). Estimating northern peatland CO2 exchange from MODIS time series data. *Remote Sens. Environ.* 114 (6), 1178–1189. doi:10.1016/j.rse.2010.01.005

Segura, J. H., Nilsson, M. B., Schleucher, J., Haei, M., Sparrman, T., Székely, A., et al. (2019). Microbial utilization of simple carbon substrates in boreal peat soils at low temperatures. *Soil Biol. Biochem.* 135, 438–448. doi:10.1016/j.soilbio.2019.06.006

SGU (1963). *Geological survey of Sweden, bedrock map, 1:50000*. Retrieved from https://apps.sgu.se/kartvisare/kartvisare-berg-50-250-tusen.html.

SGU. (1990). *Geological survey of Sweden, quaternary deposits map 1:25000*. Retrieved from https://apps.sgu.se/kartvisare/kartvisare-jordarter-25-100.html.

Shen, X., Liu, Y., Zhang, J., Wang, Y., Ma, R., Liu, B., et al. (2022). Asymmetric impacts of diurnal warming on vegetation carbon sequestration of marshes in the qinghai tibet plateau. *Glob. Biogeochem. Cycles* 36 (7), e2022GB007396. doi:10.1029/2022gb007396

SLU (2021). *Reference measurements of the climate at the experimental forests at SLU*. Retrieved September 20, 2021, from https://www.slu.se/en/departments/field-based-forest-research/environment/climate-data/referenceclimate/.

SMHI (2021). *Swedish Climate data*. Retrieved September 20, 2021, from http://www.smhi.se/data/meteorologi.

Sponseller, R. A., Blackburn, M., Nilsson, M. B., and Laudon, H. (2018). Headwater mires constitute a major source of nitrogen (N) to surface waters in the boreal landscape. *Ecosystems* 21 (1), 31–44. doi:10.1007/s10021-017-0133-0

St. Louis, V. L., Rudd, J. W. M., Kelly, C. A., Beaty, K. G., Flett, R. J., and Roulet, N. T. (1996). Production and loss of methylmercury and loss of total mercury from boreal forest catchments containing different types of wetlands. *Environ. Sci. Technol.* 30 (9), 2719–2729. doi:10.1021/es950856h

Swindles, G. T., Morris, P. J., Baird, A. J., Blaauw, M., and Plunkett, G. (2012). Ecohydrological feedbacks confound peat-based climate reconstructions. *Geophys. Res. Lett.* 39 (11), 4. doi:10.1029/2012gl051500

Swindles, G. T., Morris, P. J., Wheeler, J., Smith, M. W., Bacon, K. L., Turner, T. E., et al. (2016). Resilience of peatland ecosystem services over millennial timescales: Evidence from a degraded British bog. *J. Ecol.* 104 (3), 621–636. doi:10.1111/1365-2745.12565

Turetsky, M. R., Kotowska, A., Bubier, J., Dise, N. B., Crill, P., Hornibrook, E. R. C., et al. (2014). A synthesis of methane emissions from 71 northern, temperate, and subtropical wetlands. *Glob. Change Biol.* 20 (7), 2183–2197. doi:10.1111/gcb.12580

Ueyama, M., Knox, S. H., Delwiche, K. B., Bansal, S., Riley, W. J., Baldocchi, D., et al. (2023). Modeled production, oxidation, and transport processes of wetland methane emissions in temperate, boreal, and Arctic regions. *Glob. Change Biol.* 00 (2022), 2313–2334. doi:10.1111/gcb.16594

Virkkala, A.-M., Natali, S. M., Rogers, B. M., Watts, J. D., Savage, K., June Connon, S., et al. (2022). The ABCflux database: Arctic–boreal CO₂ flux observations and ancillary information aggregated to monthly time steps across terrestrial ecosystems. *Earth Syst. Sci. Data* 14, 179–208. doi:10.5194/essd-14-179-2022

Vuichard, N., and Papale, D. (2015). Filling the gaps in meteorological continuous data measured at FLUXNET sites with ERA-Interim reanalysis. *Earth Syst. Sci. Data* 7 (2), 157–171. doi:10.5194/essd-7-157-2015

Wania, R., Ross, I., and Prentice, I. C. (2009). Integrating peatlands and permafrost into a dynamic global vegetation model: 2. Evaluation and sensitivity of vegetation and carbon cycle processes. *Glob. Biogeochem. Cycles* 23 (3), 15. doi:10.1029/2008gb003413

Wiedermann, M. M., Gunnarsson, U., Ericson, L., and Nordin, A. (2009a). Ecophysiological adjustment of two Sphagnum species in response to anthropogenic nitrogen deposition. *New Phytol.* 181 (1), 208–217. doi:10.1111/j.1469-8137.2008.02628.x

Wiedermann, M. M., Gunnarsson, U., Nilsson, M. B., Nordin, A., and Ericson, L. (2009b). Can small-scale experiments predict ecosystem responses? An example from peatlands. *Oikos* 118 (3), 449–456. doi:10.1111/j.1600-0706.2008.17129.x

Wiedermann, M. M., and Nilsson, M. B. (2020). Peatland vegetation patterns in a long term global change experiment find no reflection in belowground extracellular enzyme activities. *Wetlands* 40 (6), 2321–2335. doi:10.1007/s13157-020-01377-3

Wiedermann, M. M., Nordin, A., Gunnarsson, U., Nilsson, M. B., and Ericson, L. (2007). Global change shifts vegetation and plant–parasite interactions in a boreal mire. *Ecology* 88 (2), 454–464. doi:10.1890/05-1823

Wißkirchen, K., Tum, M., Günther, K. P., Niklaus, M., Eisfelder, C., and Knorr, W. (2013). Quantifying the carbon uptake by vegetation for Europe on a 1 km^2 resolution using a remote sensing driven vegetation model. *Geosci. Model Dev.* 6, 1623–1640. doi:10.5194/gmd-6-1623-2013

Wu, J., and Roulet, N. T. (2014). Climate change reduces the capacity of northern peatlands to absorb the atmospheric carbon dioxide: The different responses of bogs and fens. *Glob. Biogeochem. Cycles* 28 (10), 1005–1024. doi:10.1002/2014gb004845

Wu, J., Roulet, N. T., Nilsson, M., Lafleur, P., and Humphreys, E. (2012). Simulating the carbon cycling of northern peatlands using a land surface scheme coupled to a wetland carbon model (CLASS3W-mwm). *Atmosphere-Ocean* 50 (4), 487–506. doi:10.1080/07055900.2012.730980

Yi, C., Li, R., Wolbeck, J., Xu, X., Nilsson, M., Aires, L., et al. (2010). Climate control of terrestrial carbon exchange across biomes and continents. *Environ. Res. Lett.* 5 (3), 034007. doi:10.1088/1748-9326/5/3/034007

Yu, Z. C. (2012). Northern peatland carbon stocks and dynamics: A review. *Biogeosciences* 9 (10), 4071–4085. doi:10.5194/bg-9-4071-2012

Yurova, A., Wolf, A., Sagerfors, J., and Nilsson, M. (2007). Variations in net ecosystem exchange of carbon dioxide in a boreal mire: Modeling mechanisms linked to water table position. *J. Geophys. Res.* 112 (G2), G02025. doi:10.1029/2006jg000342

Zhao, J., Peichl, M., and Nilsson, M. B. (2016a). Enhanced winter soil frost reduces methane emission during the subsequent growing season in a boreal peatland. *Glob. Change Biol.* 22 (2), 750–762. doi:10.1111/gcb.13119

Zhao, J., Peichl, M., Öquist, M., and Nilsson, M. B. (2016b). Gross primary production controls the subsequent winter CO2 exchange in a boreal peatland. *Glob. Change Biol.* 22 (12), 4028–4037. doi:10.1111/gcb.13308

Zhou, S., Zhang, Y., Caylor, K. K., Luo, Y., Xiao, X., Ciais, P., et al. (2016a). Explaining inter-annual variability of gross primary productivity from plant phenology and physiology. *Agric. For. Meteorology* 226–227, 246–256. doi:10.1016/j.agrformet.2016.06.010

Zhou, Y., Wu, X., Ju, W., Chen, J. M., Wang, S., Wang, H., et al. (2016b). Global parameterization and validation of a two-leaf light use efficiency model for predicting gross primary production across FLUXNET sites. *J. Geophys. Res. Biogeosciences* 121 (4), 1045–1072. doi:10.1002/2014jg002876

Zhu, Q., Liu, J., Peng, C., Chen, H., Fang, X., Jiang, H., et al. (2014). Modelling methane emissions from natural wetlands by development and application of the TRIPLEX-GHG model. *Geosci. Model Dev.* 7, 981–999. doi:10.5194/gmd-7-981-2014

Photo: Andreas Palmén

frontiers

Supplementary Material

The Kulbäcksliden Research Infrastructure: a unique setting for northern peatland studies

Koffi Dodji Noumonvi*, Anneli M. Ågren, Joshua L. Ratcliffe, Mats G. Öquist, Lars Ericson, Cheuk Hei Marcus Tong, Järvi Järveoja, Wei Zhu, Stefan Osterwalder, Haijun Peng, Charlotta Erefur, Kevin Bishop, Hjalmar Laudon, Mats B. Nilsson, Matthias Peichl

*** Correspondence:** Corresponding Author: koffi.noumonvi@slu.se

Table of content

1. APPENDIX A: Areal cover of different combinations of quaternary deposits and land use

In the main article, percentage shares of the different quaternary deposits and land use are presented separately. Here in Table S1, different combinations of the 2 themes are presented separately.

Table S1: Areal cover (in ha) of different combinations of quaternary deposits and land use.

Sites	Quaternary deposit \ Landuse	Forests	Open lands	Water
Degerö Stormyr	Peat	82.68	112.32	
	Rock outcrops	0.13		
	Till	76.15	0.71	
	Water			0.50
Stortjärn	Peat	5.44	8.11	
	Till	15.83	0.16	
	Water			0.03
Hålmyran	Peat	9.28	15.89	
	Rock outcrops	0.31	0.00	
	Till	6.49	0.21	
	Water			0.88
Hälsingfors-mire	Peat	10.17	32.03	
	Rock outcrops	5.67		
	Till	14.80	0.47	
	Water			1.67
Hälsingfors-forest dense section	Peat	7.85		
	Rock outcrops	2.26		
	Till	3.54		
Hälsingfors-forest open section	Peat	2.63		
	Rock outcrops	3.64		
	Till	5.60		

2. APPENDIX B: Catchment delineation details

In order to illustrate the groundwater movements, the 0.5 m DEM was aggregated to 2 m and 6 m resolution DEMs to smooth out the micro-topography. In fact, in high resolution DEMs hummocks and hollows might act as “dams” and route the water in the wrong direction in the model, while the water actually drains perpendicularly to these features and underneath the surface of the mire. The DEMs were pre-processed using the optimal method for the Swedish landscape (Lidberg et al., 2017), using the Breach function in WhiteboxTools 2.0 and the modelled stream lines indicate where the flow accumulation is larger than 1 ha. Two different watershed delineations were calculated for each catchment based on the different resolution DEMs. The delineation was overall similar for the two DEM resolutions, and at locations

where the delineation depended on the DEM resolution, additional field survey was conducted to verify the flow direction and correct the delineated catchment borders.

3. APPENDIX C: Climate stations

Several climate stations exist in the vicinity of the study area. In a radius of 30 km from the common centroid of all catchments, this includes nine climate stations of the Swedish Meteorological and Hydrological Institute (SMHI, 2021) and two reference climate stations of the Swedish University of Agricultural Sciences (SLU, 2021) (Table S2).

Table S2: Air temperature and precipitation data availability in a radius of 30 km from the peatland complex. The data is provided by the Swedish University of Agricultural Sciences (SLU) and the Swedish Meteorological and Hydrological Institute (SMHI)

Station name	Data provider	Distance to study area (km)	Time span	Air temperature	Precipitation
Kulbäcksliden	SLU	1.84	1990 - Ongoing	Yes	Yes
Vindeln-Sunnansjönäs	SMHI	10.99	1989 - Ongoing	Yes	Yes
Hällnäs-Lund	SMHI	11.3	1961 - 1989	Yes	Yes
Svartberget	SLU	13.1	1990 - Ongoing	Yes	Yes
Granö D	SMHI	14.48	2008 - Ongoing	No	Yes
Harrsele	SMHI	17.2	1961 - 1998	No	Yes
Malkälen D	SMHI	25.28	1989 - Ongoing	No	Yes
Pengfors	SMHI	27.37	1961 - 1975	No	Yes
Örträsk	SMHI	27.67	1973 - 2012	No	Yes
Vännäs	SMHI	29.3	1961-1976	Yes	No
Tavelsjö D	SMHI	29.59	1989 - Ongoing	No	Yes

4. APPENDIX D: Mire vegetation classification workflow

4.1. Introduction

The present classification of mire vegetation is mainly based on the Finnish mire system (Eurola et al., 1984, 1995, 2015) with some additions. The Finnish system also has some similarities with the system utilized in the Swedish Wetland Survey for northern Sweden (Forslund et al., 1993), which in large is based on a system finally published in Vegetationstyper i Norden (Påhlsson, 1994). The latter however covers all Nordic countries and as a result the marked regional differences in the mire vegetation and its response on various directions of variation have been difficult to grasp. One advantage with the Finnish system is that it is easily applicable for mires in boreal Sweden. In order to enable comparisons, naming utilized in other classification systems are sometimes given.

Classification of forest vegetation also follows the Finnish system as outlined by (Kalela, 1961) which shows great similarities with the forest site types described by (Ebeling, 1978) for northern Sweden. In accordance with the Finnish system forests on moist and wet sites (“swamp forests”) are here included in the mire vegetation. As a consequence also thin-peated forest types are included among the mire sites, and the border of the mire massif is set by the mineral soil. Where to draw the limit depends upon focus. In vegetational-ecological studies

mire is often preferred, while peatland sets the limit at a peat depth of 30 cm thus including drained peatland (Joosten and Clarke, 2002).

Mire terminology follows Eurola et al. (1984, 1995, 2015), Laitinen et al. (2005, 2007), Rydin et al. (1999), and Rydin and Jeglum (2013).

4.2. Mire types

KRI is located in the middle boreal zone, an area where the gradual, latitudinal, transition from southern to northern mire types has received much attention in Finland (Laitinen et al., 2007; Ruuhijärvi, 1983) while until recently less so in Sweden due to its more complicated topography (Gunnarsson and Löfroth, 2009; Rydin et al., 1999). The extensive interest for zonal, climatic, vegetation systems in Finland, has demonstrated a zonal, climatic mire system continuum from ordinary raised bog systems (in temperate and south boreal areas), to a northward gradually increasing proportion of fens compared to bogs within the aapa mire zone (Laitinen et al., 2007; Ruuhijärvi, 1983). Thus aapa mires are mixed peatland complexes where the central fen areas, with patterned and unpatterned fens, are surrounded by marginal areas also including bogs close to the divides (Laitinen et al., 2007; Ruuhijärvi, 1983). A bog is a convex to flat structure under ombrotrophic influence while an aapa mire is a concave structure under minerotrophic influence. An aapa mire is a mire system (complex) where the central parts are characterized by minerotrophy, and that these parts (as well as the marginal areas) may receive supplementary nutrients also from snow-melt water; the definition is vegetational-ecological (Eurola et al., 1995). Aapa mires (according to the present broad concept) are morphologically variable and three main types have been described (Laitinen et al., 2007; Ruuhijärvi, 1983): (1) a lawn aapa mire where lawns dominate but the flark level often occurs in form of longitudinal soaks (e.g. the westernmost part of Stortjärn); (2) a lawn-flark aapa mire where peripheral lobes and different flark fens (string flark fens, stringless flark fens, flark outlets) dominate (e.g. Hålmyran); (3) a flark aapa mire where the mire massif is dominated by the flark level (e.g. Hälsingfors-mire). However, there are at least two intermediate massif types (Laitinen et al., 2007). First, an aapa mire–raised bog intermediate with the morphology of a hummock ridged raised bog but with minerotrophic hollows/flarks; a string mixed mire (Sw. strängblandmyr) often easy to identify on air photos (e.g. Hälsingfors-mire). Second, an aapa mire–raised bog intermediate with the morphology of a lawn aapa mire although with ombrotrophic vegetation (e.g. some central parts of Degerö Stormyr approach this situation; extremely poor fen (Sjörs and Gunnarsson, 2002).

A characteristic feature of KRI is the nutrient poor conditions. Most fens are oligotrophic, and the result is a remarkably species poor mire vegetation. For example, many common mire plants indicating mesotrophic conditions, e.g. *Molinia caerulea, Carex chordorhiza, C. livida,* do not occur or are very rare. This species poverty implies that the dichotomy ombrotrophic-minerotrophic may be elusive when focusing on species composition as stressed by (Ruuhijärvi, 1960, p. 35). For that reason areas that are judged to represent ombrotrophic vegetation have been specifically marked in Figure 6. Here belongs two flat bog areas of northern type (Rydin et al., 1999); unpatterned bog/*Fuscum* bog in (Eurola et al., 1995) at Degerö and Hälsingfors, one area with the structure of reticulate bog (Gunnarsson and Löfroth, 2009) at Hälsingfors, and several sloping, clearly patterned mires in the marginal areas close to the divides (northern eccentric bog in (Eurola et al., 2015)). However the species poor biota in combination with that several minerotrophic indicators tend to show a northward increasing occurrence in bog communities (Økland, 1990; Pakarinen and Ruuhijärvi, 1978; Rydin et al., 1999) should be kept in mind. The issue of how well species

composition, and particularly so scattered occurrences of fen indicators, mirrors the movement of minerotrophic water was already treated by (Sjörs, 1948). The winter conditions, the duration and magnitude of snowpack and timing of snowmelt may play a role here.

The following are some major characteristics of mire vegetation at KRI:

- The area is characterized by aapa mire – raised bog complexes; central patterned and unpatterned fens + bogs in marginal areas
- The presence of different aapa mire types: lawn type (Stortjärn), lawn-flark type (Hålmyran), flark type (Hälsingfors)
- The presence of intermediate types: with the morphology of a hummock ridged raised bog with minerotrophic hollows/flarks; or morphology of a lawn aapa mire with ombrotrophic vegetation (approaching nutrient availability similar to ombrotrophic conditions)
- A very species poor flora as most fens are oligotrophic and only a few slightly mesotrophic which makes the ombrotrophic – minerotrophic dichotomy elusive
- Vegetation types indicate important differences in hydrology, from unstable to stable (in the order Stortjärn –Hålmyran –Hälsingfors –Degerö)
- A strong groundwater outflow from surrounding mineral soils resulting in dominance of minerotrophic pine and spruce mire forests

4.3. Vegetation types

The Finnish mire system distinguishes four main types (Eurola et al., 1984; Ruuhijärvi, 1983): letto (L) eutrophic fens, which does not occur in the area; neva (N) fens, remaining open wet, ombrotrophic (Om), oligotrophic (Ol) and mesotrophic (Me) mires, dominated by graminoids and Sphagna; korpi (K) spruce and birch-dominated minerotrophic (Mi) mires; and räme (R) ombrotrophic pine mires and hummocks characterized by dwarf shrubs and Sphagna. However, due to extensive groundwater influence from the mineral soil in the area, most pine-dominated mires have a clear minerotrophic influence. It should be noted that the open treeless neva mire has no sharp border between ombrotrophy and minerotrophy; thus the transition may be gradual. Another important feature of the system is the identification of a large number of combination site types. For occurrence of ombrotrophic vegetation and wet combination types see Figure S2 and for different mire-forest and forest types see Figure S3.

The information in the below text has the following structure:

Numbering and acronyms refer to unpublished field notes.

E 84/95: Naming mainly following Eurola et al. (1984, 1995, 2015), if not otherwise stated. Acronyms refer to the Finnish names

ViN 1994: Naming in Vegetationstyper i Norden (Påhlsson, 1994)

E 1978: Naming (in Swedish) in (Ebeling 1978) for forest site types

F 1993: Naming (in Swedish) in (Forslund et al., 1993)

M 1923: Naming in (Malmström, 1923). Note that “mosse” (bog) at that time was used for *Sphagnum*-dominated vegetation types.

Short information on species composition and environmental conditions

The four mires are referred to as follows: De Degerö Stormyr, Hå Hålmyran, Hä Hälsingfors-mire, St Stortjärn.

Minerotrohic communities

Flark level types have been split up into several smaller units as it is assumed that these are likely to be particularly sensitive to global change (Granlund et al., 2022; Sallinen et al., 2022). Also note that *Trichophorum cespitosum* dominated fens with *Sphagnum compactum* (*i.e.* n° 2, 4, and 8) are indicative of an unstable hydrology (Laitinen et al., 2007) – in contrast to the different *Sphagnum papillosum* fens. These two types are distinguished in (Eurola et al., 1995) while treated more collectively in (Eurola et al., 2015). As they differ in hydrology they are separated here.

1b EvCpSa

E 84/95: oligotrophic true short-sedge fen, OlVLkN; oligotrophic ordinary low-sedge fen, OlLkN (Eurola et al., 1995, 2015)

ViN 1994: *Carex pauciflora-Eriophorum vaginatum-Sphagnum angustifolium*-var., 3.2.3.1.a

F 1993: taggstarr-*S. angustifolium*-var. av fastmattekärr av tuvull-vitmosstyp

An oligotrophic lawn of peripheral lobes characterized by *Carex pauciflora* and *Eriophorum vaginatum* and the rich occurrence of *Sphagnum angustifolium* and a regular occurrence of *S. fuscum*, *S. medium* and *S. rubellum*, Often only as a narrow border towards the surrounding mire forest; important type in sparsely treed pine fens or in combination with pine hummocks. Often mapped as a combination type, oligotrophic short-sedge pine fen (n° 40, see further below).

1 EvCp

E 84/95: true *Sphagnum papillosum* short-sedge fen, OlKaN; oligotrophic *Papillosum* low-sedge fen, OlKaN (Eurola et al., 2015)

ViN 1994: *Eriophorum vaginatum-Sphagnum papillosum*-type, 3.2.3.1

F1993: fastmattekärr av tuvull-vitmosstyp

M 1923: *Eriophorum vaginatum-Sphagnum balticum*-mosse (Sw. tuvdunmosse)

An oligotrophic lawn of peripheral lobes characterized by *Eriophorum vaginatum*, *Carex pauciflora* and *Trichophorum cespitosum* and a closed *Sphagnum* layer with *S. balticum* and *S. papillosum* as most important species. Dwarf shrubs, *Andromeda polifolia* and *Oxycoccus palustris*, of limited importance.

2 TcEv

E 84/95: oligotrophic true *Sphagnum papillosum-S. compactum* short-sedge fen, OlKaN (Eurola et al., 1995); poor *Sphagnum compactum* fen (Laitinen et al., 2005). The *Compactum* fens are included among the *Papillosum* fens in (Eurola et al., 2015) although I prefer to keep them separated.

ViN 1994: *Eriophorum vaginatum-Sphagnum papillosum-S. compactum*-var., 3.2.3.1.b

F 1993: tuvsäv-*S. papillosum-S. compactum*-variant av fastmattekärr av tuvull-vitmosstyp

M 1923: *Scirpus austriacus-Sphagnum balticum*-mosse (Sw. “jämn” tuvsävmosse). Malmström differs between “jämn” (“smooth”) and “tuvig” (“tussocky”) *Scirpus austriacus*-mosse (see further n° 4 below).

An oligotrophic lawn, characterized by the dominance of *Trichophorum cespitosum*. *Eriophorum vaginatum* of regular although variable occurrence. Replaces the preceding type on sites with a stronger water flow from surrounding mire forests (fen type). Key indicator in the bottom layer *Sphagnum compactum*, otherwise similar species composition as in n° 1. Characterized by unstable hydrology (as n° 4, 8 and 9; cf. (Laitinen et al., 2005; Ruuhijärvi, 1960)). A dominant community of peripheral lobes in the western half of St; also important at Hå and Hä.

At St, northern side, also “short-sedge pine fens dominated by *S. compactum*”, LkNR (Laitinen et al., 2005) in the transition to surrounding mire forest. This combination type is also mentioned by Malmström (1923) as: trädbevuxen *Sphagnum fuscum*-rismosse-*Scirpus austriacus*-mosse.

3 EvS

E 84/95: oligotrophic true *Sphagnum papillosum* short-sedge fen (with small flarks), OlKaN; oligotrophic *Papillosum* low-sedge fen, OlKaN (Eurola et al., 2015)

ViN 1994: included in *Eriophorum vaginatum-Sphagnum papillosum*-type, 3.2.3.1

F 1993: Mjukmattekärr av starr-vitmosstyp starr-*S. papillosum*-variant

M 1923: included in *Eriophorum vaginatum-Sphagnum balticum*-mosse (Sw. tuvdunmosse)

Eriophorum vaginatum lawns and carpets, often with *Carex pauciflora*, and a closed *Sphagnum* carpet (*S. papillosum* and *S.* subgenus *Cuspidata*). Characteristic in gently sloping peripheral lobes, in stringless central flark fens with a stable hydrology (De, Hä) or in string flark fens as mosaic with n° 5.

4 Tc(Ev)Sb(p+co)

E 84/95: oligotrophic true *Sphagnum papillosum-S. compactum* short-sedge fen with larger flarks (>1/5 of the area), OlRiKaN (Eurola et al., 1995); oligotrophic *Papillosum* fen with flarks (around ½ the area), RiKaN (Eurola et al., 2015). *Sphagnum compactum* Weissmoor ((Ruuhijärvi, 1960), Tab. 9).

ViN 1994: included in *Eriophorum vaginatum-Sphagnum papillosum-S. compactum*-var., 3.2.3.1.b

F 1993: included in “tuvsäv-*S. papillosum-S. compactum*-variant av fastmattekärr av tuvull-vitmosstyp” (see n° 2 above).

M 1923: *Scirpus austriacus-Sphagnum compactum-S. balticum*-mosse (Sw. “tuvig” tuvsävmosse).

An oligotrophic lawn-carpet community dominated by *Trichophorum cespitosum* and linked to an unstable water regime (cf. (Laitinen et al., 2005, 2007; Ruuhijärvi, 1960) indicated by the presence of *Sphagnum compactum* in the bottom layer. A more “smooth” type often occurs in the transition between hummock strings and loose-bottom flarks, or dominates flark carpets on slightly sloping mires; it is characterized by a continuous cover of *S.* subgenus

Cuspidata and fits the description of ORiKaN (Hä). On more sloping mires forming narrow strings (with *S. balticum, S. compactum, S. rubellum, S. papillosum*) alternating with narrow flarks (with different *S.* subgenus *Cuspidata*) (Hå) which corresponds more to OlKaN. At stronger slopes (particularly at St north of the small lake) clear string-flark fen structure characterized by a mixture of liverworts (*Cladopodiella fluitans*), Sphagna and lichens (e.g. *Cetrariella delisei*, *Cladonia mitis*, and *C. squamosa* (the mire ecotype)) with features similar to moist heath vegetation (e.g. *Empetrum nigrum*; see also n° 15), indicating regular occurrence of longer drought periods.

5 SchS

E 84/95: oligotrophic *Sphagnum* flark fen, OlSphRiN; oligotrophic *Sphagnum* flark fen, OlRsRiN (Eurola et al., 2015)

ViN 1994: *Carex* spp.-*Scheuchzeria palustris*-*Sphagnum* spp.-var., 3.2.4.1c

F 1993: kallgräs-vitmoss-varianten av mjukmattekärr av starr-vitmosstyp

An oligotrophic carpet community characterized by *Scheuchzeria palustris* and a closed layer of *Sphagnum* subgenus *Cuspidata* (*S. balticum, S. majus, S. lindbergii*, and some *S. jensenii*); scanty occurrence of *Eriophorum vaginatum* and *Trichophorum cespitosum*. Forms extensive flarks in central string flark fens (De, Hå, Hä, St). Also a frequent component forming small carpets in soaks (in combination with n° 3 and 12).

6 (Sch)S

E 84/95: ~*Sphagnum dusenii* (=*S. majus*) flark fen, OlSphRiN (Eurola et al., 1984); oligotrophic *Sphagnum* flark fen, OlRsRiN (Eurola et al., 2015).

ViN 1994: included in *Carex* spp.-*Scheuchzeria palustris*-*Sphagnum* spp.-var. (see n° 5 above).

F 1993: Mjukmattekärr av starr-vitmosstyp, 3.6.2.1; similar to alpin starr-*S lindbergii*-variant.

M 1923: included in *Scheuchzeria-Sphagna Cuspidata*-mosse (Sw. kallgräs-mosse)

The name is here used for very wet areas (loose bottoms) in stringless central flark fens with a stable hydrology and a covering *Sphagnum* subgenus *Cuspidata* carpet with *S. majus* as dominant, and with scanty occurrence of vegetative *Scheuchzeria palustris* (large areas at De, Hå, Hä).

7 ClS

E 84/95: oligotrophic *Sphagnum* flark fen, OlSphRiN, Rimpiartiges Weissmoor in (Eurola et al., 1984), Oligotrophes moos-armes Rimpiweissmor in (Ruuhijärvi, 1960)

ViN 1994: included in *Carex* spp.-*Scheuchzeria palustris*-*Sphagnum* spp.-var. (see n° 5 above).

F 1993: kallgräs-vitmoss-varianten av mjukmattekärr av starr-vitmosstyp

M 1923: *Carex limosa-Sphagna Cuspidata*-mosse (Sw. *Carex limosa*-mosse),

A loose-bottom community characterized by *Carex limosa* (and vegetative *Scheuchzeria palustris*) and *Sphagnum* subgenus *Cuspidata* (particularly *S. majus*, *S. lindbergii* and *S. jensenii*) of variable cover. Regular occurrence of *Drosera longifolia*. Best developed in central stringless flark fens with a stable water regime (De); may form small flarks in soaks (together with n° 12). Often seen with suffering, loose-lying Sphagna, transitional to n° 9 (see below).

8 Tctuss

E 84/95: poor mud-bottom flark fen (Rimpiartiges Weissmoor), OlRuRiN (Eurola et al., 1984); Oligotrophes moos-armes Rimpiweissmoor in (Ruuhijärvi, 1960)

ViN 1994: included in *Carex* spp.-*Gymnocolea inflata-Sphagnum* spp.-type, 3.2.4.2 (Sw. fattig mossfattig torvslamtyp)

F 1993: most likely included in "lösbottenkärr av oligotrof typ" (oligotrophic loose-bottom fen)

M 1923: may be included in his *Carex limosa*-dykärr

Characterized by the occurrence of scattered *Trichophorum cespitosum* tussocks (sometimes also *Eriophorum vaginatum* tussocks), suffering loose-lying Sphagna, often replaced by the liverwort *Cladopodiella fluitans*. The occurrence of Sphagna and liverworts varies between years depending on precipitation (and growth of green algae). Tussock dieback affected by frost heave and formation of needle ice during severe cold spells during dry autumns. Unstable hydrology. Important community at St and Hä. Forms the transition between n° 4 and n° 9.

A few larger flarks with *Rhynchospora alba* tussocks in a string mixed mire occur at St and are included in this type.

9 Clad

E 84/95: poor mud-bottom flark fen, OlRuRiN

ViN 1994: included in *Carex* spp.-*Gymnocolea inflata-Sphagnum* spp.-type, 3.2.4.2 (Sw. fattig mossfattig torvslamtyp)

F 1993: lösbottenkärr av oligotrof typ

M 1923: referred to as "vegetationslösa flarkar" (flarks without any vegetation)

Mud-bottom flarks (St, Hå, Hä, less so at De) with a more or less covering dark brown liverwort carpet (that is *Cladopodiella fluitans*), which typically show large between-year variations in cover due to variation in precipitation with marked declines in rainy years.

10 (mud)

E 84/95: poor mud-bottom flark fen

Here used for flark pools with more or less permanent water.

11 CrSf

E 84/95: oligotrophic true tall-sedge fen, OlVSN; oligotrophic ordinary tall-sedge fen, OlSN (Eurola et al., 2015); mesotrophic true tall-sedge fen, MeVSN; mesotrophic ordinary tall-sedge fen, MeSN (Eurola et al., 2015).

ViN 1994: *Carex* spp.-*Sphagnum fallax*-var., 3.2.4.1a

F 1993: Starr-*S. fallax*-variant av mjukmattekärr av starr-vitmosstyp

M 1923: *Carex rostrata*-mosse

Forms extensive carpet/loose bottom stands, in the wettest parts of central, stringless flark fens (De in northeast, Hä in northwest), characterized by vigorous *Carex rostrata* and a bottom layer with *Sphagnum fallax* (dominant), *S. angustifolium*, and sometimes *S. lindbergii* and *S. majus*. In the wettest areas (at De, Hä) with increasing occurrence of *Drepanocladus fluitans* (*Warnstorfia f.*), indicating more mesotrophic conditions. Also important in various combination types (see n° 45-47 below), as well as in old ditches (see n° 62 below) at the mire margin (De, Hä).

12 (Cr)S

E 84/95: oligotrophic *Sphagnum papillosum* tall-sedge fen, OlKaSN; also with some weak mesotrophic influence, MeKaSN; oligotrophic *Papillosum* tall-sedge fen, OlKaSN, and mesotrophic *Papillosum* tall-sedge fen, MeKaSN, respectively in (Eurola et al., 2015)

ViN 1994: *Carex* spp.-*Sphagnum papillosum*-var., 3.2.4.1b

F 1993: Starr-*S papillosum*-variant of “mjukmattekärr av starr-vitmosstyp” (Eng. fen carpet of *Carex*-*Sphagnum*-type)

M 1923: *Carex rostrata*-*Sphagnum papillosum*-*Sphagna Cuspidata*-mosse

A tall sedge community (*Carex rostrata*, often with scattered, in the area vegetative, *Eriophorum angustifolium*, *Carex lasiocarpa*) and a closed *Sphagnum* carpet (*S. papillosum* + *S.* subgenus *Cuspidata*). Inhabits somewhat drier sites compared with n° 11, often bordering ponds in stringless flark fens, in longitudinal soaks in lawn aapa mires, in soaks or areas of strong groundwater influence (Hä eastern part) in marginal lobes (in combination with n° 5 and 7), or in bogs. Similar communities around small lakes and ponds are classified as n° 14 (see below).

13 MeT = *Menyanthes* type

E 84/95: *Sphagnum* flark fen (Eurola et al., 1984), poor oroarctic flark fen (Eurola and Virtanen, 1991), oligotrophic mud-bottom flark fen, OlRuRiN (Eurola et al., 2015)

ViN 1994: *Menyanthes trifoliata*-*Sphagnum* spp.-var., 3.2.4.1d (Sw. vattenklöver-vitmoss-variant)

F 1993: -

M 1923: *Menyanthes*-*Sphagna Cuspidata*-mosse (vattenklövermosse)

Forms a characteristic border around small pools both in central stringless flark fens (De, St) and where groundwater discharges from the surrounding mineral forest (Hä, the eastern side). Covering Sphagna (*S. balticum*, *S. lindbergii*, *S. majus*) and *Menyanthes trifoliata* together with *Carex rostrata*, *C. magellanica*, *C. lasiocarpa*, and *Eriophorum angustifolium*, indicative of slight mesotrophic influence. Stable hydrology in contrast to n° 9.

14 Cr

This classification was used for the *Carex rostrata* stands that frequently border small ponds and water- covered flarks in stringless central flark fens. In the area often together with the *Menyanthes* type (n° 13) and the two may be united. See also the comment on quagmires under n° 15 below.

M 1923: *Carex limosa-C. rostrata* dykärr

15 SSquag

A short-sedge quagmire with a mosaic of carpets (*Carex limosa*) and lawns (*Trichophorum cespitosum*) with dying Sphagna (*S. compactum, S. lindbergii*, *S. medium, S. papillosum, S. rubellum*) colonized by liverworts (*Cladopodiella fluitans*), lichens (*Cetrariella delisei, Cladonia squamosa*, the mire ecotype) and dwarf shrubs (*Empetrum nigrum, Calluna vulgaris*). As quagmire only seen around the small lake at St. Similar vegetation types in lawns in the outlet area at Hä. Here interpreted as a drought effect due to unstable hydrology. Eurola et al. (1984 p. 80) suggests that the floating moss carpets overgrowing the water surface of pond and lakes, with a mixture of swampy and tall-sedge fens, flark fens, and short-sedge lawns (that is n° 13, 14, 15), can be united under the name “poor fen marginal to a pool”. This pragmatic view is suitable for vegetation mapping.

Malmström (1923, Tab 3:1-5): describes the quagmire vegetation around ponds as a zonation from a *Menyanthes-Sphagna Cuspidata*-mosse, over a *Carex limosa-Sphagna Cuspidata*-mosse, to a *Scheuchzeria-Sphagna Cuspidata*-mosse.

Ombrotrophic communities

Hollow communities

16 EvSb

E 84/95: ombrotrophic short-sedge flark-level bog, KuN; ombrotrophic low-sedge bog, OmLkN (Eurola et al., 2015)

ViN 1994: *Eriophorum vaginatum-Sphagnum balticum*-type, 3.1.3.5

F 1993: included in ”mjukmattemosse av vitag-kallgräs-*S.balticum*typ” (ombrotrophic carpet of *Rhynchospora alba-Scheuchzeria palustris-Sphagnum balticum*-type)

M 1923: *Eriophorum vaginatum-Sphagnum balticum*-mosse

Carpet community characterized by *Eriophorum vaginatum* and *Trichophorum cespitosum* and covering Sphagna with *S. balticum* (dominant), *S. tenellum* and *S. rubellum*. Characteristic for the driest bog hollows. Differs from n° 3 due to the absence of *S. papillosum*.

17 SchScu

E 84/95: ombrotrophic flark-level bog, SphKuN; *Scheuchzeria-Sphagnum balticum*-Weissmoor (Eurola, 1962). Schlenken Weissmoor (Ruuhijärvi, 1960); ombrotrophic hollow bog, KuN (Eurola et al., 2015)

ViN 1994: *Rhynchospora alba-Scheuchzeria palustris-Sphagnum balticum*-type, 3.1.4.1

F 1993: Mjukmattemosse av vitag-kallgräs-*S.balticum*typ

M 1923: *Scheuchzeria-Sphagna Cuspidata*-mosse

Very characteristic for flarks (hollows) in bogs or transitional mires. Carpet community characterized by *Eriophorum vaginatum*, *Scheuchzeria palustris*, *Trichophorum cespitosum*, *Carex limosa* and covering *Sphagnum balticum*, *S. lindbergii*, and *S. tenellum*. The absence of *S. papillosum* (and *S. majus*) is diagnostic towards oligotrophic flark communities. In the area, *Rhynchospora alba* does not occur in this type (however see the comment under n° 8 above).

18 SchSm

E 84/95: *S. dusenii* (=*majus*) flark-level bog (Eurola 1962), SphKuN

ViN 1994: *Rhynchospora alba-Scheuchzeria palustris-Sphagnum majus*-type, 3.1.4.4

F 1993: mjukmattemosse av vitag-kallgräs-*S.majus*typ

A carpet/loose-bottom community with scattered *Scheuchzeria palustris* and *Carex limosa* and covering Sphagna (*S. balticum*, *S. lindbergii*, *S. tenellum* and *S. majus*) that is very close to n° 17. Confined to the lowest flarks of bogs/transitional mires in the transition to unpatterned central flark fens. Most likely transitional between ombrotrophic and minerotrophic and maybe best united with n° 5. As to *Rhynchospora alba* see the comment under n° 17.

Lawn communities

20 EvSb

E 84/95: short-sedge intermediate-level bog, OmLkN; *Sphagnum balticum*-Weissmoor (Eurola, 1962); ombrotrophic low-sedge bog, OmLkN (Eurola et al., 2015)

ViN 1994: *Eriophorum vaginatum-Sphagnum balticum*-type, 3.1.3.5

F 1993: Fastmattemosse av tuvull-*S.balticum*typ; Fastmattemosse av tuvull-*S.angustifolium*typ

M 1923: *Eriophorum vaginatum-Sphagnum balticum*-mosse

A species poor lawn community characterized by *Eriophorum vaginatum*, the occurrence of *Andromeda polifolia*, *Oxycoccus palustris*, *Rubus chamaemorus*, and a closed *Sphagnum* carpet (*S. balticum*, *S. angustifolium*, *S. rubellum*, and some *S. fuscum*). Often in mosaic with n° 24 (see below).

Comment: occurs often together with the close "short-sedge intermediate-level bog", OmLkN; *Sphagnum parvifolium*-Weissmoor (Eurola, 1962); ViN 1994: *Eriophorum vaginatum-Sphagnum angustifolium*-type, 3.1.3.4. This type differs through the dominance of *S. angustifolium*. The two types have been treated collectively.

Hummock communities

21 Anfu

E 84/95: A*ndromeda-Sphagnum fuscum* bog, OmLkNR (Eurola, 1962).

ViN 1994: *Eriophorum vaginatum-Sphagnum fuscum*-type 3.1.3.1

F 1993: Fastmattemosse av tuvull-*S.fuscum*-typ; Fastmattemosse av tuvull-*S.angustifolium*-typ.

M 1923: shows similarities with his "*Andromeda*-rik trädbevuxen *Fuscum*-mosse" except for the absence of a tree canopy.

The driest lawn/hummock community dominated by *Eriophorum vaginatum* and dominant *S. fuscum* in the bottom layer; often with some *S. medium* and *S. rubellum*. Other regular species in this species poor community are *Andromeda polifolia*, *Drosera rotundifolia*, *Oxycoccus* spp. Often as mosaic and particularly so together with n° 1. May be difficult to separate from n° 20 and n° 24.

22 Empfu = *Empetrum nigrum-Sphagnum fuscum* bog

E 84/95: Empetrum-Sphagnum fuscum bog *pro parte*, VmRaR; *Empetrum-Fuscum* bog *pro parte*, VaRaR (Eurola et al., 2015); Eigentliches *Empetrum-Sphagnum fuscum* Reisermoor (Eurola, 1962)

The two *Empetrum* species differ in their ecology. *E. nigrum* is a species of vitally growing *Sphagnum fuscum*, while *E. hermaphroditum* is a species of stagnant *Sphagnum* growth (Eurola, 1962), mirroring their differences in shoot growth.The above name is here used for the *Sphagnum fuscum* hummocks with *Empetrum nigrum* that form a characteristic feature in island mixed mires. Frequently co-occurring species are *Andromeda polifolia*, *Oxycoccus microcarpus*, *Rubus chamaemorus*, and *Eriophorum vaginatum*. The circumscription accords with the true *Empetrum–Sphagnum fuscum* bog (Eurola, 1962) and with the comment by (Ruuhijärvi, 1960), p. 151, concerning his *Empetrum – Sphagnum fuscum* – Reisermoor, namely that *E. nigrum* is light demanding ("Lichtplanze") and thus a species of the mire expanse. These *E. nigrum-Sphagnum fuscum* hummocks of island mixed mires form a characteristic feature in the area (and throughout the boreal forest land). Here, they are not included in the broader *Empetrum-Sphagnum fuscum* bog in Eurola et al. (1984, 1995, 2015) which also includes hummocks at the mire margin (and on open concentric bogs) with stagnant *Sphagnum* growth where *Empetrum hermaphroditum* prevails. *E. nigrum* is also a characteristic species in hummock communities of raised bogs in temperate and south boreal areas (Eurola, 1962; Sjörs, 1948) with vitally growing Sphagna. The hybrid can be found on hummocks at the mire edge. For *E. hermaphroditum* see also n° 23-25 further below.

23 Ulfu

E 84/95: *Empetrum-Sphagnum fuscum* bog, VmRaR; *Empetrum-Fuscum* bog, VaRaR (Eurola et al., 2015)

ViN 1994: *Calluna vulgaris-Empetrum* spp.-*Sphagnum fuscum*-type, 3.1.2.2

F 1993: Rismosse av *Sphagnum fuscum*-typ

M 1923: included in his "rismossesträngar" (hummock strings)

In the field notes referred to Ulfu, *Uliginosum-Sphagnum fuscum*-type, in order to avoid confusion with n° 22.

A characteristic community for open bogs and higher strings and higher hummock islands in mixed mires. Dwarf-shrubs dominate (*Andromeda polifolia*, *Empetrum hermaphroditum*, *Ledum palustre*, *Vaccinium uliginosum*, *V. vitis-idaea*) together with *Rubus chamaemorus*, and *Betula nana*; regular occurrence of low pines. *Sphagnum fuscum* gradually replaced by *S. angustifolium*, lichens (*Cladonia mitis*, *C. stygia*, and various cup lichens) and forest mosses (*Pleurozium schreberi*).

24 Cvfu

E 84/95: *Calluna-Sphagnum fuscum* bog, KrRaR (Eurola et al. 1984); *Calluna-Fuscum* bog, KaRaR (Eurola et al., 2015)

ViN 1994: *Calluna vulgaris-Empetrum* spp.-*Sphagnum fuscum*-type, 3.1.2.2

F 1993: included under n° 23

M 1923: included in his "*Calluna*-rik trädbevuxen *Fuscum*-mosse" (see n° 26 below) forming the transition between his *Andromeda*- and *Ledum*-types

The most important bog community in the area, both fringing the open mire areas and on lower hummock strings and islands. Differs from n° 23 through the dominance of *Calluna vulgaris* (and co-dominant *E. hermaphroditum*). Sphagna (*S. fuscum, S. angustifolium*) dominate the bottom layer together with *Pleurozium schreberi*. Whether the striking dominance of *Calluna* in the area may mirror an unstable hydrology (Laitinen et al., 2005) or a more local continental climate, or both, resulting in a reduced peat growth remains to be understood.

The type merges gradually over to n° 26 – the most important pine bog community fringing the open mire in the area.

25 Lifu = Lichen-*Sphagnum fuscum* bog

E 84/95: Similar to the following descriptions: *Calluna - Sphagnum fuscum - Cladonia* Reisermoor (Eurola, 1962); *Dicranum-Sphagnum fuscum* bog, KsRaR (Eurola et al., 1984); Oroarctic dwarf-shrub bog vegetation (Eurola and Virtanen, 1991)

ViN 1994: *Empetrum hermaphroditum-Vaccinium microcarpum-Sphagnum fuscum*-type, 3.1.2.1

F 1993: –

The driest hummock community on treeless bogs, characterized by declining dwarf-shrubs (most important *Empetrum hermaphroditum*) and Sphagna (*S. fuscum*, *S. angustifolium*, *S. medium*, *S. rubellum*) overgrown by liverworts (e.g. *Mylia anomala*), crustaceous (e.g. *Ochrolechia frigida*) and mat-forming lichens (e.g. *Cladonia mitis*, *Cetraria nivalis* (syn. *Flavocetralia n*)), and mosses (*Dicranum undulatum*, *Polytrichum strictum*, *Pleurozium schreberi*). Confined to the driest hummocks on open treeless, wind-exposed bogs typically with thin snow cover; only present at Hä.

Dwarf-shrub pine bogs

26 PCv

E 84/95: Pine-*Calluna* bog; Dwarf-shrub pine bog, *Calluna* variant, RaIR, OmIR; Dwarf-shrub pine mire, VIR (Eurola et al., 2015)

ViN 1994: *Pinus sylvestris*-*Vaccinium uliginosum*-type, *Calluna* var., 3.1.1.3

F 1993: included in “tallmosse av ristyp” (Eng. Pine bog, dwarf-shrub-type)

M 1923: *Calluna*-rik trädbevuxen *Fuscum*-mosse (trädbevuxen ljung-mosse)

A sparsely treed pine bog community forming the transition between the open mire and the surrounding mire forest. Due to the marked minerotrophic influence from surrounding mineral soils, the bog community inhabits smaller areas only, while it is frequently present as a combination type: low sedge pine fen (see n° 40 further below).

27 PLe

E 84/95: Pine-*Ledum* bog; Dwarf-shrub pine bog, *Ledum* variant, RaIR, OmIR; Dwarf-shrub pine mire, VIR (Eurola et al., 2015)

ViN 1994: *Pinus sylvestris*-*Ledum palustre*-type, 3.1.1.2

F 1993: Tallmosse av skvattramtyp (Eng. Pine bog, *Ledum*-type)

M 1923: *Ledum*-rik trädbevuxen *Fuscum*-mosse (trädbevuxen skvattram-mosse)

Similar to n° 28 (see below) but *Ledum palustre*, *Vaccinium uliginosum*, *Betula nana* dominate the forest floor. Sphagna of decreasing and *Pleurozium schreberi* (and lichens) of increasing importance.

Pine bog communities, with a rather closed tree canopy, approaching this type have a limited occurrence in the area. A few smaller patches close to small lakes (Hå at the western side of the small lake, St north of the small lake), not in the mire forest fringing the open mire, approach this vegetation type. However, *Ledum* does not reach that dominance characteristic for areas closer to the Bothnian coast. In the area *Ledum* is a characteristic species on higher strings in mixed mires (see n° 23 above), in the true spruce pine mire (see n° 34 below), in Pine-*Uliginosum* bogs (see n° 28 below) and in many heath forest types (see n° 51-52 below).

28 PUl

E 84/95: Pine-*Uliginosum* bog; Dwarf-shrub pine bog, *Uliginosum* variant, RaIR, OmIR; Dwarf-shrub pine mire, VIR (Eurola et al., 2015)

ViN 1994: *Pinus sylvestris*-*Vaccinium uliginosum*-type, *Vaccinium uliginosum*-var., 3.1.1.3

F 1993: Tallmosse ristyp

M 1923: included in his *Ledum*-rik trädbevuxen *Fuscum*-mosse (trädbevuxen skvattram-mosse); se n° 27 above

Characterized by the dominance of *Empetrum hermaphroditum*, *Vaccinium uliginosum*, *V. vitis-idaea*, and rich occurrence of *Calluna vulgaris*, *Ledum palustre*, and *Betula nana*. Well-developed bottom layer with dominant Sphagna (*S. fuscum*, *S. angustifolium*, *S. divinum*, *S. russowii*) and *Pleurozium schreberi*.

A more densely treed pine bog replacing n° 26, although with limited areal extension in the area, mirroring the minerotrophic influence from surrounding mineral forests.

The following three pine bog communities (Eurola et al., 2015) (mentioned in Forslund et al., 1993) do not occur in any of the four study areas: Pine-*Betula nana* bog, OmVkR (for a close type see n° 37), Pine-*Vaginatum* bog, OmTR (for a close type see n° 38), Pine-*Carex globularis* bog, OmPsR (for a close type see n° 36). However, they may occur within KRI, although all close vegetation types observed were minerotrophic.

Forest vegetation included in the mire series

In Finnish classification, these communities are included in the mire vegetation, while in Swedish classification (Ebeling, 1978) they are generally included in forest vegetation as "swamp forests". The paludified types (n° 30 and 31) are transitional between heath (moor) and mire (peat) forests; the remaining with peat formation. In classification of mire forest types the occurrence of, and relative proportion of, heath-forest and hummock-level species play an important role. The forest types are mapped in Figure S3.

30 moistP

E 84/95: Paludified pine forest

ViN 1994: *Picea abies*-*Vaccinium* spp.–*Sphagnum* spp.-type, 2.1.2.3

E 1978: fuktig ristyp (moist dwarf-shrub type)

F 1993: included in sumptallsskog av ristyp

M 1923: risbevuxna *Sphagnum acutifolium*-tuvor (syn. *S. capillifolium*)

Heath forest species (*Calluna vulgaris*, *Empetrum hermaphroditum*, *Vaccinium myrtillus*, *V. vitis-idaea*) dominate over hummock level species. However, Sphagna (*S. capillifolium*, *S. angustifolium*, *S. russowii*) of regular occurrence. Of fragmentary occurrence in the area due to rather steep forest slopes.

31 moistS

E 84/95: Paludified spruce forest

ViN 1994: *Picea abies-Vaccinium* spp.–*Sphagnum* spp.-type, 2.1.2.3

E 1978: fuktig ristyp (moist dwarf-shrub type)

F 1993: granskog av lågörtstyp sumpvariant, 2.1.2.3

M 1923: blåbärs-rik gransumpskog (see also n° 33 below)

Similar to n° 30, heath forest species dominate over hummock level species. A closed bottom layer of forest mosses *Dicranum majus*, *Hylocomium splendens*, *Barbilophozia lycopodioides*, and in slight depressions Sphagna (*S. girgensohnii*, *S. angustifolium* and *S. russowii*). Scattered occurrence of deciduous shrubs (*Alnus incana*). Of limited occurrence in the four areas although common within KRI.

32 wetP

E 84/95: Thin-peated pine mire, KgR; the type is close to dwarf-shrub pine bogs, IR, n° 26-28, and transitional types can be named minerotrophic dwarf-shrub pine bog, MiIR.

ViN 1994: *Pinus sylvestris-Vaccinium uliginosum*-type, 2.1.1.3 (Sw. sumptallskog av ristyp); cf. *Pinus sylvestris-Vaccinium uliginosum*-type, 3.1.1.3 (Sw. tallmosse av ristyp, Eng. dwarf shrub pine bog) close to n° 28 (see above).

E 1978: våt ristyp (wet dwarf-shrub type)

F 1993: included in sumptallskog av ristyp

M 1923: -

A mosaic type where hummock level species dominate over heath forest species. Important species in the bottom layer besides ordinary heath forest mosses are *Polytrichum commune*, *Sphagnum angustifolium*, *S. fuscum*, *S. capillifolium* (syn. *S. nemoreum*), *S. russowii*. Scattered *Carex globularis* tussocks are characteristic. Very limited occurrence in the area, often only as a narrow border of a few m.

33 wetS

E 84/95: Thin-peated spruce mire, KR (if including pine spruce forest, KgKR); divided in two types: thin-peated *Myrtillus* spruce mires, MKgK; thin-peated *Vitis-idaea* spruce mires, PKgK.

Note: The thin-peated spruce mires are close to true spruce mires which are diveded in the following four types: *Myrtillus* spruce mire, MK; *Vitis-idaea* spruce mire, PK; *Rubus chamaemorus* spruce mire, MrK; *Equisetum sylvaticum* spruce mire, MkK. Due to their fragmentary occurrence in the four areas they are here treated collectively, in spite of the quantitative differences in species composition.

ViN 1994: *Picea abies-Vaccinium* spp.–*Sphagnum* spp.-type, 2.1.2.3; *Picea abies-Equisetum sylvaticum*-var., 2.1.2.3b

E 1978: våt ristyp (wet dwarf-shrub type)

F 1993: Sumpgranskog av ristyp, hjortronvariant + skogsfräkenvariant.

M 1923: describes the following types: hjortron-rik (*Rubus chamaemorus*) gransumpskog; *Equisetum silvaticum*-rik gransumpskog; blåbärs-rik gransumpskog (which also seems to include n° 31 above)

In common with n° 32 is that hummock level species dominate over heath forest species. In the field layer *Rubus chamaemorus*, *Equisetum sylvaticum* and *Carex globularis* together with *Vaccinium* spp., particularly *V. myrtillus*. A closed bottom layer with rich occurrence of *Sphagnum giergensohnii, S. russowii* and *S. angustifolium* together with *Dicranum majus*, *Hylocomium splendens*, *Ptilium crista-castrensis*, *Polytrichum commune* and *Barbiolophozia lycopodioides*. The true spruce mire types differ through the marked dominance of Sphagna (also with the rare *S. wulfianum*) and *Polytrichum commune*. The remaining two variants, with *Rubus chamaemorus*, often with covering *Polytrichum commune*, and *Equisetum sylvaticum*, both have a more marked mosaic where the intermediate and flark level dominate. In the latter case often with scattered *Alnus incana* and *Salix lapponum*, *S. phylicifolia*, *S. myrsinifolia*. Small fragments of the *Chamaemorus* type, with abundant *Eriophorum vaginatum* at the flark level, are found close to discharging brooks (Hå). Otherwise, all types only occur as fragments in the four areas, while they are important vegetation types in more gently sloping terrains within KRI.

34 wetDws

E 84/95: Ordinary spruce pine mire, VKR;

ViN 1994: Lists the following swamp forest types: *Pinus sylvestris-Vaccinium uliginosum*-type, 2.1.1.3 (KgR, IR), *Pinus sylvestris-Ledum palustre*-type, 3.1.1.2 (OmIR), and *Pinus sylvestris-Vaccinium uliginosum*-type, 3.1.1.3 (RaIR); *Picea abies-Vaccinium* spp.-*Sphagnum* spp.-type, 2.1.2.3

E 1978: våt ristyp (wet dwarf-shrub type).

F 1993: Sumptallskog av ristyp

M 1923: Trädbevuxen *Sphagnum russowii*-rismosse may include this type, although the rich occurrence of *Carex globolaris* points towards n° 35 (see below).

Tall dwarf shrubs (*Ledum palustre, Vaccinium uliginosum*) of about equal importance as *Vaccinium myrtillus* and *V. vitis-idaea*; tall-growing *Betula nana* and regular occurrence of *Carex globularis* present. A closed bottom layer as in n° 33 although with particularly rich occurrence of Sphagna (*S. angustifolium* often most important, *S. giergensohnii*, *S. divinum*, *S. russowii*) and *Polytrichum commune*. A very characteristic type in marginal pine and spruce mires.

Comment: The type is close to ombrotrotrophic pine bog communities but the minerotrophic influence is shown by the occurrence of minerotrophic species such as *Carex globularis, Dicranum majus, Sphagnum giergensohnii* and *Polytrichum commne*. An alternative name would be: minerotrophic dwarf-shrub spruce-pine mire, MiIR.

35 wetCglS

E 84/95: *Carex globularis* spruce-pine mire, PsKR

ViN 1994: seems to be included under *Picea abies*—*Vaccinium* ssp.—*Sphagnum* spp.-type, 2.1.2.3; (Sw. sumpgranskog av ristyp)

E 1978: våt ristyp (wet dwarf-shrub type); included in n° 34 (above)

F 1993: Sumptallskog av ristyp, klotstarrvariant

M 1923: trädbevuxen *Sphagnum russowii*-rismosse (klotstarr-rik gransumpskog); the placement here based on the rich occurrence of dwarf shrubs.

Similar to n° 34 (see above) but differs in the following respects: Tall dwarf shrubs (*Ledum palustre*, *Vaccinium uliginosum*) dominate over *Vaccinium myrtillus* and *V. vitis-idaea*. *Carex globularis* of increasing importance. Increasing role of *S. angustifolium*, *S. divinum*, *S. russowii*, and *Polytrichum commune* in the bottom layer. A transitional type approaching n° 36.

36 wetCglP

E 84/95: *Carex globularis* pine mire, PsR

ViN 1994: *Pinus sylvestris*-*Carex globularis*-type, 3.2.1.1

F 1993: tallkärr av klotstarrtyp

M 1923: trädbevuxen *Sphagnum russowii*-rismosse (trädbevuxen klotstarrismosse)

Tall dwarf shrubs of limited importance, *Carex globularis* dominant together with *Eriophorum vaginatum* and *Carex pauciflora* in the depressions. *Sphagnum angustifolium* and *S. fuscum* dominant in the bottom layer. Of limited occurrence in the four studied areas except for the southern part of St.

37 wetBn

E 84/95: close to *Betula nana* pine bog, OmVkR; in the area best characterized as ”*Betula nana* pine mire”, MiVkR, VkR (Eurola et al., 2015)

ViN 1994: listed as a transitional type towards sumptallskog ristyp, 2.1.1.3; våt ristyp (wet dwarf-shrub type)

E 1978: våt ristyp (wet dwarf-shrub type)

In the area this type is best characterized as ”*Betula nana* pine mire”; a sparsely treed type, fringing the open mire, characterized by a rich occurrence of *Betula nana*; under strong mineroptrophic influence from surrounding mire forest. Also a characteristic type of strings and hummocks and particularly so in the mire cross area in the wet central parts of Hä.

Combination types

38 wetEv

E 84/95: *Eriophorum vaginatum* birch fen, TK ; Sometimes approaching minerotrophic *Eriophorum vaginatum* bog, MiTR

ViN 1994: *Pinus sylvestris –Eriophorum vaginatum*-type, 3.1.1.4

F 1993: Tallmosse av tuvulltyp (with minerotrophic features) often in mosaic with tallrismosse

M 1923: Trädbevuxen *Eriophorum vaginatum*-mosse (trädbevuxen tuvdunmosse),

Characterized by dominant, tall *Eriophorum vaginatum* tussocks, often together with *Carex pauciflora*, and the low importance of dwarf shrubs (mostly only *Andromeda polifolia* and *Oxycoccus palustris*). Insignificant role of forest and hummock level species, except close to discharging brooks. Strong minerotrophic influence from surrounding mineral soil. In the area mostly in birch/pine mires (Hå, St), more fragmentary in spruce mires.

40 EvCvP

E 84/95: oligotrophic short-sedge pine fen, OlLkNR

F 1993: Tallkärr av fattig vitmosstyp

M 1923: trädbevuxen *Sphagnum fuscum*-rismosse–*Eriophorum vaginatum*-mosse

In the field notes named *Eriophorum vaginatum-Calluna* pine mire (EvCvP).

The most important transition type between the open mire and surrounding mire forest. A combination type between true short-sedge fen (n° 1b and 1) and dwarf-shrub pine bog (n° 26). The hummocks may either form islands or strings; in the latter case resulting in a pronounced patterning parallel to the slope (Hå in the south; Hä in the north). The fen (lawn) and hummock areas easily separated on aerial photos.

45 CrB

E 84/95: oligotrophic tall-sedge birch fen, OlSK; sometimes slightly mesotrophic MeSK

M 1923: Trädbevuxen *Carex rostrata*-mosse

A combination type with low hummocks (abundant *Betula nana*) and tall-sedge communities (*Carex rostrata*). *Sphagnum angustifolium* and *S. fallax* in general most important Sphagna. Confined to ground water discharge in small forest islands on the open mire (De in the north; Hä in north-west). Also with slight mesotrophic influence (*Potentilla palustris, Salix lapponum, S. myrtilloides*). Occurrences marked with asterisk on Figure S2.

46 Crmes

E 84/95: poor birch fen NK; around some discharging brooks swampy birch fen, LuNK

ViN 1994: Gran-björkkärr av fattig vitmoss-type, 3.2.1.3; *Picea abies-Betula pubescens-Sphagnum* spp.-type

F 1993: Gran-björkkärr av fattig vitmosstyp

M 1923: Trädbevuxen *Carex rostrata*-mosse, trädbevuxen *Eriophorum vaginatum*-mosse

A combination type with tall hummocks, lawns and carpets (*Eriophorum vaginatum*) and wet depressions (loose-bottoms) with tall sedges (*Carex rostrata* and covering *Sphagnum angustifolium*, *S. fallax*, *S. flexuosum*, *S. riparium*). Mesotrophic indicators: *Dactylorhiza maculata*, *Potentilla palustris*, *Calamagrostis phragmitoides*, *Carex echinata*, *C. nigra* and low willows (*Salix phylicifolia*, *S. lapponum*, *S. myrtilloides*). Ground water discharge from the mineral soil, brooks at mire margin (Hå in north-east, although outside catchment; St in the south). Occurrences marked (hatched) on Figure S2.

47 Cr3

E 84/95: Oligotrophic tall-sedge pine fen OlSR, (incl. oligotrophic short-sedge pine fen OlLkNR)

M 1923: seems to be included in "trädbevuxen *Carex rostrata*-mosse"

A combination type, mostly 3-level type, with large wet flarks of tall sedges (*Carex rostrata*) with covering *Sphagnum riparium*, *S. angustifolium*, *S. fallax*, *S. flexuosum*). Characteristic for brook outlets and groundwater discharge close to mineral soil (Hå in south-east;) and in outlet areas (Hä in south-west). Occurrences marked (hatched) on Figure S2.

48CnJf

E 84/95: *Carex nigra* birch fen, NigNK

Was not observed in the four areas but occurs within KRI. Confined to small depressions under strong ground water influence.

Forest vegetation on mineral soil

Naming follows (Kalela, 1961) and (Ebeling, 1978). Ebeling stresses the danger of judging moisture and nutrient status only on forest site type as the moor layer may have disappeared due to past intense fire history resulting in a lichen-dominated vegetation, supposed to mirror dry, as well as nutrient poor, site conditions. To accurately judge hydrological conditions one also need to know the thickness of the E-horizon (which was ignored during the field survey). That means that moisture conditions for lichen-dominated ClT (n° 50) may in fact vary from very dry to mesic. The regular occurrence of *Vaccinium uliginosum* (and also *Ledum palustre*) in heath forests is a northern zonal feature due to increasing humidity (Kalela, 1961). In the area Norway spruce normally dominates in VMT and Scots pine dominates in the other types. The forest types are mapped in Figure S3.

50 ClT

(Kalela, 1961): *Cladina* type, ClT

(Ebeling, 1978): lavtyp (lichen type), skarp-frisk lavtyp (very dry-mesic lichen type), skarp lav-ristyp (very dry/very poor lichen – dwarf-shrub type)

ViN 1994: *Pinus sylvestris-Cladonia* spp.-typ, 2.1.1.1, tallskog av lav-ristyp

Calluna vulgaris (scattered) is the most important species in the field layer, while the bottom layer is dominated by lichens (*Cladonia* spp.) and small acrocarpous mosses. Scattered *Salix starkeana* shrubs are relicts from past forest fires; also in n° 51 and 52 below.

51 ECT

(Kalela, 1961): *Empetrum-Calluna* type, ECT

(Ebeling, 1978): Kråkris-ljungtyp (*Empetrum-Calluna*-type; mesic *Empetrum-Calluna*-type), Lavristyp (ljungtyp and kråkristyp (dry and mesic lichen–dwarf-shrub-type; both *Calluna* and *Empetrum* type)

ViN 1994: *Pinus sylvestris-Calluna vulgaris-Empetrum* spp.-type, 2.1.1.2 (tallskog av ljung-kråkris-typ)

Field layer dominated by *Empetrum hermaphroditum* and *Calluna vulgaris*. Bottom layer dominated by lichens (*Cladonia* spp.), acrocarpous mosses (*Dicranum* spp., *Polytrichum* spp.) while pleurocarpous mosses are of low importance.

52 EVT

(Kalela, 1961): *Empetrum-Vaccinium* type, EVT

(Ebeling, 1978): lingon-ristyp (*Vitis-idaea*-type; mesic *Vitis-idaea*–dwarf-shrub-type); torr lavristyp (dry lichen–*Vitis-idaea*-type), torr-frisk ristyp (semi dry dwarf-shrub type).

ViN 1994: *Pinus sylvestris-Vaccinium vitis-idaea*-type, 2.1.1.4; tallskog av lingonris-typ

Field layer dominated by *Empetrum hermaphroditum* and *Vaccinium vitis-idaea*. *Pleurozium schreberi* and acrocarpous mosses (*Dicranum polysetum, D. scoparium, Polytrichum juniperinum*) dominate the bottom layer and some *Cladonia* lichens. The first herbs may appear.

53 VMT

(Kalela, 1961): *Vaccinium-Myrtillus* type, VMT

(Ebeling, 1978): frisk blåbärsristyp (mesic dwarf-shrub type, mesic *Myrtillus*-type), frisk ristyp.

ViN 1994: *Picea abies-Vaccinium myrtillus*-type, 2.1.2.1; granskog av blåbärsristyp

Vaccinium myrtillus and *V. vitis-idaea* dominate together with a closed bottom layer of forest mosses (*Dicranum* spp., *Hylocomium splendens, Pleurozium schreberi, Ptilium crista-castrensis*) and liverworts (*Barbilophozia lycopodioides*). More frequent herbs: *Luzula pilosa, Maianthemum bifolium, Melampyrum pratense, Trientalis (Lysimachia) europaea.*

Others

60 flark pools with open water

61 Phragmites swamp (RuRl in Eurola et al., 2015), loose-bottom, mesotrophic, surrounded by n° 46 (only at Hå, in north-east, although outside the catchment area; see Figure S3).

62 Ditches

Carex rostrata tall-sedge fen. Loose bottoms with *Sphagnum fallax* dominant, *S. angustifolium*, *S. flexuosum*, *S. riparium* (De, Hä).

4.4. Vegetation classification workflow

The vegetation classification involved microtopography identification/classification, ground truth handling and model training to finally achieve the actual classification (Figure S1)

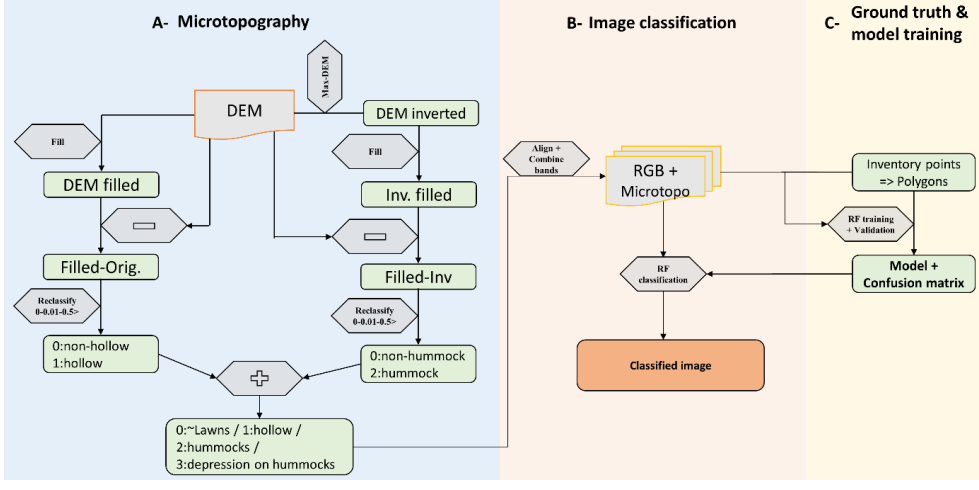

Figure S1. Mire vegetation classification workflow. The classification includes microtopography identification/classification (A), ground truth and model training (C) and image classification (B).

4.4.1 Mire microtopography modelling

Microtopography was included in the vegetation classification as it is an important factor in the differentiation of mire vegetation. The classification of microtopography as considered in this study is a mere simplification of its complexity. We only distinguished 4 classes: (i) lawns, (ii) hollows (i.e. flarks and carpets/loose-bottom), (iii) hummocks and strings, and (iv) small depressions on hummocks. The process for microtopography classification consisted of two steps. Hollows were identified by subtracting a digital elevation model (DEM) from a filled DEM (filled using the fill algorithm in ArcGIS Desktop). Hummocks and strings are identified by preceding a similar process as for the identification of hollows by the inversion of the DEM (by subtracting the DEM from the maximum value of the DEM). By reclassifying, encoding and finally summing up hollow-non hollow and hummock-non hummock layers, a microtopography classification is obtained (Figure S1-A).

4.4.2 Ground truth and model training

In November 2021, a vegetation inventory was conducted at over 50 points at each of the 4 mires considered in this study. Field controls were performed in September-October 2022.

The identified vegetation types follow the classification in APPENDIX B, section 3.3. Since it was not possible to discriminate between individual vegetation types with the limited spectral information available, these were further grouped as follows:

- Group I: Lawns, dominated by short sedges and Sphagna (vegetation types 1, 2, 3, 4 and 20)
- Group II: Carpets dominated by short sedges and *Sphagnum* subg. *Cuspidata* (vegetation types 5, 6, 12, 15, 16, 17, and 18)
- Group III: Mud/loose bottoms, tall-sedge fens,(vegetation types 7, 8, 9, 10, 11, 13, 14, and 15)
- Group IV: hummocks and sparsely treed mire (vegetation types 21, 22, 23, 24, 25, 26 and 40)
- Group V: Mire forests, including high hummocks (vegetation types 27-28, 30-38, 45-48)
- Group VI: Forests on mineral soils, outside of the mire system although within the catchment area. (vegetation types 50-53)

Group VI in the above grouping, i.e. forests on mineral soils was first clipped out before the image classification and appended to the final classification results. The observation points from the field survey were used to draw polygons or regions of interest (ROI) of the different groups abovementioned. The microtopography classification was stacked with the 6.5 cm resolution RGB image as an additional band. The RGB+microtography image was then trained using the random forest classifier in OrfeoToolbox v. 8.0.1 integrated into QGIS v. 3.22.6 (Figure S1-C). This training created the model that was then used for the classification. During the training, 80% of the pixels of the ROI were used for the actual training, and the remaining 20% were used for validation, i.e. computation of the confusion matrix and Cohen's kappa coefficient.

4.4.3 Image classification

In this step, the same image used during training (RGB + microtography) was classified with the random forest classifier based on the model obtained during the training stage (Figure S1-B). The resulting raster layer was then sieved and clusters with less than 100 pixels were merged with their surrounding class in order to reduce the normal fragmentation that occurs during image classification.

4.4.4 Classification results

The kappa coefficients obtained during validation were 0.76 for Degerö Stormyr and Stortjärn together, 0.82 for Hålmyran, and 0.75 for Hälsingfors, indicating a good classification performance overall. The mire vegetation classification results are presented in Figure S2. The vegetation in the area is essentially minerotrophic, but there are some areas where the vegetation has ombrotrophic characteristics. These areas are located essentially outside of the footprint of the EC towers, although small portions occur within the 90% footprint at all sites. These areas were visible on the orthomosaic and were drawn manually (Figure S2).

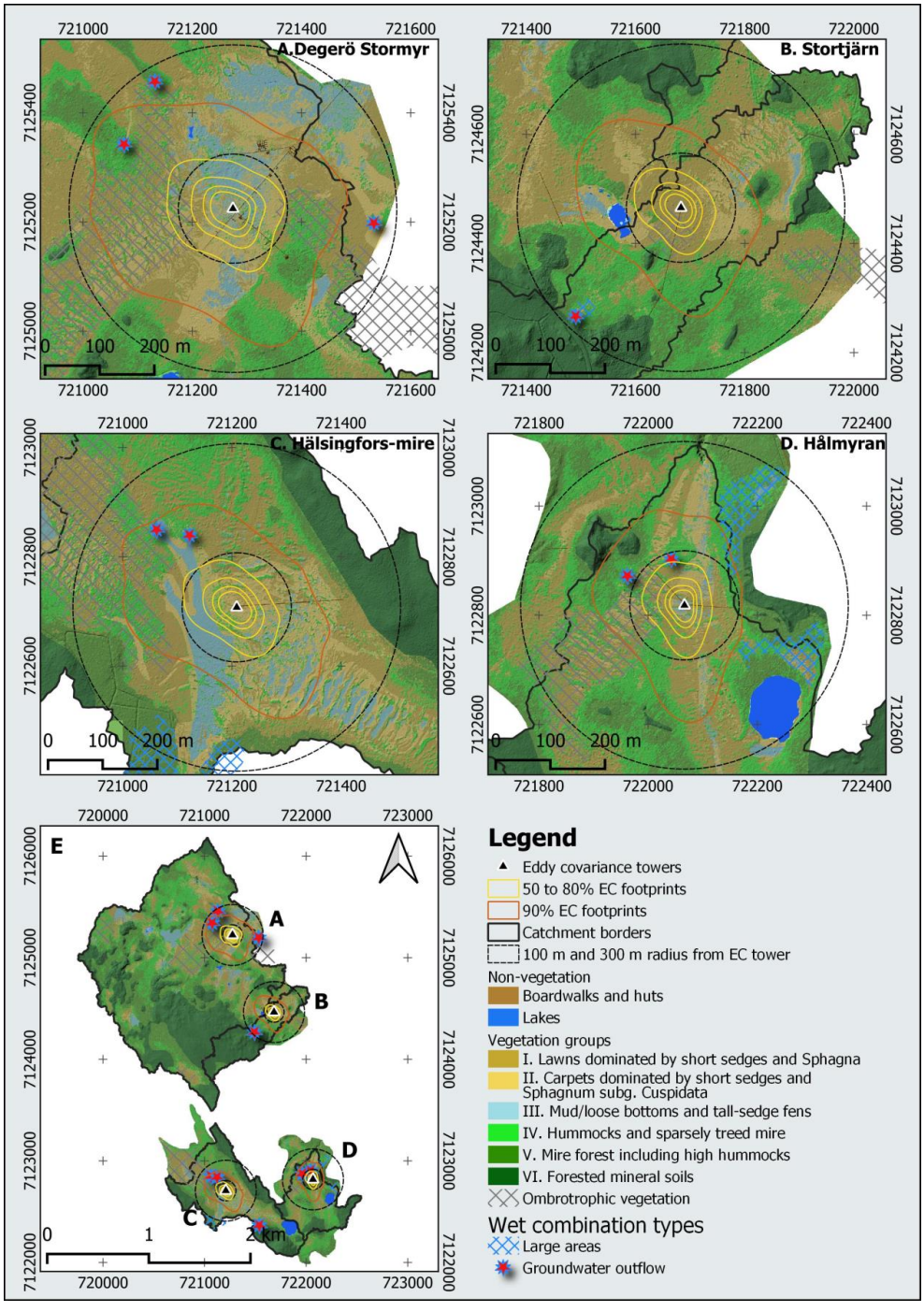

Figure S2. Vegetation classification map of the mire sites of the Kulbäcksliden peatland research infrastructure with a focus on a 300 m radius from EC towers at Degerö Stormyr (A), Stortjärn (B), Hälsingfors-mire (C), Hålmyran (D) and an overview of all four catchments (E).

The footprint climatologies were calculated from one-year data wind speed and wind direction (Mai 2020 to April 2021) based on (Kljun et al., 2015). The vegetation groups layer is blended with a hillshade derived from the 0.5 m resolution digital elevation model. Visit https://gis-slu.maps.arcgis.com/apps/View/index.html?appid=7d485f469233422aa98a5d49e031fd44 for an online version of this map.

The share of the different groups per catchment and footprint area is presented in table S3.

Table S3: Percentage share of the different groups of vegetation per catchment, 50%, 60% 70%, 80% and 90% footprint climatology area. The groups are those defined above in section 4.4.2.

Zone	Mire site	Total area (ha)	Percentage of total area							
			Group I	Group II	Group III	Group IV	Group V	Group VI	Boardwalks	Water
Catchments	Degerö Stormyr	272.93	15.5	8.1	4.4	23.0	20.6	27.9	0.2	0.2
	Stortjärn	29.64	13.9	6.6	0.6	11.4	9.8	57.5	0.1	0.1
	Hålmyran	33.11	22.7	7.0	1.6	31.0	13.8	21.2	0.1	2.6
	Hälsingfors	64.83	20.2	10.5	4.7	17.5	12.5	32.0	0.0	2.6
Footprint 50%	Degerö Stormyr	0.38	12.1	39.6	37.7	7.3	0.0	0.0	3.3	0.0
	Stortjärn	0.19	95.3	2.5	0.0	0.7	0.0	0.0	1.4	0.0
	Hålmyran	0.20	39.6	27.5	24.7	5.9	0.0	0.0	2.3	0.0
	Hälsingfors	0.25	18.1	71.6	0.3	9.0	0.0	0.0	1.0	0.0
Footprint 60%	Degerö Stormyr	0.67	11.8	40.8	38.3	7.0	0.0	0.0	2.1	0.0
	Stortjärn	0.33	92.5	5.2	0.0	1.3	0.0	0.0	1.0	0.0
	Hålmyran	0.35	46.0	30.1	16.8	5.4	0.0	0.0	1.7	0.0
	Hälsingfors	0.44	15.0	68.9	0.9	14.4	0.0	0.0	0.7	0.0
Footprint 70%	Degerö Stormyr	1.32	14.5	42.5	35.9	5.7	0.0	0.0	1.5	0.0
	Stortjärn	0.65	91.0	6.0	0.0	2.1	0.2	0.0	0.7	0.0
	Hålmyran	0.67	48.9	30.3	11.6	8.0	0.0	0.0	1.2	0.0
	Hälsingfors	0.86	12.3	65.4	5.6	16.1	0.0	0.0	0.5	0.0
Footprint 80%	Degerö Stormyr	3.29	15.9	49.1	27.2	7.0	0.0	0.0	0.9	0.0
	Stortjärn	1.65	82.9	12.5	0.0	3.3	1.0	0.0	0.4	0.0
	Hålmyran	1.61	48.6	26.5	8.1	15.8	0.3	0.0	0.7	0.0
	Hälsingfors	2.15	14.0	54.4	19.2	12.1	0.1	0.0	0.3	0.0
Footprint 90%	Degerö Stormyr	15.12	32.7	30.9	11.5	19.9	4.3	0.0	0.5	0.1
	Stortjärn	8.24	47.6	21.4	2.2	20.9	5.0	0.9	0.2	1.7
	Hålmyran	7.23	33.9	18.2	4.1	34.2	7.2	2.1	0.2	0.0
	Hälsingfors	9.97	26.7	34.9	18.7	18.8	0.7	0.0	0.1	0.0

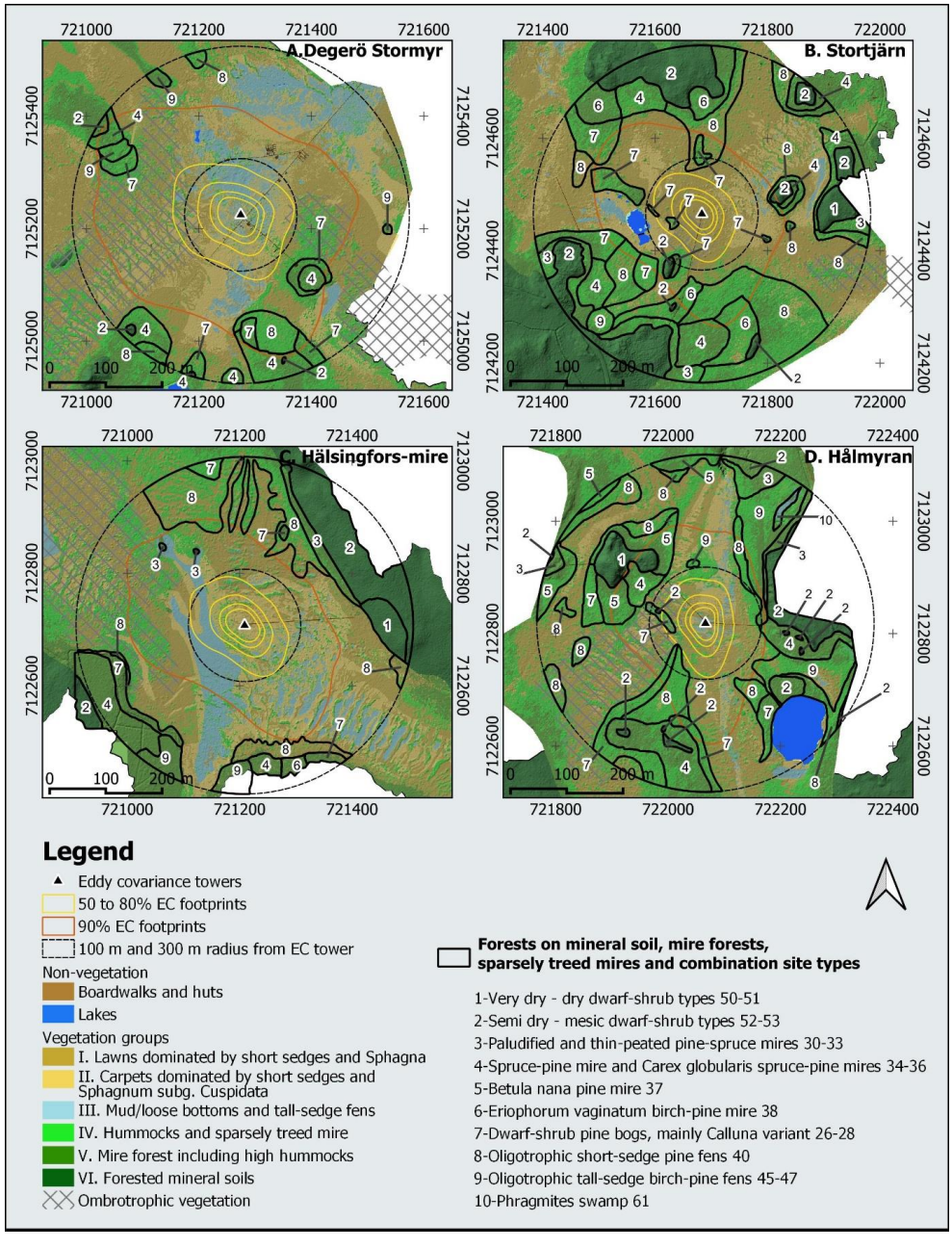

Figure S3. Simplified vegetation classification map of forests types on mineral soil, mire forests, sparsely treed mires, and various wet combination types including *Phragmites* swamps. For explanation see text. This simplified map is limited to a 300 m radius from EC towers at Degerö Stormyr (A), Stortjärn (B), Hälsingfors-mire (C), Hålmyran (D).

4.5 References:

Ebeling, F. (1978). *Nordsvenska skogstyper*. *Sveriges Skogsvårdsförbunds Tidskrift* (Vol. 76).

Eurola, S. (1962). *Über die regionale Einteilung der südfinnischen Moore* (Vol. 33(2)). Annales Botanici Societatis Zoologicae Botanicae 'Vanamo'.

Eurola, S., Hicks, S., and Kaakinen, E. (1984). Key to Finnish Mire Types. In P. D. Moore (Ed.), *European Mires* (pp. 11–117). Academic Press.

Eurola, S., Huttunen, A., Kaakinen, E., Kukko-oja, K., Saari, V., and Salonen, V. (2015). *Sata suotyyppiä : opas Suomen suokasvillisuuden tuntemiseen*. (V. Saari & V. Salonen, Eds.). University of Oulu; Thule Institute. Retrieved from https://converis.jyu.fi/converis/portal/detail/Publication/25319741?auxfun=&lang=fi_FI

Eurola, S., Huttunen, A., and Kukko-oja, K. (1995). *Suokasvillisuusopas (Mire vegetation guide)* (Oulanka Reports, Vol. 14). Oulanka Biological Station, University of Oulu.

Eurola, S., and Virtanen, R. (1991). Key to the vegetation of the northern Fennoscandian fjelds. *Kilpisjärvi Notes*, *12*, 1–28. Retrieved from https://helda.helsinki.fi/handle/10138/244529

Forslund, M., Forslund S R, and Löfroth, M. (1993). *Våtmarker i Västerbottens län*. Umeå: Länsstyrelse i Västerbotten. Retrieved from http://urn.kb.se/resolve?urn=urn:nbn:se:naturvardsverket:diva-2809

Granlund, L., Vesakoski, V., Sallinen, A., Kolari, T. H. M., Wolff, F., and Tahvanainen, T. (2022). Recent Lateral Expansion of Sphagnum Bogs Over Central Fen Areas of Boreal Aapa Mire Complexes. *Ecosystems*, *25*(7), 1455–1475.

Gunnarsson, U., and Löfroth, M. (2009). *Våtmarksinventeringen – resultat från 25 års inventeringar*. Retrieved from https://www.naturvardsverket.se/globalassets/media/publikationer-pdf/5900/978-91-620-5925-5.pdf

Joosten, H., and Clarke, D. (2002). *Wise use of mires and peatlands-background and principles including a framework for decision-making*. International Mire Conservation Group and International Peat Society. Retrieved from www.wetlands.org/projects/GPI/default.htm

Kalela, A. (1961). Waldvegetationszonen Finnlands und ihre klimatischen Parallelltypen. *Archivum Societatis 'Vanamo'*, *16*, Suppl. 65-83.

Kljun, N., Calanca, P., Rotach, M. W., and Schmid, H. P. (2015). A simple two-dimensional parameterisation for Flux Footprint Prediction (FFP). *Geoscientific Model Development*, *8*(11), 3695–3713.

Laitinen, J., Rehell, S., and Huttunen, A. (2005). Vegetation-related hydrotopographic and hydrologic classification for aapa mires (Hirvisuo, Finland). *Annales Botanici Fennici*, *42*(2), 107–121. Retrieved from https://www.jstor.org/stable/23726854#metadata_info_tab_contents

Laitinen, J., Rehell, S., Huttunen, A., Tahvanainen, T., Heikkilä, R., and Lindholm, T. (2007). Mire systems in Finland-special view to aapa mires and their water-flow pattern. *Suo*, *58*(1), 1–26.

Lidberg, W., Nilsson, M., Lundmark, T., and Ågren, A. M. (2017). Evaluating preprocessing methods of digital elevation models for hydrological modelling. *Hydrological Processes*,

31(26), 4660–4668.

Malmström, C. (1923). *Degerö Stormyr. En botanisk, hydrologisk och utvecklingshistorisk undersökning över ett nordsvenskt myrkomplex* (Meddelanden från Statens Skogsförsöksanstalt No. 20). Stockholm. Retrieved from https://pub.epsilon.slu.se/10091/1/medd_statens_skogsforskningsanst_020_01.pdf

Økland, R. (1990). Regional variation in SE Fennoscandian mire vegetation. *Nordic Journal of Botany*, *10*(3), 285–310.

Påhlsson, L. (1994). *Vegetationstyper i Norden*. (L. Påhlsson, Ed.) (Vol. TemaNord 1). Copenhagen: Nordiska ministerrådet. Retrieved from https://books.google.com/books/about/Vegetationstyper_i_Norden.html?id=0Rt4KsafjxsC

Pakarinen, P., and Ruuhijärvi, R. (1978). Ordination of northern Finnish peatland vegetation with factor analysis and reciprocal averaging. *Annales Botanici Fennici*, *15*(3), 147–157. Retrieved from https://www.jstor.org/stable/23725222#metadata_info_tab_contents

Ruuhijärvi, R. (1960). *Über die regionale Einteilung der nordfinnischen Moore* (Vol. 31(1)). Annales Botanici Societas Zoologica Botanica Fennica "Vanamo." Retrieved from https://books.google.se/books/about/Über_die_regionale_Einteilung_der_nordf.html?id=i7VQAAAAYAAJ&redir_esc=y

Ruuhijärvi, R. (1983). The Finnish mire types and their regional distribution. In A. G. P. Gore (Ed.), *Ecosystems of the World, 4 B. Mires: swamp, bog, fen and moor. Regional studies* (Vol. 47–49). Amsterdam: Elsevier.

Rydin, H., and Jeglum, J. K. (2013). *The biology of peatlands (2nd ed)*. Oxford University Press.

Rydin, H., Sjörs, H., and Löfroth, M. (1999). Mires. *Acta Phytogeographica Suecica*, *84*, 91–112. Retrieved from https://www.researchgate.net/publication/286628326_7_Mires

Sallinen, A., Akanegbu, J., Marttila, H., and Tahvanainen, T. (2022). Recent and future hydrological trends of aapa mires across the boreal climate gradient. *Journal of Hydrology*, *617*, 16.

Sjörs, H. (1948). Myrvegetation i Bergslagen (Summary: Mire vegetation in Bergslagen, Sweden). *Acta Phytogeographica Suecica*, *21*, 1–299.

Sjörs, H., and Gunnarsson, U. (2002). Calcium and pH in north and central Swedish mire waters. *Journal of Ecology*, *90*(4), 650–657.

SLU. (2021). Reference measurements of the climate at the Experimental Forests at SLU. Retrieved September 20, 2021, from https://www.slu.se/en/departments/field-based-forest-research/environment/climate-data/referenceclimate/

SMHI. (2021). Swedish Climate data. Retrieved September 20, 2021, from http://www.smhi.se/data/meteorologi

5. APPENDIX E: Instrumentation at the research infrastructure

Table S4. Instrumentation at the Kulbäcksliden peatland research infrastructure up to January 2023.

System	Variable	Degerö Stormyr		Stortjärn		Hålmyran		Hälsingfors mire		Hälsingfors forest	
Eddy covariance	CO2 & H2O	2001 - 2014:	LI-6262	2020 - Now	Picarro G2311-f	2020 - Now:	Picarro G2311-f	2020/06 - 2020/12:	EC 155 Campbell Scientific	2020 - Now:	LGR DLT-100 FGGA 908-0010
		2014 - Now:	LI-7200					2020/12- Now:	Picarro G2311-f		
		2013 - Now:	LGR FGGA 911-0010								
	CH4	2013 - Now:	LGR FGGA 911-0010	2020 - Now	Picarro G2311-f	2020 - Now:	Picarro G2311-f	2020/06 - 2020/12:	LI-7700	2020 - Now:	LGR DLT-100 FGGA 908-0010
								2020/12 - Now:	Picarro G2311-f		
	Hg(0)	2021 - Now:	Lumex RA-915 AM	-	-	-	-	-	-	2021 - Now:	Lumex RA-915 AM
	Wind speed & direction	2001 - 2014:	Gill R3-100	2020 - Now	Metek uSonic-3 Class A	2020 - Now:	Metek uSonic-3 Class A	2020/06 - 2020/12:	CSAT-3B	2020 - Now:	Metek uSonic-3 Class A
		2013-2017:	Metek uSonic-3 Class A					2021 - Now:	Metek uSonic-3 Class A		
		2017 - Now:	Gill HS-50								
		2021 - Now:	Metek uSonic-3 Class A (for eddy mercury)							2021 - Now:	Metek uSonic-3 Class A (for eddy mercury)

System	Variable	Degerö Stormyr		Stortjärn		Hålmyran		Hälsingfors mire		Hälsingfors forest	
Automated **Chambers**	CO2 & CH4	2014 - 2017:	LGR GGA-24EP	-	-	2021 - Now:	LGR UGGA 915-0011	-	-		
		2017 - Now:	Picarro G1101-I								
Manual **Chambers**	CH4	2004-2014	Gas chromatograph							2018	LGR UGGA model 908-0010-0002 Serial 12-0091
	CO2	2004-2014	PP IRGA Sytem							2019 - Now	GasScouter TM G4301
	CO2 & CH4	2014-2018	LGR UGGA								
Ancillary data	Air temperature and humidity	2001 - 2014:	Rotronic MP102H-331000	2020 - Now:	HC2S3 Campbell Scientific	2020 - Now:	HC2S3 Campbell Scientific	2020 - Now:	HC2S3 Campbell Scientific	2020 - Now:	HC2S3 Campbell Scientific
		2013 - Now:	Rotronic MP102H-331000								
		2018 - Now:	Rotronic MP102H-331000								
	Soil temperature	2001-2014	TO3R TOJO Skogsteknik	2020 - Now:	TO3R TOJO Skogsteknik	2020 - Now:	TO3R TOJO Skogsteknik	2020 - Now:	TO3R TOJO Skogsteknik	2020 - Now:	TO3R TOJO Skogsteknik
		2013-2019	105 type E thermocouple								
		2019-2021	Micro-step Pt100 probe								
		2021-Now:	Fischer Pt100								

System	Variable	Degerö Stormyr		Stortjärn		Hålmyran		Hälsingfors mire		Hälsingfors forest	
	Water table depth	2001 - Now:	CS450	2020 - Now:	CS451	2020 - Now:	CS451	2020 - Now:	CS451	2020 - Now:	CS451
	Precipitation	2001 - Now:	ARG100	2020 - Now:	ARG100	2020 - Now:	ARG100	2020 - Now:	ARG100		
		2013-2021	Geonor T200b								
		2022-Now	Lambrecht Rain[e]H3								
	Global radiation	2013-Now	CMP21	-	-	-	-	-	-	-	-
	SW & LW radiation	2013-Now	CNR4	2020 - Now:	NR01 Campbell Scientific	2020 - Now:	NR01 Campbell Scientific	2020 - Now:	NR01 Campbell Scientific	2020 - Now:	NR01 Campbell Scientific
	PAR	2013-2017	SQ-110	2020 - Now:	LI-190	2020 - Now:	LI-190	2020 - Now:	LI-190	2020 - Now:	LI-190
		2017-Now	LI-190								
	NDVI	2014 - now	SKYE sensors (also measure PRI and SWIR)	2020 - Now:	Decagon SRS	2020 - Now:	Decagon SRS	2020 - Now:	Decagon SRS	2020 - Now:	Decagon SRS
		2017 - now	Decagon SRS								
Phenology cameras	Images	2011 - 2014	Canon A480	2020 - Now:	Canon	2020 - Now:	Canon	2020 - Now:	Canon	2020 - 2021:	Wingscapes Timelapse
		2014 - 2022	CanonPowershot A810	2022-Now	Stardot Netcam SC	2022-Now	Stardot Netcam SC	2022-Now	Stardot Netcam SC	2022-Now	Stardot Netcam SC

System	Variable	Degerö Stormyr		Stortjärn		Hålmyran		Hälsingfors mire		Hälsingfors forest	
		2022 - now	Mobotix Mx-M26B-6D								
		2016 - now	Stardot Netcam SC(ICOS)								
		2016 - now	Mobotix Mx-M26B-6D061(SITES Spectral)								

Acta Universitatis Agriculturae Sueciae

Doctoral Thesis No. 2025:13

Northern peatlands are significant methane sources, yet their contribution to the global budget remains uncertain. This thesis investigated methane flux dynamics across a mire complex using eddy covariance data from multiple locations. Key findings revealed that C:N ratio controls spatial patterns while temperature and plant productivity drive temporal dynamics. Based on flux source-area analysis, a data-driven upscaling approach was developed to estimate the methane budget of the peatland complex. Thus, this work contributes to a better understanding of peatland-climate feedbacks.

Koffi Dodji Noumonvi received his PhD education at the Department of Forest Ecology and Management, SLU, Umeå. He has a double MSc. in Forest Sciences from the Universities of Padova (Italy) and Lisbon (Portugal) and a Water and Forest Engineering degree from Morocco.

Acta Universitatis Agriculturae Sueciae presents doctoral theses from the Swedish University of Agricultural Sciences (SLU).

SLU generates knowledge for the sustainable use of biological natural resources. Research, education, extension, as well as environmental monitoring and assessment are used to achieve this goal.

ISSN 1652-6880
ISBN (print version) 978-91-8046-448-2
ISBN (electronic version) 978-91-8046-498-7